

# Tsunami Modelling along the East Queensland Coast

---

## Report 3: Moreton Bay



Australian Government



Queensland  
Government

### Prepared by

Paul Boswood, Robert Wall, and Leo Peach  
Coastal Impacts Unit  
Science Delivery and Knowledge  
Department of Environment and Science  
GPO Box 2454  
BRISBANE QLD 4001

© The State of Queensland (Department of Environment and Science) 2018

The Queensland Government supports and encourages the dissemination and exchange of its information. The copyright in this publication is licensed under a Creative Commons Attribution 3.0 Australia (CC BY) licence



Under this licence you are free, without having to seek permission from DES, to use this publication in accordance with the licence terms.

You must keep intact the copyright notice and attribute the State of Queensland, Department of Environment and Science as the source of the publication.

For more information on this licence visit <http://creativecommons.org/licenses/by/3.0/au/deed.en>

### Disclaimer

This document has been prepared with all due diligence and care, based on the best available information at the time of publication. The department holds no responsibility for any errors or omissions within this document. Any decisions made by other parties based on this document are solely the responsibility of those parties. Information contained in this document is from a number of sources and, as such, does not necessarily represent government or departmental policy.

If you need to access this document in a language other than English, please call the Translating and Interpreting Service (TIS National) on 131 450 and ask them to telephone Library Services on +61 7 3170 5725

### Citation

Boswood PK, Wall R, Peach L. 2018. Tsunami Modelling along the East Queensland Coast, Report 3: Moreton Bay. Brisbane: Department of Environment and Science, Queensland Government.

### Acknowledgements

This project is a joint initiative of the Australian and Queensland Government through the Natural Disaster Resilience Program.

Tsunami scenarios were provided by Geoscience Australia. The authors wish to particularly thank Dr Jane Sexton and Dr Gareth Davies for their advice and support.

Front cover image – snapshot of modelled water levels for a 10,000 year average recurrence interval event originating in the Kermadec-Tonga subduction zone, eight hours after the tsunami was generated.

December 2018

---

## Document Log

Doc Version	Change	Editor
DRAFTv01	Document version for Department of Local Government, Racing and Multicultural Affairs. Not for public release.	Paul Boswood, Robert Wall, and Leo Peach
DRAFTv02	Review by P. Pinjuh, L. Peach (DES), Dr J. Sexton (GA), and Dr G. Davies (GA).	Paul Boswood
DRAFTv03	For final comment	Paul Boswood
FINAL	For public release	Paul Boswood
FINAL 2	Included amplification factors	Paul Boswood

This page intentionally left blank

---



## Executive summary

The 2004 Indian Ocean tsunami that devastated Indonesia, Thailand and Sri Lanka, brought about a heightened interest and focus into the science and disaster management for this hazard. In 2011, the Queensland Government commenced a project through the Natural Disaster Mitigation Programme (NDMP) to better understand the potential tsunami hazards along the east Queensland coastline. The first stage undertook nearshore tsunami modelling to identify regions of increased hazard to focus future detailed inundation modelling.

This current project has been undertaken through the Natural Disaster Resilience Program (NDRP), to continue the recommendations of Stage 1 by assessing the potential for tsunami inundation within and around Moreton Bay. This is achieved through demonstrated examples of hypothetical tsunami events for various average return intervals (ARI) from Geoscience Australia's revised probabilistic tsunami hazard assessment (PTHA) event database. Hydrodynamic modelling was undertaken using DHI's Mike21 flexible mesh software for events originating from the three primary subduction zones contributing to the hazard as identified in the revised PTHA. The ARIs chosen in Stage 2 as being representative of possible inundation and extreme (worst case) conditions were also selected for this study, being 750, 3,000, and 10,000 year. One event for each ARI was modelled at mean sea level (MSL) to examine the influence of the stage of tide. All other scenarios were modelled at Highest Astronomical Tide (HAT) to represent a worse case and to acknowledge that tsunami events occur over several hours and so could occur on high tide. Including sea level rise, a total of 23 scenarios were modelled, as well as an additional run to incorporate the detached breakwater at Redcliffe Pier.

Overall, approximately 140 km of coastline as well as waterways were modelled from Bribie Island to South Stradbroke Island, incorporating the Moreton Bay Regional, Brisbane City and Redland City Local Government Areas. The model was calibrated against predicted tides and validated against the 2007 Solomon Island tsunami event captured by the then Queensland Environmental Protection Agency's (EPA) Storm Tide Monitoring network.

The modelling provides insight into tsunami propagation characteristics within the study area. Arrival times are dependent on the source location, with those from the New Hebrides having the shortest arrival time of just over 4 hours, while events from South America arriving much later at over 18 hours. Once the leading wave reaches Cape Moreton, the additional time it takes to reach locations within the Bay is consistently between 1 and 1.5 hours, depending on the vicinity of the location with the three main entrances (North Channel, South Passage, Jumpinpin Channel), and 2.5 hours to reach Indooroopilly within the Brisbane River.

Although not modelled, there is potential for shorter steep waves to travel on top of the underlying tsunami in areas where the tsunami wave steepens significantly (particularly close to the coast at Redcliffe and over the entrance sandbanks). Although these waves may have an impact on coastal structures, the run-up and inundation that occurs is a result of the underlying longer period tsunami.

In general, the hazard is significantly greater on the ocean side of the islands that protect Moreton Bay, producing a significant marine and land hazard with maximum currents up to 8 metres per second (m/s) and maximum water levels up to 10 metres (m). Dangerous currents can also develop within the entrances as North Passage, South Passage and Jumpinpin Channel.

Within the bay, tsunami amplitudes are generally below one metre with little variation between the various ARIs and still water levels, due to significant dissipation across the various entrance sandbanks. Exceptions to this occur on the bay side of islands near North and South Passage, Redcliffe Peninsula, Brighton to Fisherman Island, Beachmere, and Wellington Point to Raby Bay. Strong currents can also develop in the entrances to marinas and canal estates. Given the relative consistency of tsunami amplitudes with increasing ARI, the inundation within the bay was found to be more sensitive to the stage of tide.

In general, the majority of the coastline will experience some inundation, especially at higher ARI and HAT levels. This may be restricted to the foreshore, with coastal properties in low lying areas being more susceptible at the higher tide levels. The communities identified as having a higher level of hazard (based on inundation extent) are in decreasing order:

- Amity Point to Point Lookout;
- Woorim;
- Moreton Island Communities (Cowan Cowan, Tangalooma, Koorinal, and Bulwer);
- Brighton to Brisbane Airport;
- Redcliffe Peninsula;
- Beachmere and Godwin Beach;
- Russell, Macleay, Coochie, Peel and St Helena islands;
- Bongaree; and
- Wynnum to Raby Bay.

Sea level rise associated with climate change may increase inundation extents within the Bay, which warrants consideration in vulnerability studies from climate change. The areas at most risk include Hemmant, Shorncliffe, Brighton, estates between Beachmere and Godwin Beach, Bongaree, Bellara and Dunwich. However, the actual impact will depend on the evolution and adaptation of the complex sandbanks throughout the North and South Passages, which was not considered in this study.

The draft revised PTHA draws upon an additional eight years of events, learnings, and scientific knowledge to provide the best present understanding of tsunami hazard near the Australian coast. A comparison of inundation extents from this study and the previous Stage 2 study for Golden Beach suggests that the revised PTHA increases the inundation hazard compared to the previous PTHA, due to an increased contribution to the hazard from the Kermadec-Tonga subduction zone. This suggests that a review of previous studies based on the original PTHA may be warranted, including those undertaken for the Sunshine Coast and Gold Coast. If these models are revised, it is also suggested that the offshore boundary be positioned offshore of the continental shelf to allow any shelf trapped wave processes to develop.

The developed overland DEM is a fixed bare earth model in that only ground points have been included, thereby removing all structures and vegetation. The influence of these features on inland inundation is introduced implicitly by the introduction of roughness factors. The DEM is also assumed to be static and non-erodible. Should a tsunami cause significant erosion of the dune system or entrance shoals to the bay, then the extent of inundation may differ to these model results. The hazard considered relates to potential inundation and broad-scale currents. There may be secondary impacts associated with the tsunami such as coastal erosion, which have not been addressed in this study.

The events selected represent the mean of the maximum water levels for the chosen ARI based on the draft revised PTHA as of February 2018. Higher levels can occur within the 95 per cent confidence limits. Also, any changes to the PTHA since February 2018 may influence the

outcomes of this report. Disaster managers may wish to consider appropriate factors of safety in any decisions based on the information provided through this study.

Overall, the study provides planners and disaster managers with a better understanding of the potential tsunami hazard within Moreton Bay and neighbouring islands.

# Contents

<b>Executive summary</b> .....	<b>i</b>
<b>Glossary</b> .....	<b>viii</b>
<b>1 Introduction</b> .....	<b>1</b>
<b>2 Tsunami Dynamics</b> .....	<b>3</b>
<b>3 Scope</b> .....	<b>5</b>
<b>4 Locality</b> .....	<b>6</b>
<b>5 Model Development</b> .....	<b>8</b>
<b>5.1 Modelling Approach</b>	<b>8</b>
<b>5.2 Supporting Data</b>	<b>8</b>
5.2.1 Bathymetric and Topographic Data	8
5.2.2 Tide Data	10
5.2.3 Probabilistic Tsunami Hazard Assessment Database	11
<b>5.3 Digital Elevation Model (DEM)</b>	<b>12</b>
<b>5.4 Model Domain and Mesh Development</b>	<b>13</b>
<b>6 Model Calibration, Validation and Sensitivity</b> .....	<b>16</b>
<b>6.1 Approach</b>	<b>16</b>
6.1.1 Adopted Parameters	16
6.1.2 Seabed Roughness	17
6.1.3 Overland Roughness	17
<b>7 Scenarios</b> .....	<b>18</b>
<b>8 Results</b> .....	<b>22</b>
<b>8.1 General Overview</b>	<b>22</b>
8.1.1 Wave Propagation	22
8.1.2 Maximum Amplitudes	27
8.1.3 Maximum Currents	32
8.1.4 Arrival Times	32
<b>8.2 Location Specific</b>	<b>35</b>
8.2.1 Southern Moreton Bay Islands	35
8.2.2 Redland Bay and Victoria Point	35
8.2.3 Manly to Raby Bay	35
8.2.4 Brisbane River	35
8.2.5 Port of Brisbane and Brisbane Airport	36

8.2.6	Brighton to Nudgee	36
8.2.7	Pine River	36
8.2.8	Redcliffe Peninsula	36
8.2.9	Deception Bay and Beachmere	37
8.2.10	Godwin Beach and Sandstone Point	37
8.2.11	Pumicestone Passage (South)	37
8.2.12	Bribie Island	38
8.2.13	Stradbroke Island	38
8.2.14	Moreton Island	39
<b>8.3</b>	<b>Climate Change (Sea Level Rise)</b>	<b>40</b>
<b>9</b>	<b>Discussion</b>	<b>42</b>
9.1	Updated PTHA – Comparison at Golden Beach	42
9.2	Stage of Tide and Inundation	42
9.3	Offshore Boundary	44
9.4	Undular Bores (Short Waves)	45
9.5	Sub-grid Structures (Redcliffe Detached Breakwater Example)	46
9.6	Scour Implications	48
9.6.1	Entrance Shoals	48
9.6.2	Anthropogenic Structures	50
9.7	Community Vulnerability	51
9.8	Marine Hazard and Vulnerability	53
<b>10</b>	<b>Conclusion and Recommendations</b>	<b>55</b>
<b>11</b>	<b>References</b>	<b>58</b>
<b>Appendix A – Tsunami Dynamics</b>		<b>62</b>
<b>Appendix B – Model Calibration</b>		<b>93</b>
<b>Appendix C – Validation and Sensitivity Testing</b>		<b>97</b>
<b>Appendix D – Overland Roughness Mapping</b>		<b>106</b>
<b>Appendix E – Tsunami Arrival Times</b>		<b>110</b>

## List of tables

Table 1 - Bathymetric and topographic data sources. ....	9
Table 2 - Highest Astronomical Tide (HAT) levels outside of Moreton Bay (ocean side) (MSQ, 2018). ....	10
Table 3 - - Highest Astronomical Tide (HAT) levels within Moreton Bay (MSQ, 2018).....	11
Table 4 - Table of Overland Manning's values used within the model domain.....	17
Table 5 - Model run schedule.....	20
Table 6 - Statistical Summary of event time series at the defined hazard point. ....	21
Table 7 - Stage 3 results summary .....	22
Table 8 - Variation in maximum water level (in metres above SWL) at select sites for all runs. ....	28
Table 9 - Arrival times after arrival at Cape Moreton. ....	34
Table 10 - Comparable model scenarios between Stage 2 study and Stage 3 study .....	42
Table 11 - Approximate scour depths as a percentage of flow depth (D) (reproduced from FEMA, 2012). ....	50
Table 12 - Marine facility damage classification from Lynett et al. (2014).....	53

## List of figures

Figure 1 - Stage 3 study region. ....	7
Figure 2 - Stage 3 model domain. ....	14
Figure 3 - Overland mesh resolution at Sandgate. ....	15
Figure 4 - Exceedance Rate for Stage 3 defined at longitude 153.94° east, latitude 27.29° south. ....	18
Figure 5 - Source-zone contribution by ARI (provided by GA). ....	19
Figure 6 - Subduction zones around the Pacific Rim (Power, 2013).....	21
Figure 7 - Leading wave approaching the coast for run 9 (Kermadec-Tonga, 3,000 yr ARI).....	24
Figure 8 - Example of tsunami time series for the 3,000 year ARI event at HAT, originating from Kermadec-Tonga. ....	25
Figure 9 - Cross section off Southern Bribie demonstrating the complex bathymetry. ....	25
Figure 10 - Leading wave propagation into Moreton Bay for Run 16 (Kermadec-Tonga, 10,000 yr ARI). The coloured arrow indicate wave direction from North Passage (orange), South Passage (blue), and Jumpinpin Channel (purple). Grey indicates coastal trapped waves.....	26
Figure 11 - Maximum water level and spectral plot for run 16 suggesting the presence of coastal trapped edge waves along the Redcliffe Peninsula (Inset: Spectra of surface elevation for Redcliffe, logarithmically scaled (power (cm <sup>2</sup> /hz <sup>-1</sup> ) and time in minutes).....	26
Figure 12 - Maximum water level (left) and current speed (right) for run 9 (Kermadec-Tonga, 3,000 yr ARI).....	27

Figure 13 - Variation in maximum water level (above SWL) at Raby Bay for various ARI, SWL and subduction zones (note that two KT events were run for the 10,000 year ARI). .....	28
Figure 14 – Maximum water level amplification factors (relative to offshore maximum water levels at Hazard Point).....	29
Figure 15 - Maximum water level (top) and amplification factor for centre line through Moreton Bay (orange line in Figure 14). .....	30
Figure 16 - Maximum water level (top) and amplification factor across the width of Moreton Bay (yellow line in Figure 14). .....	31
Figure 17 - Variation in amplification factor across ARI for events from Kermadec-Tonga. ....	31
Figure 18 - Kermadec-Tonga wave heights by ARI at a location offshore Moreton Island for tide level HAT Bay.....	33
Figure 19 - Inundation of southern Stradbroke Island during run 16 (Kermadec-Tonga, 10,000 year ARI). .....	39
Figure 20 - Inundation extent and water depths at Amity Point and Flinders Beach during run 16 (Kermadec-Tonga 10,000 year ARI at HAT Bay). .....	39
Figure 21 - Influence of SLR on maximum water level relative to HAT (left) and MSL (right) case for Kermadec-Tonga, 10,000 year ARI.....	41
Figure 22 - Increase of inundation extent for SLR condition (run 18 relative to run 16). .....	41
Figure 23 - Kermadec-Tonga 10,000 year ARI (Event ID 34890) modelled maximum water levels by stage of tide .....	43
Figure 24 - Influence of stage of tide on tsunami amplitude for Kermadec-Tonga 10,000 year ARI (Event ID 34890).....	44
Figure 25 - Continental shelf between Moreton Island and the Great Sandy National Park (dots represent PTHA points).....	45
Figure 26 - Tsunami wave profile snapshots during run 9 through North Passage (top) and off Redcliffe (bottom).....	46
Figure 27 - Maximum water levels and currents in the vicinity of the Redcliffe Pier for run 16 (Kermadec-Tonga, 10,000 year ARI). .....	47
Figure 28 - Maximum water levels and currents in the vicinity of the Redcliffe Pier for run 16 after mesh refinement (Kermadec-Tonga, 10,000 year ARI). .....	47
Figure 29 - Shallow sandbanks within North and South Passage.....	48
Figure 30 - Amplification factor (relative to based condition, run 16) for two scour scenarios of North and South Passage. ....	49
Figure 31 - Additional inundation extent and depths for Scenario 1 (scouring of North and South Passage to RL -5m). .....	49
Figure 32- Combination of general vulnerability curves for tsunami inundation. ....	51
Figure 33 - Example of application of hazard levels for run 16 at Woorim (top) and Amity Point. ..	52
Figure 34 - Example of marine vulnerability for run 16, based on the criteria of Lynett et al. (2014). .....	54

## Glossary

AEST	Australian Eastern Standard Time
ARI	Average Recurrence Interval
ATWS	Australian Tsunami Warning System
BoM	Bureau of Meteorology
DEM	Digital Elevation Model
DES	Queensland Department of Environment and Science
DHI	Danish Hydraulic Institute
DSITIA	Queensland Department of Science, Information Technology, Innovation and the Arts
EHP	Queensland Department of Environment and Heritage Protection
EMA	Emergency Management Australia
EPA	Queensland Environmental Protection Agency
GA	Geoscience Australia
GBR	Great Barrier Reef
HAT	Highest Astronomical Tide
JATWC	Joint Australian Tsunami Warning Centre
IofA	Index of Agreement
LGA	Local Government Authority (or Area)
MSL	Mean Sea Level
NDMP	Natural Disaster Mitigation Program
NDRP	Natural Disaster Resilience Program
NOAA	National Oceanic and Atmospheric Administration
NSW	New South Wales
NTHA	Nearshore Tsunami Hazard Assessment of Australia
PTHA	Probabilistic Tsunami Hazard Assessment of Australia
R <sup>2</sup>	Coefficient of Determination
RANSE	Reynolds averaged Navier-Stokes equations
RMSE	Root Mean Square Error
SEQ	South-east Queensland
SWL	Still Water Level
TsuDAT	Tsunami Data Access Tool
USGS	United States Geological Survey



# 1 Introduction

Following the 2004 Indian Ocean tsunami that devastated Indonesia, Thailand and Sri Lanka, the Australian Government through Geoscience Australia (GA), the Bureau of Meteorology (BoM) and Emergency Management Australia (EMA) developed the Australian Tsunami Warning System (ATWS) to provide independent advice of potential tsunami events through the Joint Australian Tsunami Warning Centre (JATWC).

To support the end-to-end warning system, GA undertook a probabilistic assessment of tsunami hazard (PTHA) along the Australian coastline in terms of tsunami amplitude (water level height above MSL) at the 100 m depth contour (Burbidge et al., 2008a and 2008b). The study was funded by EMA as part of the community awareness and capacity building component of the ATWS. The study was intended to assist the relevant state government departments to assess the tsunami risk along the coast and to prioritise regions that require further detailed assessment. However the study was limited in that for Queensland, the 100 m depth contour is offshore of the continental shelf and the Great Barrier Reef (GBR). Therefore, the influence of these significant features on tsunami propagation was uncertain.

To better understand the impact of the complex bathymetric features across the Australian continental shelf on tsunami propagation, GA undertook a national nearshore modelling study to examine the relative amplification of tsunami at 20 m depth compared to the 100 m depth contour for select locations (Fountain et al., 2009b). However that study did not include some locations such as the Sunshine Coast.

In 2012, the then Department of Science, Information Technology, Innovation and the Arts (DSITIA) was awarded a Natural Disaster Mitigation Program (NDMP) grant to further assess the tsunami hazard along the Queensland coast. The project was undertaken in two stages. Stage 1 undertook nearshore tsunami modelling to supplement the work undertaken by GA (Boswood, 2013a and 2013c). The study utilised hydrodynamic modelling software developed by the Danish Hydraulic Institute (DHI) together with the latest detailed digital elevation model (DEM) to examine the nearshore amplification to 10 m depth along the east Queensland coast from Cooktown to the NSW border. Stage 1 identified that South-east Queensland (SEQ) from Fraser Island to the New South Wales (NSW) border, was at higher risk to larger tsunami propagation than the rest of the east Queensland coast. The report identified the following regions of higher nearshore tsunami hazard in decreasing order of magnitude:

- Gold Coast (completed by GA (Fountain et al., 2009a));
- Ocean side of Bribie, Moreton, and Stradbroke Islands;
- Sunshine Coast (completed by DSITIA (Boswood, 2013b));
- Fraser Island;
- Bundaberg;
- Flying Fish Point;
- Capricorn Coast;
- Agnes Waters; and
- Hervey Bay.

The report also concluded that detailed inundation modelling would be required to assess the full risk to coastal communities.

Tsunami inundation modelling for the Gold Coast had previously been undertaken by GA (Fountain et al., 2009a), by examining three scenarios: an event representing the JATWC land inundation

warning wave amplitude of 0.3 m (1 in 200 year event); an event representing overtopping of the coastal dunes; and the largest credible event (1 in 10,000). These scenarios were modelled at both Mean Sea Level (MSL) and Highest Astronomical Tide (HAT). In 2013, DSITIA (Boswood, 2013b) undertook Stage 2 of the NDMP grant study that involved tsunami inundation modelling for the Sunshine Coast. A similar methodology to GA was used whereby three scenarios representing average recurrence intervals (ARI) of 750, 3,000 and 10,000 years were modelled at both MSL and HAT. The lowest ARI chosen to represent an event that produces inundation beyond the beach.

In 2016, the then Department of Science, Information Technology and Innovation (DSITI) and now Department of Environment and Science (DES), was awarded a Natural Disaster Resilience Program (NDRP) grant to continue the previous work by examining the potential for tsunami inundation for two more regions identified in the list above. The final two regions within SEQ were selected and are identified as Stages 3 and 4. The model domains cover the following Local Government Areas (LGA):

- Stage 3: Moreton Bay Regional, Brisbane City and Redland City; and
- Stage 4: Gympie Regional, Fraser Coast Regional and Bundaberg Regional.

These model domains represent four of the locations identified in the list above.

This report describes the processes that influence tsunami propagation and documents the tsunami inundation modelling undertaken for Stage 3.

## 2 Tsunami Dynamics

To better understand tsunami hazard, this section will briefly describe the processes that influence tsunamis. In basic terms, a tsunami is a series of long period waves generated by a disturbance in the ocean water column arising from abrupt geophysical events. These disturbances are more likely from movement of tectonic plates along faults in the form of submarine earthquakes, but could also be from submarine landslides, volcanic eruptions or a possible meteorite strike (in the extreme). More than 80 per cent of the world's tsunamis were caused by earthquakes (IOC, 2016). The earthquake scenario is the focus of this report.

A simple analogy would be dropping a pebble in a pond. The pebble generates a deformation of the water surface. This in turn creates a wave or series of waves that radiate or spread away from the source in concentric circles of increasing circumference as they propagate away. As the circumference increases, the amplitude decreases or attenuates due to energy being transferred along the wave crest. In reality, tsunami generation is not a point source but a complex pattern of bed movements. The three main stages are: tsunami generation; propagation; and run-up/inundation.

The main source of tsunamigenic earthquakes (that is, capable of generating tsunami) that could produce tsunami hazard along the east Queensland coast come from the subduction zones along the Pacific Rim. Friction between the continental and oceanic plates opposes movement until energy build-up causes the plates to suddenly slip past one another, generating an earthquake. The resulting uplift of the seabed generates a vertical rise in the full water column, which splits to propagate as a tsunami in all directions. The resulting tsunami propagates as a set of waves whose energy is concentrated at wavelengths corresponding to the earth movements (~100 km), at wave heights determined by vertical displacement (typically <1 m), and at wave directions determined initially by fault shape and orientation, and later by the adjacent coastline geometry. Because each earthquake is unique, every tsunami has unique wavelengths, wave heights, and directionality (NOAA, 2018).

As the displacement occurs through the entire water column, and wave lengths are much greater than depth, the tsunami behaves as a shallow water wave even in deep water. The wave period is generally in the range of 5 to 40 minutes. In general, the tsunami may experience the same processes that influence short period wind waves, not limited to attenuation, shoaling, scattering, focusing, diffraction, reflection, trapping and resonance, but at a larger scale and at greater depths. These processes produce an extended wave train of many waves even though the original source was a single impulse. The latter waves in a tsunami form very complicated patterns in which it is difficult to determine the relationship of a latter wave to the initial source. Hence, only the observations of the first few waves at a site are used for comparison with model simulations and estimation of the earthquake source parameters (Mofjeld et al., 2004). A tsunami event can therefore last for several hours, and the first wave may not necessarily be the largest. However, IOC (2016) suggest that the largest wave is usually one of the first five waves.

As the tsunami approaches the coastline, it is influenced by coastal features (such as bays and headlands) and nearshore bathymetry such that the amplitude can amplify and vary along the coastline. Unlike wind waves, which steepen, break and dissipate on beaches; the length to wave height ratio of tsunamis rarely steepens to breaking point. As tsunamis reach the coast, the approaching tsunami can appear as a fast moving tide or surge. The leading edge of some may decay and can appear like a fast moving tidal bore. The flow is horizontal in pattern (more like river flow) and can be very strong and turbulent. The momentum of these waves can push water much further inland than wind waves, and the currents can be too strong for a person to remain upright.

Of course the ability to inundate depends on a number of factors including tsunami height and period, stage of tide, height of any barriers (such as seawalls and beach dunes), obstacles (such as buildings), and land coverage (for example a dense forest will impede tsunami movement more than cleared pastoral land). For small amplitude tsunamis, the stage of tide may be a critical factor. As well as inundating low lying coastal regions, tsunamis will also propagate up rivers and waterways much faster than they inundate some coastal zones.

For coastal structures such as ports and marinas, strong currents can develop at the entrances. Within the port, circulation systems can develop as well as potential resonance that will amplify the tsunami amplitude.

Further detail about tsunami dynamics is provided in Appendix A.

### 3 Scope

The overall aim of this work is to provide local government authorities and disaster managers a better understanding of the potential tsunami hazards (focused on inundation) along the east Queensland coastline, through demonstrated examples of hypothetical tsunami events for various average return periods (ARI).

This study is one in a series of reports to assess the tsunami hazard through numerical modelling. The project, Tsunami Modelling along the East Queensland Coast, originated in 2011. Two reports were completed in 2013:

- **Report 1:** Regional Modelling (nearshore modelling to 10 m depth along the east Queensland coast to assess amplification factors relative to the 100 m depth contour, and to assess regions requiring more detailed studies (Boswood, 2013a)); and
- **Report 2:** Sunshine Coast (detailed tsunami inundation modelling for select synthetic scenarios of various ARI (Boswood, 2013b).

This study is a continuation of the initial project by examining tsunami inundation for two more regions as identified in Report 1:

- **Stage 3:** Moreton Bay Region, Brisbane City and Redland City local government areas; and
- **Stage 4:** Gympie Region, Fraser Coast Region and Bundaberg Region local government areas.

This is Report 3 in a series of 4, which describes Stage 3 model development and hazard assessment.

The reports focus on earthquake generated tsunamis from GA's draft revised PTHA (as of February 2018), and the broad scale inundation on the open coast and the major river systems where bathymetry data is available. It does not include small waterways and has limited resolution within small scale features such as ports, marinas and canal estates. The study is limited to the data that was available at the time of the project as detailed in the following sections.

All reports can be accessed through the Queensland Government website (<https://www.qld.gov.au/environment/coasts-waterways/beach/studies>), and the Queensland Government Open Data Portal (<https://data.qld.gov.au/>).

## 4 Locality

The Stage 3 region comprises the Moreton Bay Region, Brisbane City and Redland City Local Government Areas (LGAs) (Figure 1), with a cumulative coastline of approximately 140 km in length stretching from Bribie Island in the north to South Stradbroke Island. Brisbane is the state capital and is the highest populated city in Queensland. The combined population of the three LGAs is about 1.77 million over an area of 392,080 hectares (ABS, 2016). The largest population is located within the Brisbane City LGA (67%), whereas Moreton Bay Region has the largest area (52%). Most of the population is situated on the mainland within the bay, with only small communities on the islands.

The mainland coastline within Moreton Bay is heavily developed, with numerous revetments and groynes to protect infrastructure. The northern suburbs of Scarborough and Redcliffe have pockets of sandy beaches between rocky headlands. The coastline further to the south is of finer material with wide intertidal flats and regions of mangroves. A number of waterways flow into the bay, the largest being Brisbane River, Logan–Albert Rivers, North Pine River, Kedron Brook and Caboolture River. Port of Brisbane is located at the mouth of the Brisbane River. There are also a number of smaller marinas and canal estates within the bay, including those at Newport, Scarborough, Manly, Birkdale, and Raby Bay. Within the southern end of Moreton Bay, there are a number of small islands forming complex channels. The smaller inhabited islands within Redlands include Peel Island (QPWS Rangers), Coochiemudlo Island, MacLeay Island, Garden Island (one family), Lamb Island, Karragarra Island and Russell Island at the southern extent.

Most of the larger island communities are located on the bayside. The more exposed communities are located on the southern tip of Bribie Island (Woorim), the southern tip of Moreton Island (Koorimal) and the northern tip of North Stradbroke Island (Amity Point and Point Lookout). The islands are popular destinations for camping and recreational activities, and there are a number of camping grounds on the ocean side of the islands requiring four wheel drive access. The coastline on the ocean side consists of sandy beaches with narrow intertidal zones.

Ocean side coastal processes are dominated by the high energy wave climate, similar to that of the Gold Coast. Wave energy within Moreton Bay is dominated by local wind waves. The islands shelter the bay from the predominant southerly swells. Ocean wave energy that enters Moreton Bay and reaches the coastline is greatly attenuated by refraction, diffraction, bed friction and breaking across the shallow shoals at the bay entrance (BMT WBM, 2014).

Golden Beach, although part of the Sunshine Coast Region LGA, has been included within this study to allow for comparison between Stage 2 (Boswood, 2013b) results, to better understand the impacts of the revised PTHA (refer to Section 5.2.3).



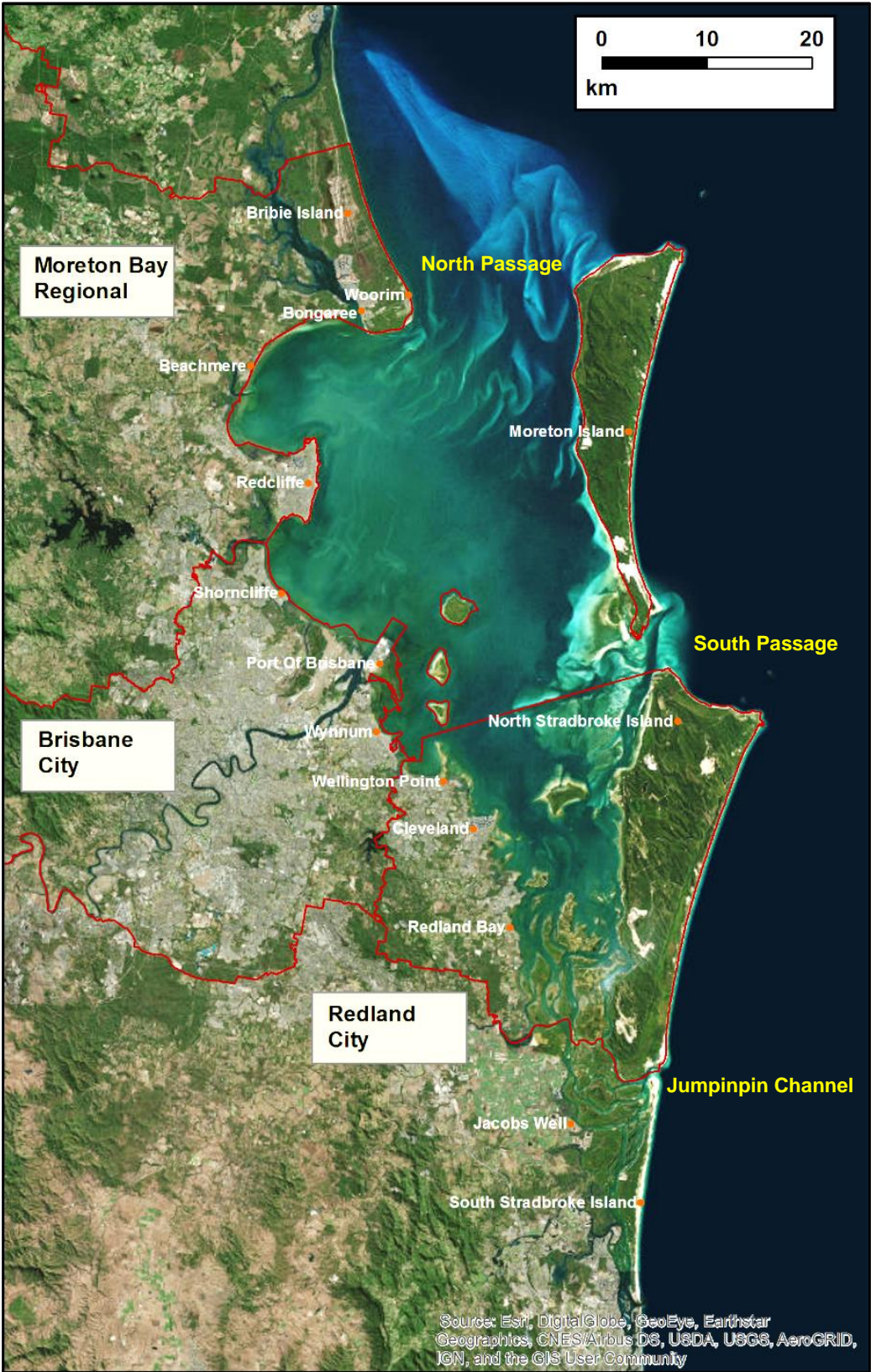


Figure 1 - Stage 3 study region.

## 5 Model Development

### 5.1 Modelling Approach

The tsunami inundation modelling was undertaken using DHI's MIKE21 flexible mesh hydrodynamic modelling software (MIKE21FM), which was successfully applied to Stages 1 and 2. The hydrodynamic model is based on the numerical solution of the two-dimensional (depth averaged) incompressible Reynolds averaged Navier-Stokes equations (RANSE) invoking the assumptions of Boussinesq and of hydrostatic pressure (DHI, 2017a). The model consists of the continuity, momentum, temperature, salinity and density equations and it is closed by a turbulent closure scheme. The spatial discretisation of the primitive equations is performed using a cell-centred finite volume method. Unstructured meshes can be generated comprising both triangular and quadrilateral elements in either Cartesian or spherical coordinate systems. An explicit scheme is adopted for time integration.

Modelling software that solves the shallow water equations have been successfully applied to tsunami propagation and inundation. Horrillo et al. (2014) undertook benchmarking of a number of models ranging from full 3D Navier-Stokes implementations to 2D long wave models with frequency dispersion (Boussinesq) or without dispersion (nonlinear shallow water equations – similar to the selected modelling software). The results indicating that all models tested were suitable for inundation modelling for the benchmark problems investigated. Further details on the suitability of this software can be found in Boswood (2013a).

The modelling approach involves developing a mesh of the study area that represents the topographic and bathymetric characteristics that will influence tsunami propagation, including bed roughness characteristics, and applying forcing conditions that represent the range of conditions expected within the study area. The following sections will go through the data and model development in more detail.

### 5.2 Supporting Data

#### 5.2.1 Bathymetric and Topographic Data

A number of bathymetric and topographic datasets were sourced during the project to develop the digital elevation model (DEM) employed for mesh interpolation (refer to Section 5.3 for more detail). Table 1 details the datasets and sources.



**Table 1 - Bathymetric and topographic data sources.**

Source	Description	Resolution	Usage
International Hydrographic Organization (IHO) and the Intergovernmental Oceanographic Commission (IOC) of UNESCO	The GEBCO_08 Grid, version 20100927, <a href="http://www.gebco.net">http://www.gebco.net</a>	unknown	Solomon Validation Model (areas outside the GA250 extent).
Geoscience Australia (GA)	Australian Bathymetry and Topography, June 2009 (GA250) (Webster, 2005),  <a href="https://data.gov.au/dataset/australian-bathymetry-and-topography-grid-june-2009">https://data.gov.au/dataset/australian-bathymetry-and-topography-grid-june-2009</a>	250 m	Solomon Validation Model (areas outside the gbr100 extent).
James Cook University (JCU)	High-resolution depth model for the Great Barrier Reef and Coral Sea 2017 (gbr100) (Beaman, 2010),  <a href="https://www.deepreef.org/bathymetry/65-3dgb-r-bathy.html">https://www.deepreef.org/bathymetry/65-3dgb-r-bathy.html</a>	100 m	Solomon Validation Model.
GA / Dr R Beaman	High-resolution depth model for the Great Barrier Reef – 30 m (gbr30) (GA, 2017),  <a href="http://pid.geoscience.gov.au/dataset/ga/115066">http://pid.geoscience.gov.au/dataset/ga/115066</a>	30 m	Moreton tsunami model.
GA	Digital Elevation Model (DEM) of Australia derived from LiDAR 5 Metre Grid – State Mosaic QLD,  <a href="https://data.gov.au/dataset/digital-elevation-model-dem-of-australia-derived-from-lidar-5-metre-grid">https://data.gov.au/dataset/digital-elevation-model-dem-of-australia-derived-from-lidar-5-metre-grid</a>	5 m	Moreton tsunami model.
DES Hydrology	Brisbane River Catchment Flood Study, 2017, DEM,  <a href="https://www.business.qld.gov.au/industries/mining-energy-water/water/maps-data/brisbane-river-catchment">https://www.business.qld.gov.au/industries/mining-energy-water/water/maps-data/brisbane-river-catchment</a>	1 m/5 m	Moreton tsunami model.
GA	Intertidal Extents Model Confidence Layer (ITEM CL),  <a href="http://pid.geoscience.gov.au/dataset/ga/100464">http://pid.geoscience.gov.au/dataset/ga/100464</a>	25 m	Moreton tsunami model.

Source	Description	Resolution	Usage
Queensland Government	Queensland Land Use Mapping Program (QLUMP), <a href="https://www.qld.gov.au/environment/land/vegetation/mapping/qlump">https://www.qld.gov.au/environment/land/vegetation/mapping/qlump</a>	N/A	Roughness Map.
Queensland Government	Queensland Digital Cadastral Database (DCDB) <a href="https://www.business.qld.gov.au/running-business/support-assistance/mapping-data-imagery/data/digital-cadastral">https://www.business.qld.gov.au/running-business/support-assistance/mapping-data-imagery/data/digital-cadastral</a>	N/A	Roughness Map.
Queensland Government	Queensland Wetland Mapping, <a href="https://wetlandinfo.ehp.qld.gov.au/wetlands/facts-maps/wetland-background/">https://wetlandinfo.ehp.qld.gov.au/wetlands/facts-maps/wetland-background/</a>	N/A	Roughness Map.

### 5.2.2 Tide Data

The tidal harmonics used to develop the large scale tidal model boundary conditions were supplied by the National Tidal Centre (NTC), Commonwealth Bureau of Meteorology. For locations further east than longitude 156° east, tidal constituents from NASA's GOT00.2 global tidal model were provided by NTC. The eight primary tidal constituents were provided for 63 locations along the perimeter of the tidal model domain, the constituents being K1, O1, M2, P1, S2, N2, K2 and Q1.

For calibration purposes, tidal constituents at a number of monitoring sites were provided by Maritime Safety Queensland (MSQ).

Highest Astronomical Tide (HAT) levels for the tsunami modelling scenarios were obtained from MSQ (2018), and are reproduced below in Table 2 and Table 3 for the ocean side of the study area and within the bay respectively.

**Table 2 - Highest Astronomical Tide (HAT) levels outside of Moreton Bay (ocean side) (MSQ, 2018).**

Site	AHD (m LAT)	HAT (m LAT)	HAT (m AHD or m MSL)
Snapper Rocks	0.98	2.11	1.13
Gold Coast Seaway	0.76	1.91	1.15
Amity Point	1.02	2.24	1.22
Woorim (Bribie)	0.93	2.16	1.23
Caloundra Head	0.99	2.05	1.06
Mooloolaba	0.99	2.17	1.18
<b>AVERAGE:</b>	<b>0.95</b>	<b>2.11</b>	<b>1.16</b>

**Table 3 - - Highest Astronomical Tide (HAT) levels within Moreton Bay (MSQ, 2018).**

Site	AHD (m LAT)	HAT (m LAT)	HAT (m AHD or m MSL)
Beachmere (Caboolture R)	1.26	2.62	1.36
Margate	1.23	2.59	1.36
Sandgate	1.31	2.62	1.31
Nudgee Beach	1.31	2.62	1.31
Brisbane Bar	1.243	2.73	1.49
Manly	1.29	2.81	1.52
Wellington Point	1.26	2.84	1.58
Redland Bay	1.41	2.98	1.57
Rocky Pt (Logan R mouth)	1.1	2.63	1.53
Russell Is (Canaipa Pt)	1.39	2.89	1.50
Dunwich	1.3	2.7	1.40
Tangalooma	1.15	2.51	1.36
<b>AVERAGE:</b>	<b>1.27</b>	<b>2.71</b>	<b>1.44</b>

### 5.2.3 Probabilistic Tsunami Hazard Assessment Database

A Probabilistic Tsunami Hazard Assessment (PTHA) was undertaken by GA to provide a means of assessing the hazard along the Australian coastline to assist state government agencies in identifying potential areas at risk and so requiring more detailed studies (Burbidge et al., 2008a). The assessment provided deep water return period curves for maximum tsunami amplitude along the 100 m depth contour and relative tsunami hazard rankings for locations around Australia. Tsunami propagation modelling was undertaken using a finite difference model based on the linear shallow water equations. Over 70,000 tsunamis were modelled and the time series were recorded at points along the 100 m depth contour. GA developed the Tsunami Data Access Tool (TsuDAT) so that state governments could access this database to assess the potential hazard along their coastline and to undertake inundation modelling (GA, 2010).

Tsunami scenarios for Stages 1 and 2 were obtained from TsuDAT at defined hazard points along the 100 m depth contour based on user define criteria of area of interest, ARI and subduction zone. As the probabilistic assessment varies for each hazard point, one hazard point within the area of interest is selected to define the return period statistics for event selection. TsuDAT provided a time series of water level and momentum (velocity x depth) along the two major axes ( $u_h$  (positive east) and  $v_h$  (positive north)) at defined points along the 100 m contour.

In 2017, GA advised DES that a major revision of the PTHA was in progress, with a planned release in 2018. The scenarios used to define the hazard for the Stage 3 and Stage 4 assessments are events from the draft revised PTHA provided directly to DES by GA prior to the official release of the update.

The revised PTHA incorporates the latest best-practice methods for modelling earthquake for tsunami generation, with updated global elevation data, and validation against observational data

not previously available during the development of the original PTHA. Specifically, the update utilises:

- Subduction zone geometries from Slab1.0 (Hayes, 2012);
- Subduction zones discretised at a resolution of 50 x 50 km<sup>2</sup> (previously 100 x 50 km<sup>2</sup>);
- Stochastic slip earthquake models (previously uniform-slip); and
- Different method to set earthquake rates based on Davies et al. (2017) leading to higher tsunami event exceedance rates (events per year) than the original PTHA.

The revision also provides some flexibility with output locations, with outputs available along the RL -20 m, RL -100 m and RL -1000 m contour lines, as well as offshore model grid points. The format of the return period curves have also been updated to account for uncertainty by including the mean and 95 percentile (refer Figure 4). For this study, events were selected based on the mean exceedance curve.

It is noted that any changes to the final PTHA release from that provided by GA in February 2018 may influence the results provided in this report.

### 5.3 Digital Elevation Model (DEM)

A tsunami is a long wave that is felt through the whole water column, even in relatively deep water. As such, the propagation of the tsunami will be sensitive to the underlying bathymetric data used in the model. Considerable effort was therefore directed towards producing a Digital Elevation Model (DEM) that best represented the overland, nearshore and deep water bathymetry within the model domain based on the most complete set of available data.

The Stage 3 model DEM was developed from a range of sources including (see Table 1):

- Bathymetry and topography from the gbr30;
- Topography from the 5 m State Mosaic QLD DEM; and
- Bathymetric river data from inputs to the Brisbane River Catchment Flood Study (BMT WBM, 2017).

The gbr30 is a comprehensive compilation of available bathymetric and topographic data collected from 1967 to 2017 covering the GBR and Coral Sea extending along the entire Queensland east coast. The dataset is provided in raster format with a spatial resolution of 0.0003 decimal degrees (approximately 30 metres). It is noted that although the gbr30 is of relatively high resolution, the underlying bathymetry data within the nearshore can be sparse. The intertidal zone can be dynamic, particularly on the beaches exposed to the open ocean.

The State Mosaic QLD DEM contains topographic data from various airborne Light Detection and Ranging (LiDAR) surveys conducted along the Queensland coastline between 2009 and 2015. Data for the study area was extracted from this dataset. The DEM include some areas of erroneous reflections from water surfaces within the intertidal zone giving incorrect elevations. This required processing before integrating with the other datasets. Satellite overlays along with the Intertidal Extents Model (ITEM) Confidence Layer (GA, 2016) were used to identify these error areas within the data, which were then removed. The ITEM Confidence Layer's use as a mask for the topographic data was further verified with a field survey conducted at Sandgate-Brighton Foreshore in November 2017.

Hydrographic survey data of the lower Brisbane River and surrounding tributaries conducted in 2014 for the Brisbane River Catchment Flood Study (BMT WBM, 2017) was provided by the Hydrology group within DES. This included a 1 m spatial resolution DEM of the main lower

Brisbane River channel and various 5 m DEMs for the tributaries of Bulimba Creek, Breakfast Creek, Norman Creek and Kedron Brook.

Considerable effort was invested in creating a seamless transition at the coastline interface between the topographic and bathymetric datasets, where artificial steps could develop at the interface of the higher resolution (and higher accuracy) 5 m topographic DEM and the lower resolution gbr30 DEM. A 1 km wide transition zone was created based on nearest neighbour interpolation performed on each of the datasets where they met to create a smooth transition.

Within residential canals on south Bribie Island, Newport and Raby Bay, data was either non-existent or of poor quality. Assumptions were required of bed levels in these areas. The developed overland DEM is a bare earth model in that only ground points have been included, thereby removing all structures and vegetation. The influence of these features on overland inundation is introduced implicitly by the introduction of roughness factors. The DEM is also assumed to be static and non-erodible. Should a tsunami cause significant damage to soft/natural defences (such as dune systems), then this could significantly impact the inundation extent provided in this report.

The final DEM was developed over the duration of the project, as more data became available. The gbr30 DEM did not become available until January 2018. The initial model domain and mesh size testing (refer to Section 5.4) was undertaken with the gbr100, with further mesh size testing conducted after receiving the gbr30. All model validation and scenario modelling was undertaken with the final DEM, which is a layered compilation of all quality assured DEMs to maintain available resolution, as well as the transition zone mentioned above.

## 5.4 Model Domain and Mesh Development

The entire model domain for Stage 3 is shown in Figure 2. A number of test runs using 10,000 year ARI events (refer to Section 7) were undertaken to optimise the inland extent of the model and mesh resolution in the offshore (that is depths > 10 m) to maintain feasible computation times whilst reducing numerical dispersion and adequately representing key geomorphological features within the bathymetry.

The offshore boundary was set to correspond with GA's PTHA tsunami event database output locations. The original PTHA database (TsuDAT (GA, 2010)) provided event time series at the 100 m depth contour. The draft revised PTHA (refer to Section 5.2.3) can provide output at the 100 m and 1,000 m depth contour. As the 100 m depth contour comes in close to Cape Moreton (about 7.5 km offshore), an offshore boundary at the 1,000 m depth contour was selected for this study to maximise the distance of the offshore boundary from the study area. This is a variation to the Stage 2 study (Boswood, 2013b) where the offshore boundary was set along the 100 m depth contour, being the only available output location for the original PTHA database. The land boundary provides for flooding and drying associated with inundation. The model domain extends to the north and south of the study area to allow tsunami propagation into this region and to mitigate any numerical boundary effects.

MLITT (2012) suggests that grid sizes should be selected such that 20 grid points represent a wavelength. For wave periods in the range of 5 to 10 minutes, this would suggest grid sizes of 1.5 to 3.0 km at 1000 m depth, and 150 to 300 m at 10 m depth. Generally, finite volume models refer to mesh area rather than mesh dimension. The Sunshine Coast tsunami inundation study (Boswood, 2013b) examined the impact of mesh resolution on tsunami inundation extents by comparing the results for two mesh resolutions (200,000 m<sup>2</sup> offshore to 75,000 m<sup>2</sup> at 10m depth against 35,000 m<sup>2</sup> offshore to 10,000 m<sup>2</sup> at 10 m depth). The comparison showed a reduction in spatial resolution by about half, resulting in over a two fold increase in computation time for an

average three per cent increase in maximum amplitude, with little difference in inundation extent. The area modelled for the Sunshine Coast was significantly smaller than the area being modelled in this study. A balance is required to assure the processes that influence tsunami inundation are replicated, whilst maintaining reasonable computation times based on the number of elements and the time step for model stability governed by the Courant-Friedrich-Lévy (CFL) number (DHI, 2017b).

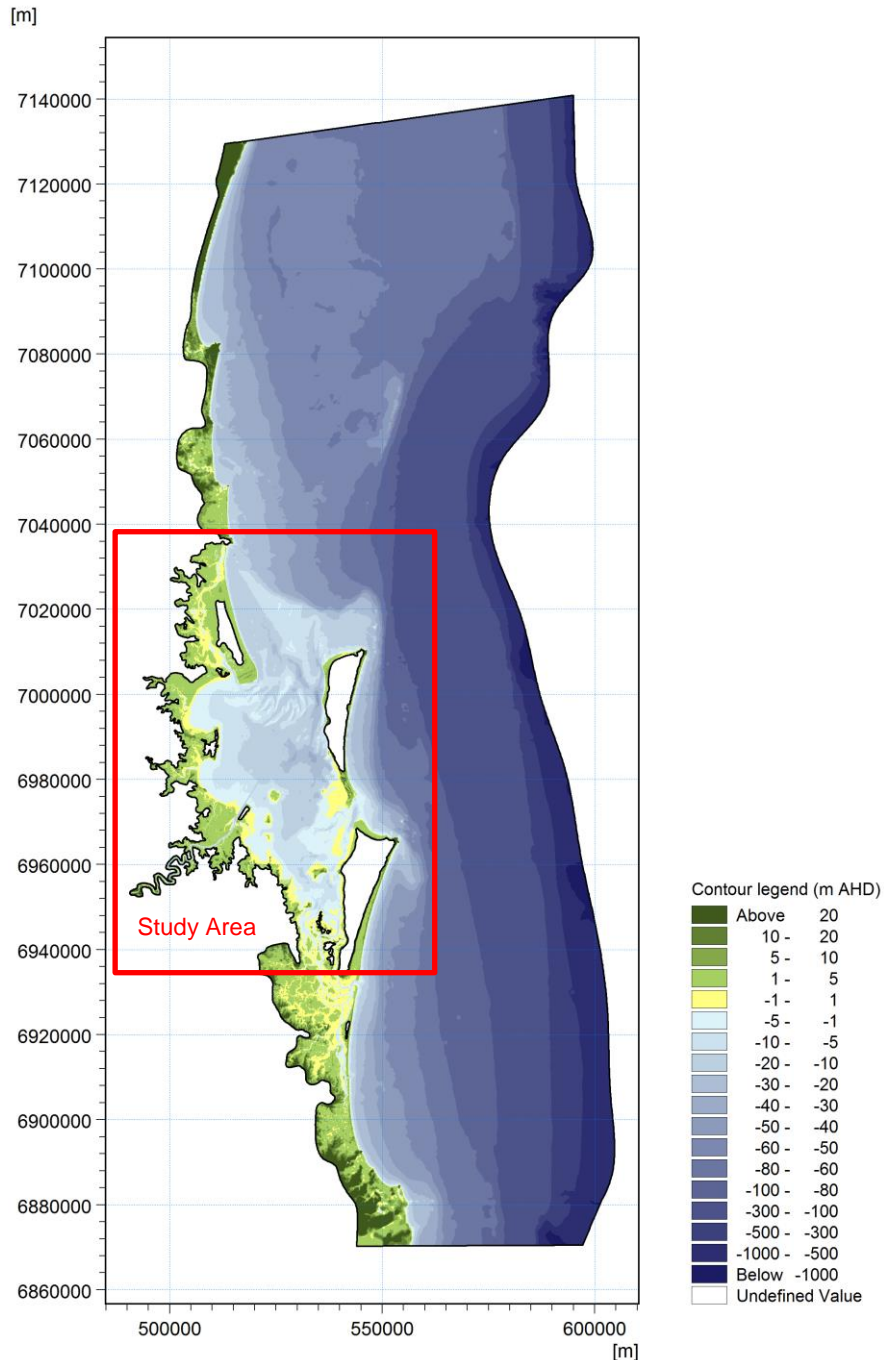


**Figure 2 - Stage 3 model domain.**

The final mesh comprises 2,295,036 triangular mesh elements. The maximum offshore resolution is 120,000 m<sup>2</sup> (an equivalent spatial resolution ( $dx$ ) of about 490 metres). A more detailed mesh is adopted within the study area, with maximum resolution of 7,500 m<sup>2</sup> ( $dx \approx 120$  m) within Moreton Bay and the nearshore zone on the ocean side. This is sufficient to capture tsunami shoaling and refraction processes, but does not capture features in the nearshore whose length scales (length



or width) are less than the adopted mesh sizes, such as the detached breakwater off the end of the Redcliffe Jetty. Major rivers were modelled up to the limit of reliable bathymetric data, which is typically not to the tidal limit. The replication of smaller waterways is reliant on the hydrographic datasets obtained. Although, the gbr30 DEM (refer to Section 5.2.1) is of high resolution, the nearshore data used to generate it can be sparse.

Meshes for developed inland areas, rivers, marinas and canal estates are typically  $800 \text{ m}^2$ , ( $dx \approx 40 \text{ m}$ ) going down to  $400 \text{ m}^2$  ( $dx \approx 30 \text{ m}$ ). This overland mesh size was considered adequate for emergency management purposes as it approximately represents a large residential lot, but is not too fine to cause unreasonable simulation times. This will provide general inundation extents, but will not provide detailed flow characteristics around buildings or along residential streets, as demonstrated in Figure 3. Sensitivity testing on overland mesh size indicated that coarser meshes would be more conservative. In undeveloped inland areas, a coarser resolution of  $1,200$  to  $2,400 \text{ m}^2$  ( $dx = 50$  to  $70 \text{ m}$ ) was adopted. Care was taken to capture potential barriers to tsunami inundation such as coastal ridges, dunes and the crest of revetments.

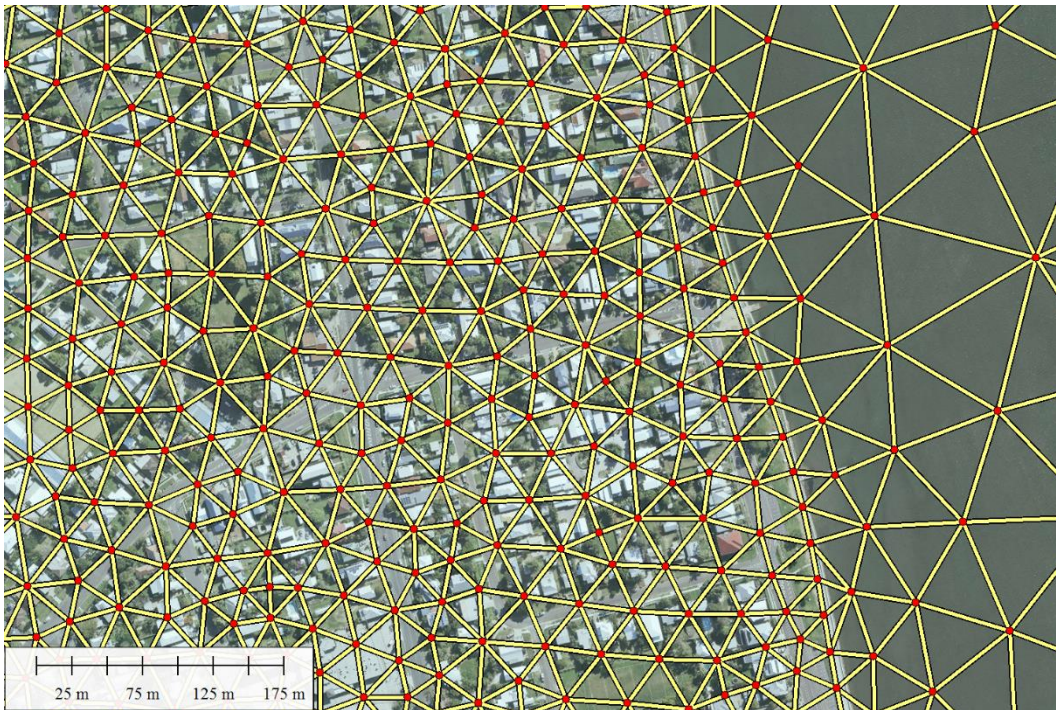


**Figure 3 - Overland mesh resolution at Sandgate.**

## 6 Model Calibration, Validation and Sensitivity

### 6.1 Approach

The standard approach to calibrating 2D hydrodynamic models involves adjusting model parameters such as bed roughness, horizontal eddy viscosity, and bathymetry to match measured water level and/or velocity data collected within the study area. This may involve a range of conditions that are expected to influence the local hydrodynamics. Once calibrated, the model is then validated against measured events.

As explained in Boswood (2013a), the availability of measured tsunami events along the Queensland coast is scarce, and inundation mapping from historic events is non-existent. As water level data associated with tides are more readily available, the 2013 study (Stage 1) calibrated the regional models against tidal predictions for 83 sites over a spring tide period in January to February 2011. The calibrated models were then validated for a specific tsunami event originating from the Solomon Islands in 2007 that was measured by the DES storm tide network (EPA, 2007). Boundary conditions consisting of water level time series was provided by GA.

To have further confidence in the detailed mesh developed for the current project, this process of calibration and validation was again undertaken, the detail of which is provided in Appendix B and Appendix C for calibration and validation respectively.

Calibration was undertaken against astronomical tides for six prediction sites that were available within the study area: Caloundra Head; Tangalooma Point; Bongaree; Brisbane Bar; Brisbane Port Office; and Gold Coast Seaway. For the validation event, only two sites were available within the model domain: Gold Coast Seaway; and Mooloolaba. Unfortunately there were no measurements available within Moreton Bay. Calibration parameters considered were seabed roughness and horizontal eddy viscosity.

Overall, the model performed well in reproducing both the tides and 2007 Solomon Island tsunami event with minimal adjustment required to the parameters. As there were no monitoring sites within the bay for validation, sensitivity testing was undertaken of these two parameters based on a 10,000 year ARI event provide by GA (refer to Appendix C). The results indicated minimal sensitivity along the open coast, supporting previous findings of Cardno (2013) for the NSW coast. However, within the bay the model is more sensitive to roughness and to a lesser extent, eddy viscosity. For the 2007 Solomon Island event, there was no noticeable sensitivity for either parameter. However, the Solomon event was a small magnitude tsunami in the order of 10 cm on the open coast, compared to the 10,000 year event with maximum amplitude of over 5 m along the open coast.

#### 6.1.1 Adopted Parameters

Given the lack of validation data within the bay and the findings of the sensitivity analysis described above, the final parameter settings were chosen on the more conservative side to produce slightly higher amplitudes but within commonly accepted values for coastal applications. Horizontal eddy viscosity is defined by the Smagorinsky formulation (Smagorinsky, 1963), adopting a constant coefficient of 0.28 (default value).



### 6.1.2 Seabed Roughness

The seabed roughness is defined by the Manning's coefficient ( $n$ ), a commonly adopted parameter for both riverine and coastal applications. Calibration suggested a constant seabed value of 0.025. Sensitivity testing showed this parameter to be the more sensitive within the bay for larger events. Therefore a lower roughness value of 0.02 was adopted, as applied by Cardno (2013).

### 6.1.3 Overland Roughness

As a tsunami travels overland, it will experience obstacles and land cover that will obstruct or impede its motion. The adoption of a "bare earth" topography requires the application of overland roughness values that represent the expected effect of the removed obstacles on inundation extent for each overland cell. Roughness coefficients are typically adjusted to match measured inundation levels. However, such data for a tsunami event is lacking for the study region.

Bricker et al. (2015) conclude that tsunami models would benefit from leveraging roughness values from open channel flow literature, and cites the work of Bunya et al. (2010), which provides an extensive list of Manning's values based on land use mapping for a storm surge modelling study. The approach applied to the current study was the development of a detailed roughness map based on land use. Further detail is provided in Appendix D.

Manning's values for overland areas were chosen following a literature review of values as discussed in Appendix D. The final list of values is reproduced in Table 4, based on the work of Bricker et al. (2015), Bunya et al. (2010), and Cardno (2013). This list has been purposely kept to a minimum, to prevent undue complexity that at present cannot be verified. It is expected that this will produce a more conservative result.

**Table 4 - Table of Overland Manning's values used within the model domain.**

Land Use Category	Manning's $n$	Manning's $M (1/n)$
Coastal Waters	0.025	40.00
Roads	0.020	50.00
Wetland Barren	0.030	33.33
Wetland Shrub	0.045	22.22
Grassland	0.030	33.33
Farmland	0.040	25.00
Coastal Woody Wetland	0.070	14.28
Forest	0.070	14.28
Low Density Urban	0.050	20.00
Medium Density Urban	0.100	10.00

## 7 Scenarios

As previously mentioned in Section 5.2.3, model time series were provided by GA based on a defined hazard point, area of interest, ARI and subduction zone. The hazard was defined at a point offshore from Moreton Island and North Stradbroke Island (longitude 153.94° east, latitude 27.29° south) from which the exceedance rate based on maximum tsunami amplitude (peak stage) is derived (Figure 4). The PTHA considers only earthquakes as source to the tsunami hazard, which contribute to approximately 80 per cent of all tsunami events (Davies, 2017 and Appendix A).

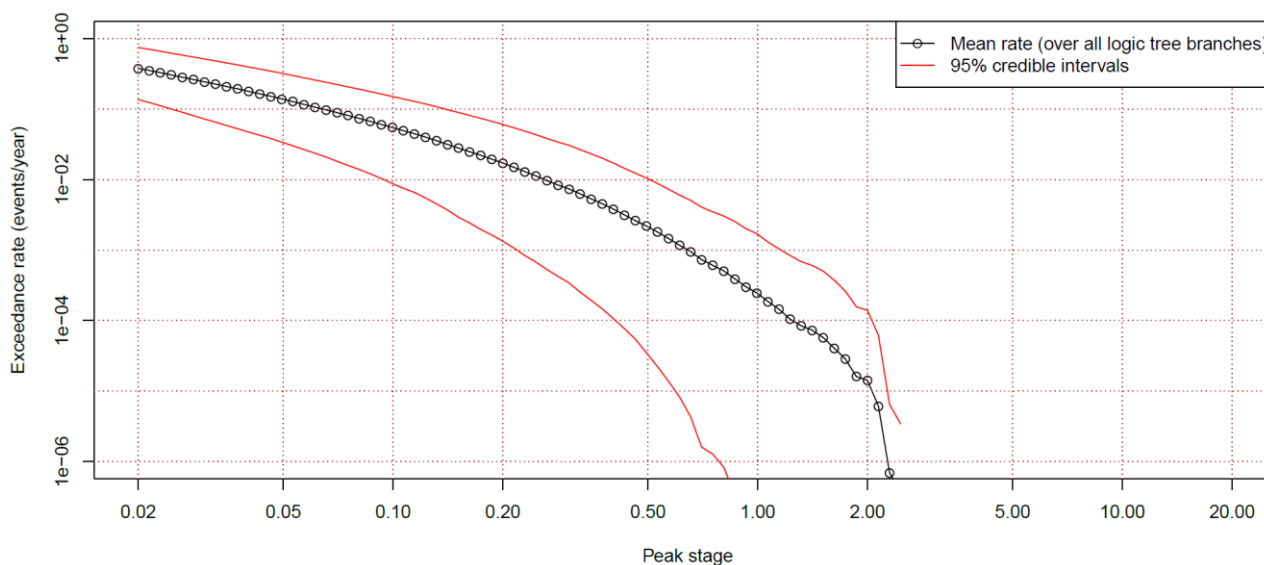


**Figure 4 - Exceedance Rate for Stage 3 defined at longitude 153.94° east, latitude 27.29° south.**

Events are then extracted for ARI (inverse of the exceedance rate) at 750, 3,000 and 10,000 years (based on the mean rate) consistent with the Stage 2 Sunshine Coast study (Boswood, 2013b). The higher ARI being the largest credible event and the other two arbitrarily chosen to demonstrate inundation that would overtop the coastal dunes. Figure 5 shows the contribution to the hazard at the defined offshore point by earthquake subduction zone with Figure 6 showing subduction zones within proximity to the east Queensland coast. It can be seen that the Kermadec-Tonga trench has the highest contribution across all ARI, followed by New Hebrides and South America. This is a change to the Sunshine Coast study, which showed the New Hebrides Trench as having the highest contribution to the hazard (based on the original PTHA).

It is noted that although the study has adopted the mean rate, there can be considerable spread in maximum stage between the 95 per cent creditable intervals. For example, the mean 100 year ARI event is about 0.3 m, but could also be between 0.1 and 0.5 metres. The upper limit being only seven centimetres below the 750 year ARI events provided in Table 5. So although the events modelled may seem extreme, they can also occur at lower recurrence intervals. It is also noted that the events provided by GA are from the draft revised PTHA as of February 2018. Any changes in the final release may influence the results and conclusions provided in this report.

The model run schedule is shown in Table 5 listing all Stage 3 runs varying over ARI, subduction zone and still water level. Models were run with still water levels at MSL, HAT, and HAT with sea level rise (SLR). The MSL condition is provided for one event each ARI, being the level applied to the PTHA. Given that a tsunami event can persist over several hours, it is likely that waves will occur on high tide. To demonstrate the variation that can occur with different tide stages the remainder of the runs are undertaken at HAT. Adopting HAT will provide a conservative result and is consistent with the NSW study (Cardno, 2013). HAT values within and outside the bay are

provided in Table 3 and Table 2 respectively. The average difference between both is 0.28 m, so it was decided to apply two HAT levels: Gold Coast Seaway for the ocean side, and Brisbane Bar for the bay. These sites are close to the average value and are also long standing monitoring sites.

Sea level rise is considered as a constant 0.8 m increase for the year 2100 from the Coastal Hazard Technical Guide (EHP, 2013). The ARI provided by the PTHA is for MSL, consequently model runs at HAT and SLR water levels may have an ARI greater than the reported values.

Each ARI is modelled for three events generated from different subduction zones at HAT. Only the Kermadec-Tonga event is considered for MSL. Along with one event from the New Hebrides, two events from Kermadec-Tonga were selected for the 10,000 year ARI, reflecting the dominance in hazard contribution and to examine the variability between different tsunami events from the same source. SLR was only considered for the worst case event (10,000 year Kermadec-Tonga; event id 35449) representing the upper-limit of the hazard for all scenarios considered in this study. Statistical properties of each event time series at the defined hazard point is summarised in Table 6.

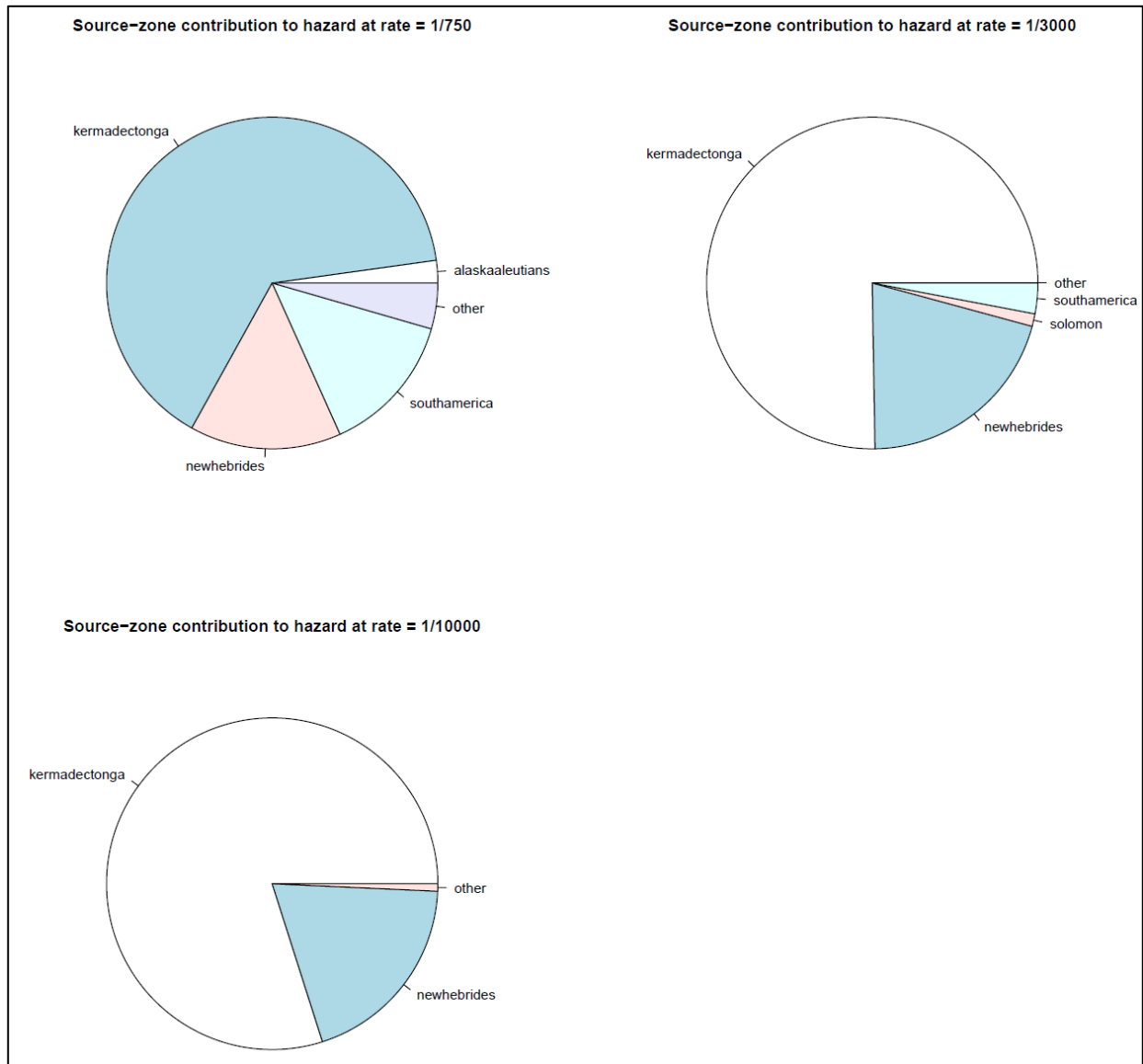


Figure 5 - Source-zone contribution by ARI (provided by GA).

**Table 5 - Model run schedule.**

Run No.	ARI	Source	PTHA Event ID	Max Amplitude (m)	Earthquake Magnitude (Mw)	Nominal Water Level	Water Level (m AHD)
1	750	Kermadec-Tonga	34745	0.578	9.2	MSL	0.00
2	750	Kermadec-Tonga	34745	0.578	9.2	HAT BAY	1.49
3	750	Kermadec-Tonga	34745	0.578	9.2	HAT OCEAN	1.15
4	750	New Hebrides	9601	0.560	8.9	HAT BAY	1.49
5	750	New Hebrides	9601	0.560	8.9	HAT OCEAN	1.15
6	750	South America	148229	0.571	9.6	HAT BAY	1.49
7	750	South America	148229	0.571	9.6	HAT OCEAN	1.15
8	3,000	Kermadec-Tonga	34890	0.903	9.3	MSL	0.00
9	3,000	Kermadec-Tonga	34890	0.903	9.3	HAT BAY	1.49
10	3,000	Kermadec-Tonga	34890	0.903	9.3	HAT OCEAN	1.15
11	3,000	New Hebrides	9774	0.935	9.0	HAT BAY	1.49
12	3,000	New Hebrides	9774	0.935	9.0	HAT OCEAN	1.15
13	3,000	South America	14798	0.811	9.6	HAT BAY	1.49
14	3,000	South America	14798	0.811	9.6	HAT OCEAN	1.15
15	10,000	Kermadec-Tonga	35449	1.295	9.4	MSL	0.00
16	10,000	Kermadec-Tonga	35449	1.295	9.4	HAT BAY	1.49
17	10,000	Kermadec-Tonga	35449	1.295	9.4	HAT OCEAN	1.15
18	10,000	Kermadec-Tonga	35449	1.295	9.4	HAT BAY + SLR	2.29
19	10,000	Kermadec-Tonga	35449	1.295	9.4	HAT OCEAN + SLR	1.95
20	10,000	New Hebrides	9743	1.267	9.0	HAT BAY	1.49
21	10,000	New Hebrides	9743	1.267	9.0	HAT OCEAN	1.15
22	10,000	Kermadec-Tonga	35375	1.196	9.4	HAT BAY	1.49
23	10,000	Kermadec-Tonga	35375	1.196	9.4	HAT OCEAN	1.15

**Table 6 - Statistical Summary of event time series at the defined hazard point.**

PTHA Event ID	Source	ARI	Max Amplitude (m)	Earthquake Magnitude (Mw)	Hm0 (m)	Tp (hh:mm:ss)	Tz (hh:mm:ss)
34745	Kermadec-Tonga	750	0.578	9.2	0.56	0:14:35	0:11:35
9601	New Hebrides	750	0.560	8.9	0.40	0:20:16	0:14:25
148229	South America	750	0.571	9.6	0.78	1:11:04	0:32:09
34890	Kermadec-Tonga	3,000	0.903	9.3	0.70	0:23:19	0:10:58
9774	New Hebrides	3,000	0.935	9.0	0.50	0:24:19	0:11:02
14798	South America	3,000	0.811	9.6	1.13	1:14:04	0:28:14
35449	Kermadec-Tonga	10,000	1.295	9.4	1.14	0:16:40	0:11:09
9743	New Hebrides	10,000	1.267	9.0	0.66	0:24:19	0:10:43
35375	Kermadec-Tonga	10,000	1.196	9.4	1.22	0:29:09	0:09:42

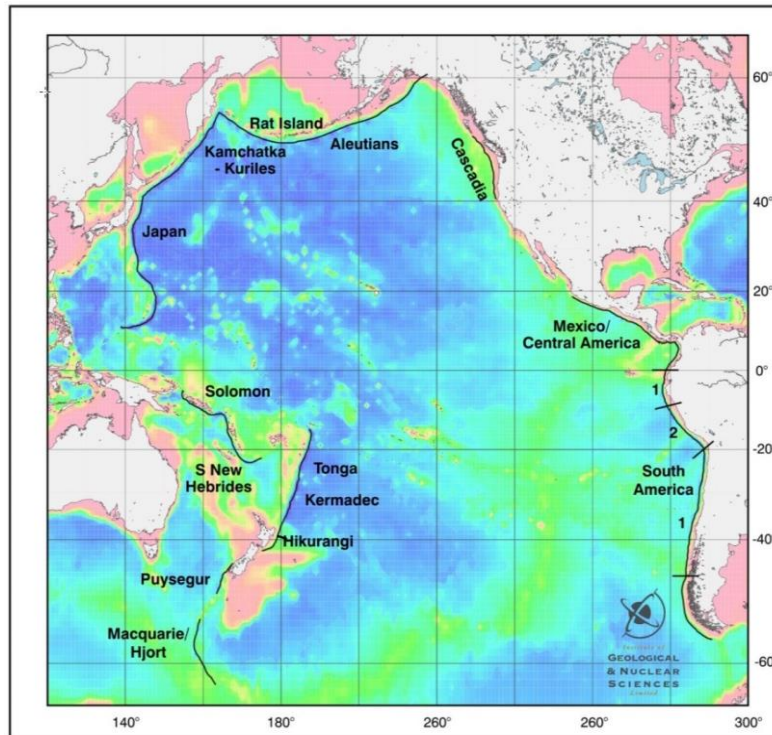


**Figure 6 - Subduction zones around the Pacific Rim (Power, 2013).**

## 8 Results

A summary of provided Stage 3 result formats is displayed in Table 7. Although a number of scenarios were modelled for each ARI at HAT, the results are provided for the worst case for each ARI. Refer to these for further context to the following sections.

**Table 7 - Stage 3 results summary**

Name	Description	Format
Appendix F	Spatial maximum water level (amplitude) and current speed of worst case scenario for each ARI at HAT (Kermadec-Tonga).	Separate PDF Map Booklets
Appendix G	Select study location maps of modelled inundation extent for each ARI at MSL (Kermadec-Tonga).	Separate PDF Map Booklet
Appendix H	Select study location maps of modelled inundation extent of worst case scenario for each ARI at HAT (Kermadec-Tonga).	Separate PDF Map Booklet
Appendix I	Select study location maps of modelled inundation extent of SLR scenario (Kermadec-Tonga).	Separate PDF Map Booklet
GIS Database	Entire study domain GIS files of modelled worst case scenario for each ARI (Kermadec-Tonga).	Separate ESRI Database

The separate documents and datasets listed in Table 7 can be accessed through the Queensland Government website (<https://www.qld.gov.au/environment/coasts-waterways/beach/studies>), and the Queensland Government Open Data Portal (<https://data.qld.gov.au/>).

### 8.1 General Overview

Across all ARI, tsunami events generated from the Kermadec-Tonga subduction zone resulted in the most extreme wave amplitudes, current speeds and inundation levels for the modelled scenarios. The spatial distribution of maximum current speeds and maximum water levels is consistent between ARI, increasing in magnitude as ARI increases (Appendix E). Further detail is provided below.

#### 8.1.1 Wave Propagation

This section provides a general description of tsunami propagation within Moreton Bay based on observation of the model results. Each tsunami will be different, but there will be characteristics that will be more generic based on coastline shape and bathymetric features. These characteristics will assist in understanding the potential hazard for Moreton Bay and are summarised below. To illustrate some of these characteristics, the model results from runs 9 and 16 in Table 5 (Kermadec-Tonga 3,000 and 10,000 year ARI events respectively) will be presented. In general, tsunami propagation into the study region can be characterised by:

- The first or leading wave, in the absence of any ambient conditions, is well formed and continuous across the study region (refer Figure 7).
- The first wave is not always preceded by a recession or drop in water level (also referred to as leading depression N-wave or LDN). Of the model scenarios considered, those from the Kermadec-Tonga subduction zone were LDN; whereas, those generated from the New Hebrides and South America had no initial recession (leading elevation N-waves or LEN).

This fits with subduction zone slip mechanics and tsunami generation discussed in Appendix A, where the coast on the overriding plate (as opposed to the subducting plate) will generally experience a LDN.

- The first wave is not necessarily the largest wave. The largest wave may occur several hours after the first wave as demonstrated in Figure 8. Of the scenarios modelled, the offshore leading wave is typically the largest wave. However, as the tsunami reaches the coast, interactions with the coastline and the shelf produce complicated patterns between the incident and reflected waves in both space and time, such that the resulting time series can look much different to the offshore wave train. The timing of the largest wave will depend on these interactions. The timing of the maximum water level will also depend on the stage of tide.
- The tsunami will impact the ocean side of the islands first. These are the locations where the largest tsunami heights will occur. However, these are also the locations of the highest dune elevations.
- The presence of shelf trapped waves and coastal trapped edge waves will influence the timing and spatial distribution of the largest tsunami amplitude, as well as the duration that the tsunami event will persist. An example of a shelf trapped wave originating on the Great Sandy National Park coast and impacting Bribie Island during run 9 to produce the maximum water level depicted in Figure 8 is illustrated in Figure A. 9.
- Coastal trapped edge waves occur on the ocean bordering islands. Generally, the tsunami impacts the most eastern points first. For Moreton island, the tsunami impacts Cape Moreton, generating progressive edge waves that propagate south on the ocean side of the island, as well as westward along the northern end and then southwards along the bay side of the island. A similar process occurs at Point Lookout on North Stradbroke Island. Coastal trapped waves on the islands may travel in either direction along the coast. However the dominant direction appears to be to the south.
- Coastal trapped edge waves can propagate in both directions along Bribie Island, but are predominantly towards the south and around the southern tip where they enter the bay. Tsunamis impacting Bribie are influenced by the complex bank patterns along North passage (refer Figure 9).
- Tsunamis enter the bay primarily through the North and South Passages, and to a lesser extent, through Jumpinpin Channel. Tsunami amplitudes are greatly attenuated by the complex sandbank patterns within these entrances as illustrated in Figure 12.
- As the tsunami enters the bay, it radiates outwards from the entrances (refer Figure 10). Tsunamis entering the North Passage will primarily influence north of the Brisbane River. Tsunamis entering South Passage predominantly impact south of the Brisbane River. The location of a site relative to these two entrances governs the arrival time. Tsunamis entering through Jumpinpin Channel are greatly attenuated by the complex and shallow channels such that this energy is greatly attenuated by the time it reaches MacLeay Island.
- Coast trapped edge waves also occur along Redcliffe Peninsula (refer to Figure 11), propagating towards the south. The largest tsunami heights within the bay occur at Redcliffe (Figure 12).
- Tsunamis will propagate up waterways and into marinas. The tsunami can propagate up the Brisbane River a considerable distance with little attenuation.



- Although not modelled, there is potential for shorter steep waves to travel on top of the underlying tsunami in areas where the tsunami wave steepens significantly (particularly close to the coast at Redcliffe and over the entrance sandbanks). This is discussed further in Section 9.4.

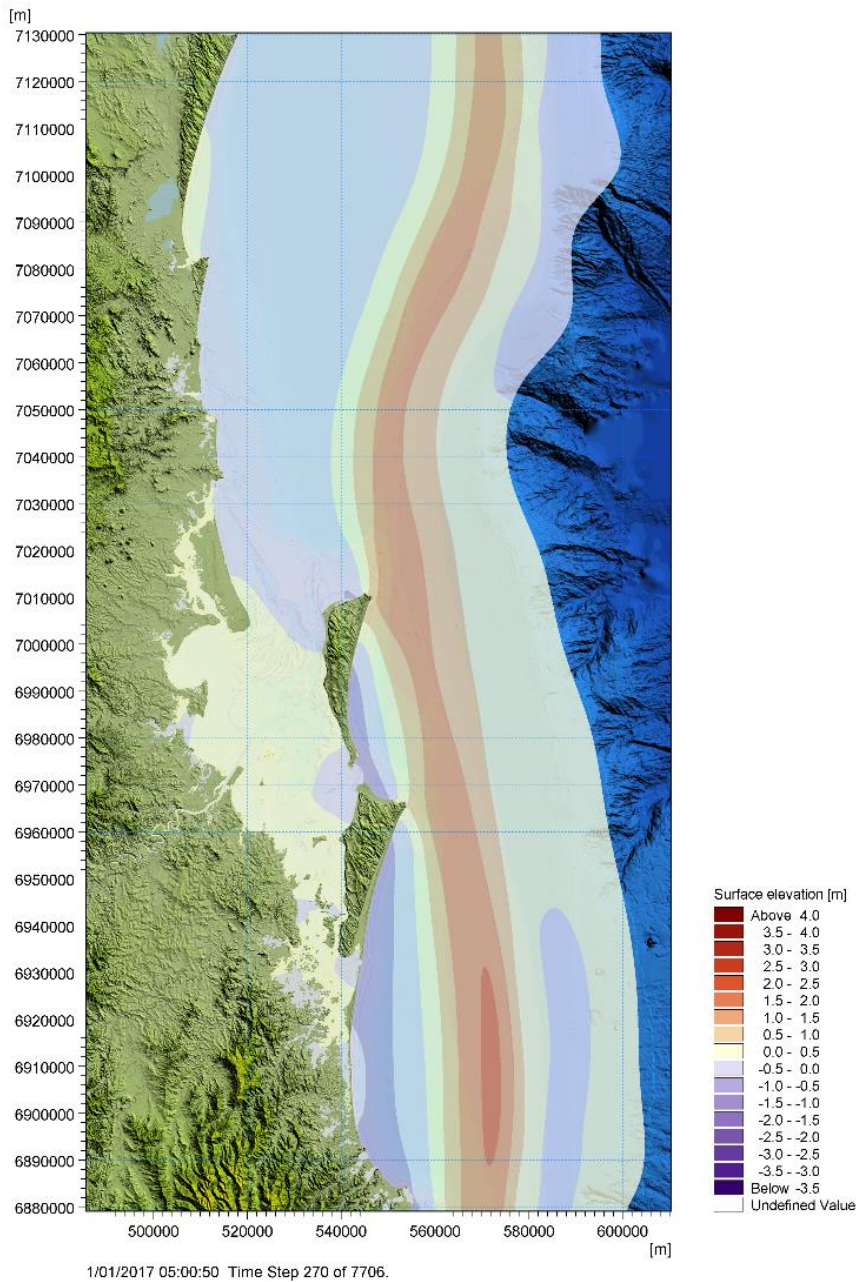
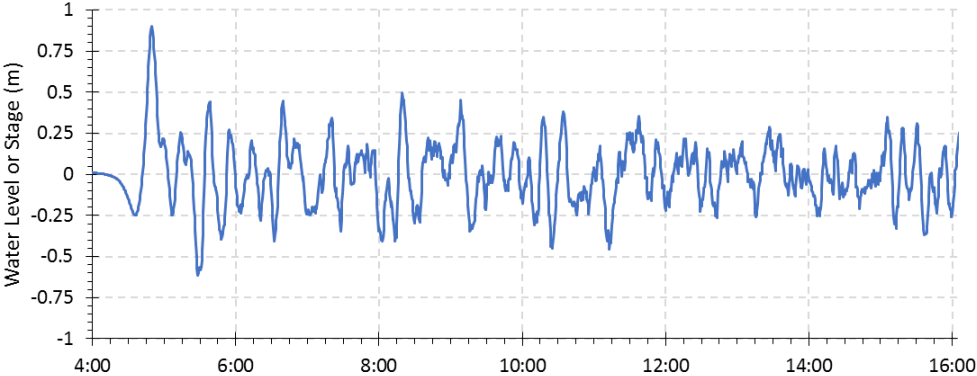


**Figure 7 - Leading wave approaching the coast for run 9 (Kermadec-Tonga, 3,000 yr ARI).**



(a) Boundary condition at defined hazard point (3000 year ARI event, depth = 1000m)



(b) Southern Bribie Island (3000 year ARI event, depth ≈ 5m)

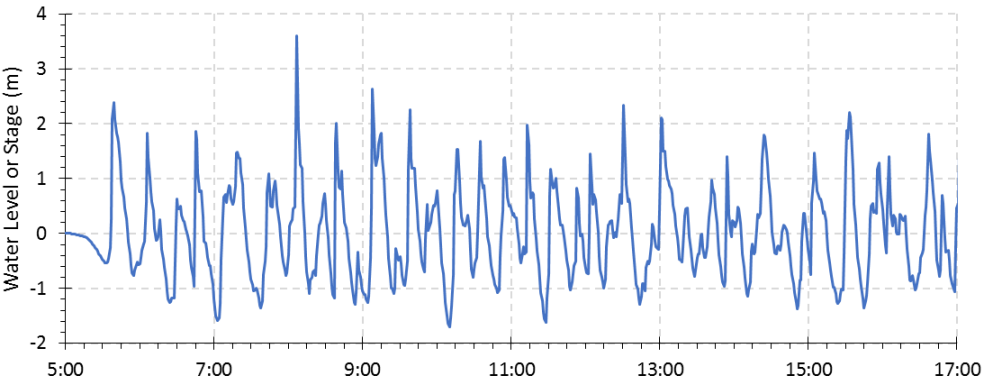


**Figure 8 - Example of tsunami time series for the 3,000 year ARI event at HAT, originating from Kermadec-Tonga.**

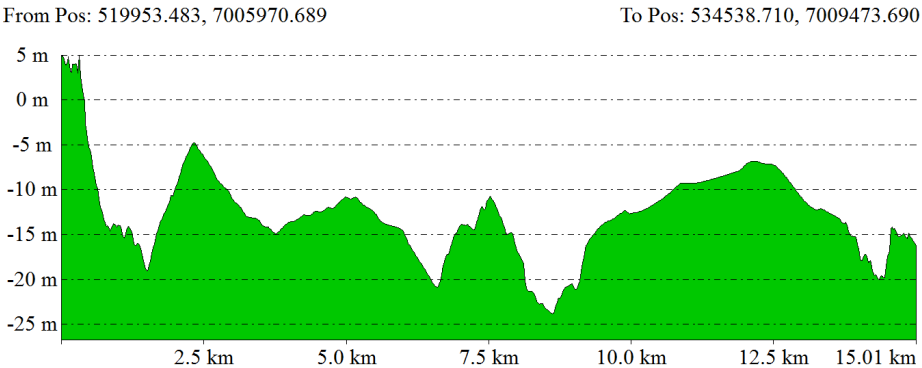


**Figure 9 - Cross section off Southern Bribie demonstrating the complex bathymetry.**

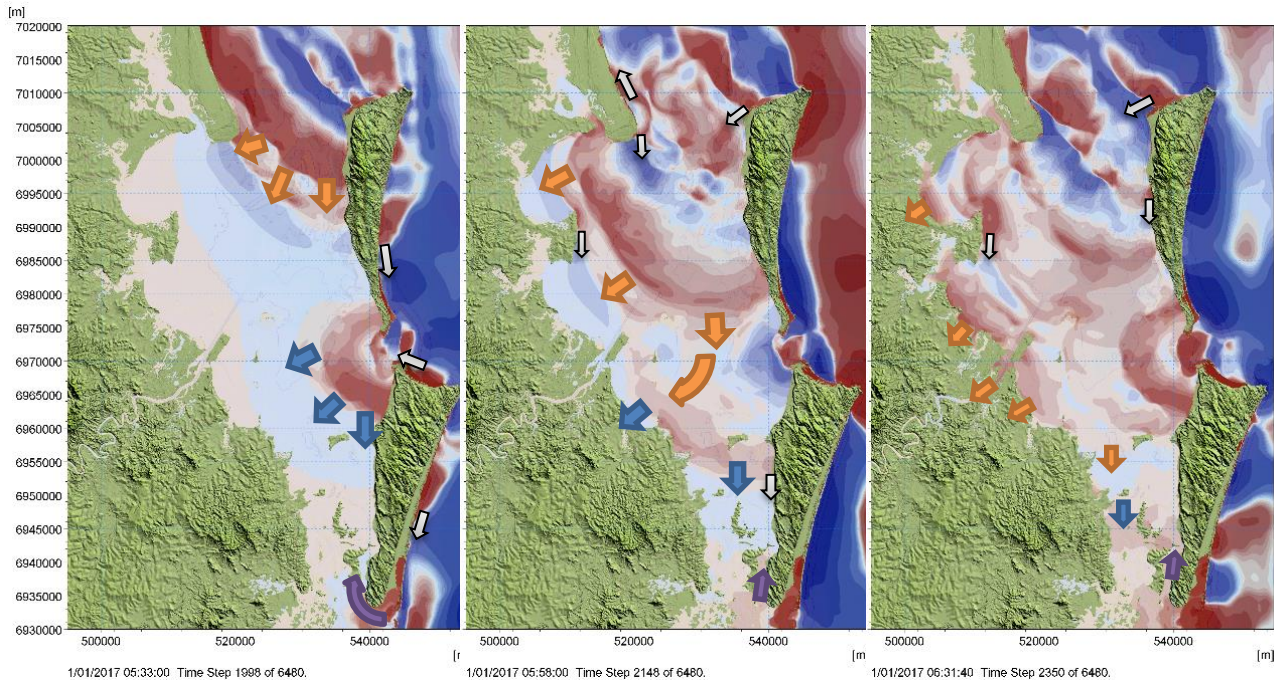


**Figure 10 - Leading wave propagation into Moreton Bay for Run 16 (Kermadec-Tonga, 10,000 yr ARI). The coloured arrow indicate wave direction from North Passage (orange), South Passage (blue), and Jumpinpin Channel (purple). Grey indicates coastal trapped waves.**

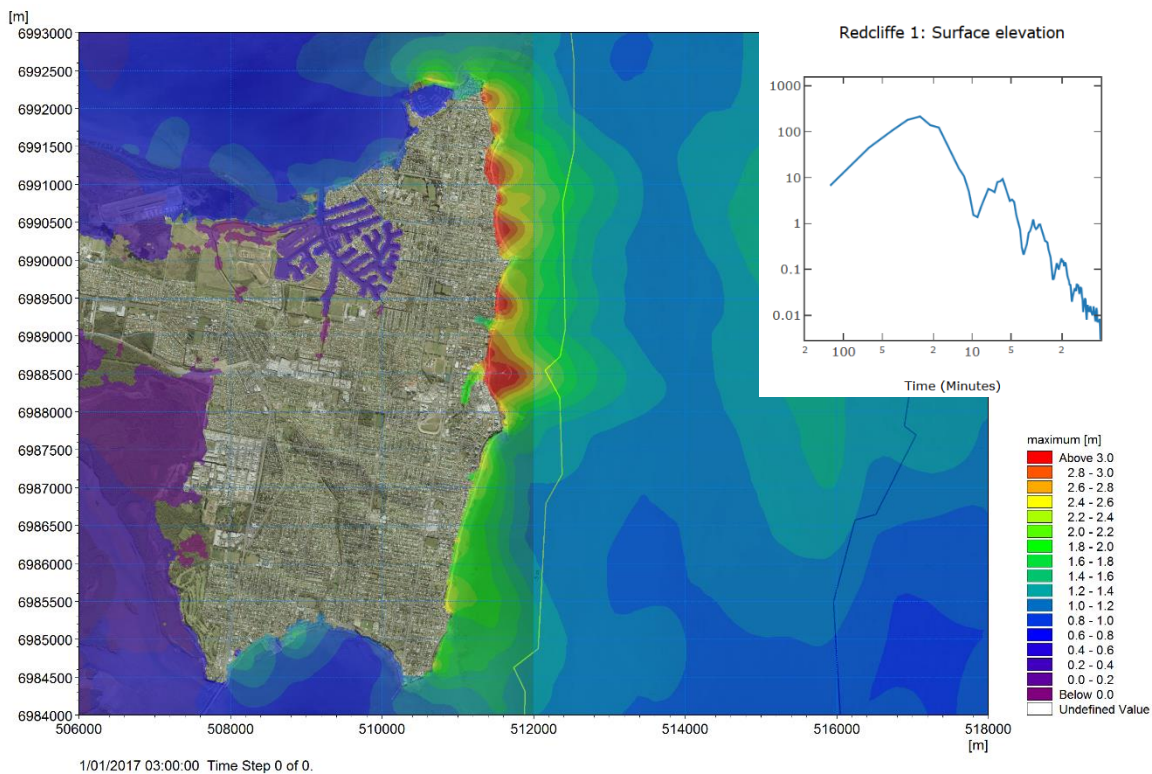


**Figure 11 - Maximum water level and spectral plot for run 16 suggesting the presence of coastal trapped edge waves along the Redcliffe Peninsula (Inset: Spectra of surface elevation for Redcliffe, logarithmically scaled (power ( $\text{cm}^2/\text{hz}^{-1}$ ) and time in minutes).**



### 8.1.2 Maximum Amplitudes

Appendix F (refer Table 7) provides maximum water level maps for the worst case scenario for each ARI at HAT, being events from the Kermadec-Tonga subduction zone. The maximum water level is relative to the still water level and so is a measure of the maximum amplitude or maximum stage. The largest wave amplitudes occur on the ocean side beaches of Stradbroke Island and Moreton Island. These islands are situated on a narrow section of the continental shelf allowing for offshore waves to propagate with little dissipation. In addition, the relatively steep seabed profile in depths less than 60 m allows substantial shoaling to occur. The islands provide protection to Moreton Bay and the complex shallow banks across the entrances (Figure 2) provide substantial dissipation of tsunami energy propagating from offshore to within Moreton Bay.

Along the ocean side of the islands, maximum water levels range from 5 m for 750 year ARI to 10 m for 10,000 year ARI (amplification factors up to 9). Within Moreton Bay wave amplitudes are generally below 1 m (amplification factors below 1), with the exception of Moreton Island, Amity Point, Redcliffe Peninsula and Scarborough, where the maximum water levels can reach 3 to 4 m (amplification factors up to 3). Amplitudes of up to 1.5 m (amplification factors up to 1) can also occur at Beachmere, Sandgate, Nudgee, Fisherman Island, Peel Island and Raby Bay. An example for run 9 is provided in Figure 12.

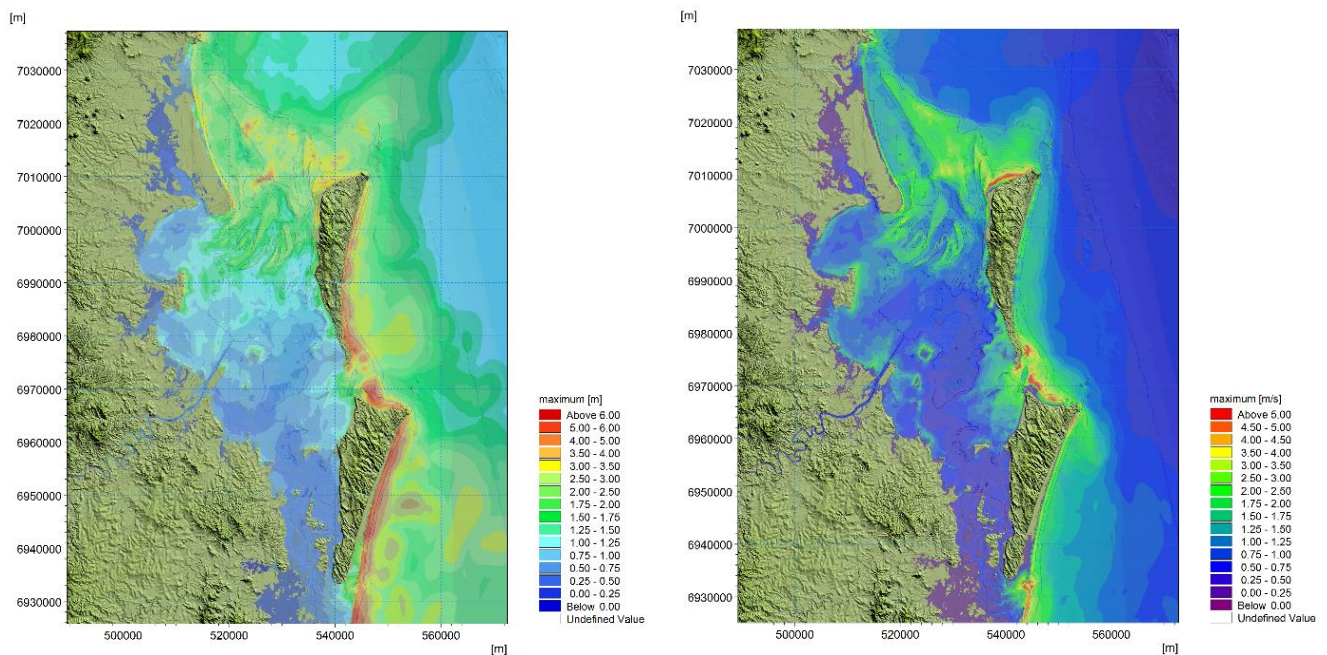


**Figure 12 - Maximum water level (left) and current speed (right) for run 9 (Kermadec-Tonga, 3,000 yr ARI).**

There are only small increases in amplitudes within the bay with increasing ARI as illustrated in Figure 13 for a coastal site at Raby Bay (the location of which is provide in Table 8). The figure also shows that there can be variation between events of the same ARI that can be of similar magnitude to that of a higher ARI.

This is further demonstrated in Table 8 for select points near the coast within the study area. The statistics represent the variation in maximum water level above SWL (a proxy for maximum amplitude) for all runs. As can be seen, the variation is larger for sites outside the bay or close to the entrances. The variation is lower on the mainland within the bay, with the exception of Redcliffe.

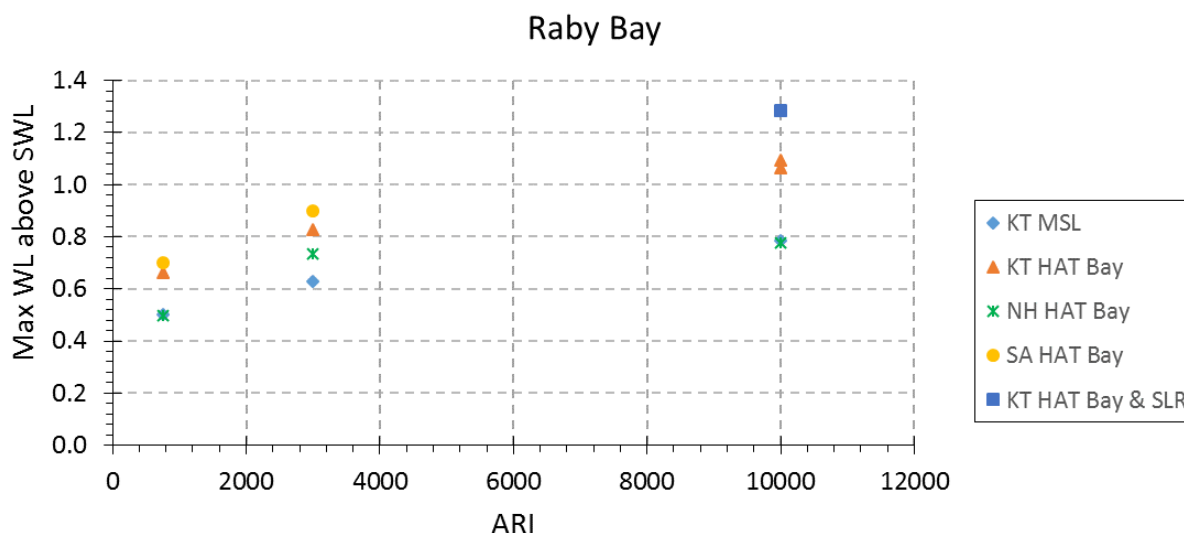


**Figure 13 - Variation in maximum water level (above SWL) at Raby Bay for various ARI, SWL and subduction zones (note that two KT events were run for the 10,000 year ARI).**

**Table 8 - Variation in maximum water level (in metres above SWL) at select sites for all runs.**

	Woorim	Beachmere	Redcliffe	Sandgate	Raby Bay	Dunwich	Bulwer	Blue Lagoon	Flinders Beach	North Stradbroke
Easting	520410	506660	511950	507580	526536	539747	536411	544430	546726	551110
Northing	7006000	6998460	6988482	6979500	6956880	6959135	7004829	7003285	6969033	6959236
Depth (m MSL)	3.6	2.5	2.9	1.6	1.7	1.5	2.4	2.5	2.6	2.4
Average	3.3	0.7	2.0	1.0	0.8	0.9	2.1	4.0	5.9	5.4
Standard Deviation	1.0	0.2	0.6	0.2	0.2	0.3	0.8	1.2	1.7	2.2
Max	4.6	1.0	3.0	1.3	1.3	1.5	3.5	5.7	9.1	9.0
Min	1.8	0.5	1.1	0.6	0.5	0.4	1.1	2.2	3.4	2.0
Max Range	2.9	0.5	1.9	0.8	0.8	1.1	2.4	3.5	5.8	6.9

The islands provide protection to Moreton Bay, and the complex shallow banks across the passages between them substantially dissipate tsunami energy propagating into Moreton Bay. Figure 14 shows typical tsunami amplification factors relative to the offshore hazard point maximum water level (Table 5) for events from the three subduction zones. There is significant shoaling on the numerous banks within the entrances followed by wave attenuation, with some focusing of energy into Redcliffe to Nudgee. There is also noticeable shoaling along the inner northern banks for events originating from both the New Hebrides and Kermadec-Tonga subduction zones. This is less obvious for the South America event, most likely due to the much longer wave periods.

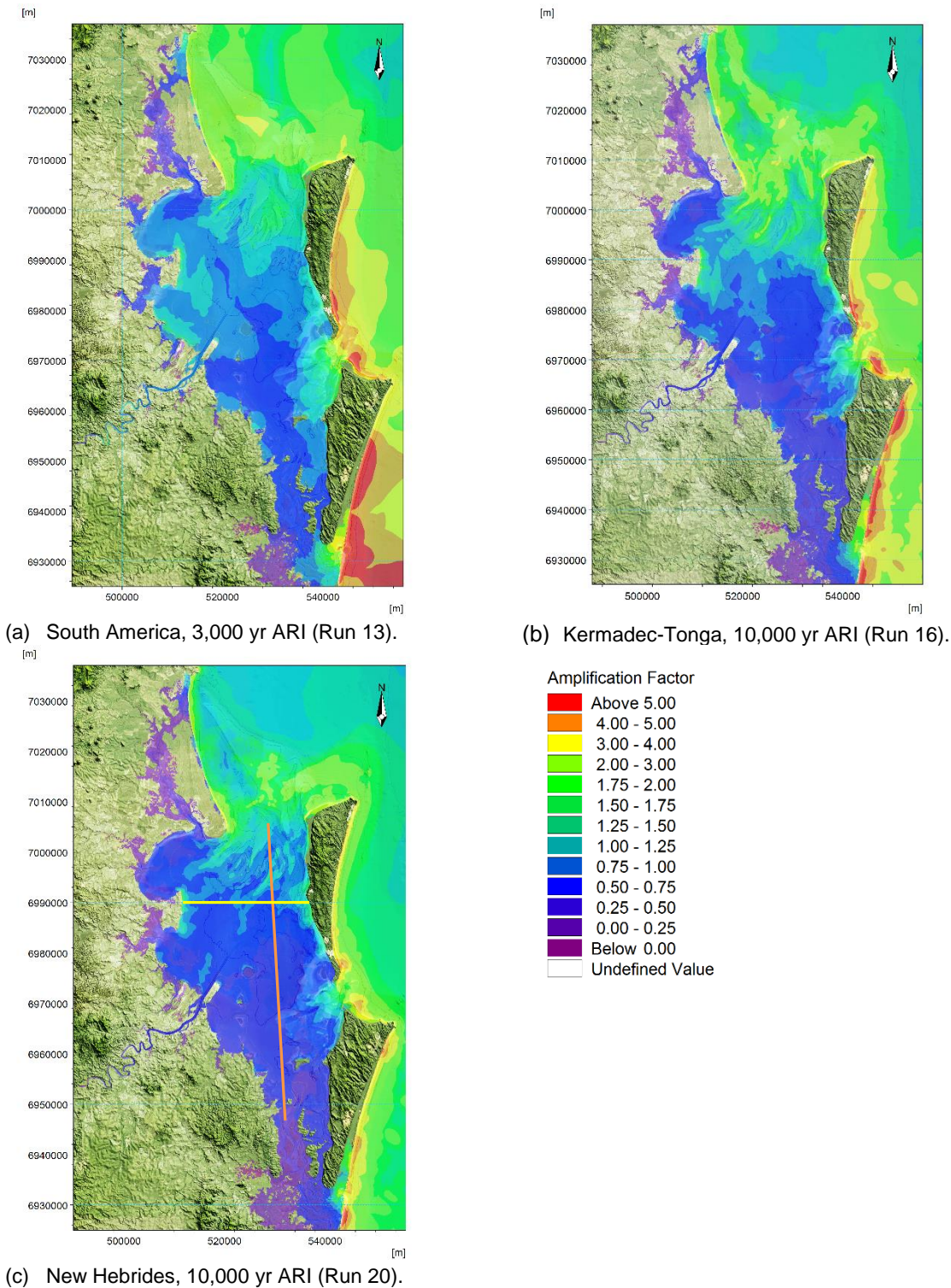


**Figure 14 – Maximum water level amplification factors (relative to offshore maximum water levels at Hazard Point).**

The dissipation across these shoals increases with increasing approaching tsunami height as illustrated in Figure 17. This is further highlighted by examining the maximum water levels along a line through the bay commencing at North Passage (Figure 15). From Figure 15 we can see that although the maximum water level at North Passage increases with ARI, the amplification factor decreases such that the water levels are relatively consistent at the southern end of the Bay.



Figure 17 also shows the wave shoaling and focusing on the inner northern banks becoming less pronounced for increasing ARI.

Along Redcliffe Peninsula and in the lee of Moreton Island, coastal trapped waves can develop, increasing the maximum water levels. This is less evident for events from South America (Figure 16).

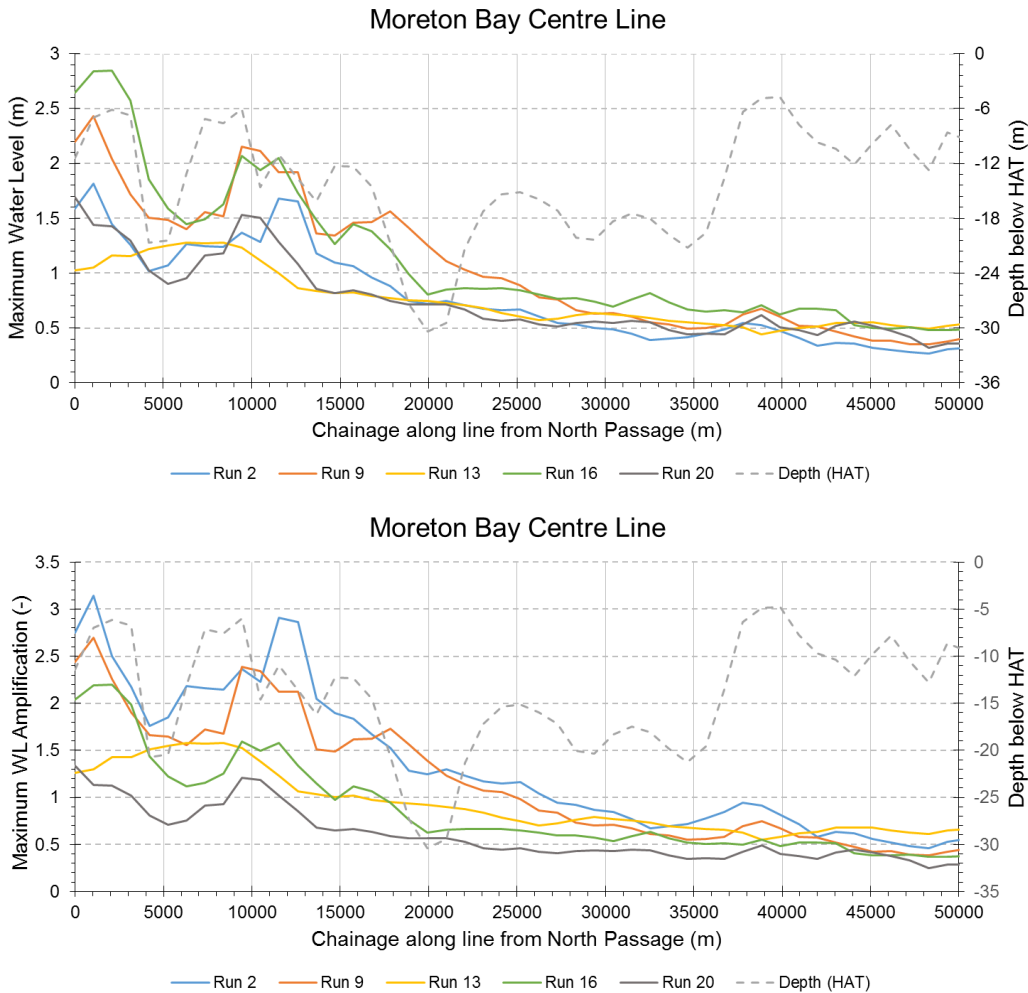


**Figure 15 - Maximum water level (top) and amplification factor for centre line through Moreton Bay (orange line in Figure 14).**

Areas identified as having a higher nearshore hazard (in terms of tsunami wave height) are in decreasing order of magnitude:

- North Stradbroke Island (ocean side);
- Moreton Island (ocean side);
- Bribie Island (ocean side);
- Amity Point;
- Bulwer;
- Redcliffe Peninsula;
- Cowan Cowan;
- Tangalooma;
- Brighton to Fisherman Island;
- Beachmere;
- Peel Island; and
- Raby Bay.

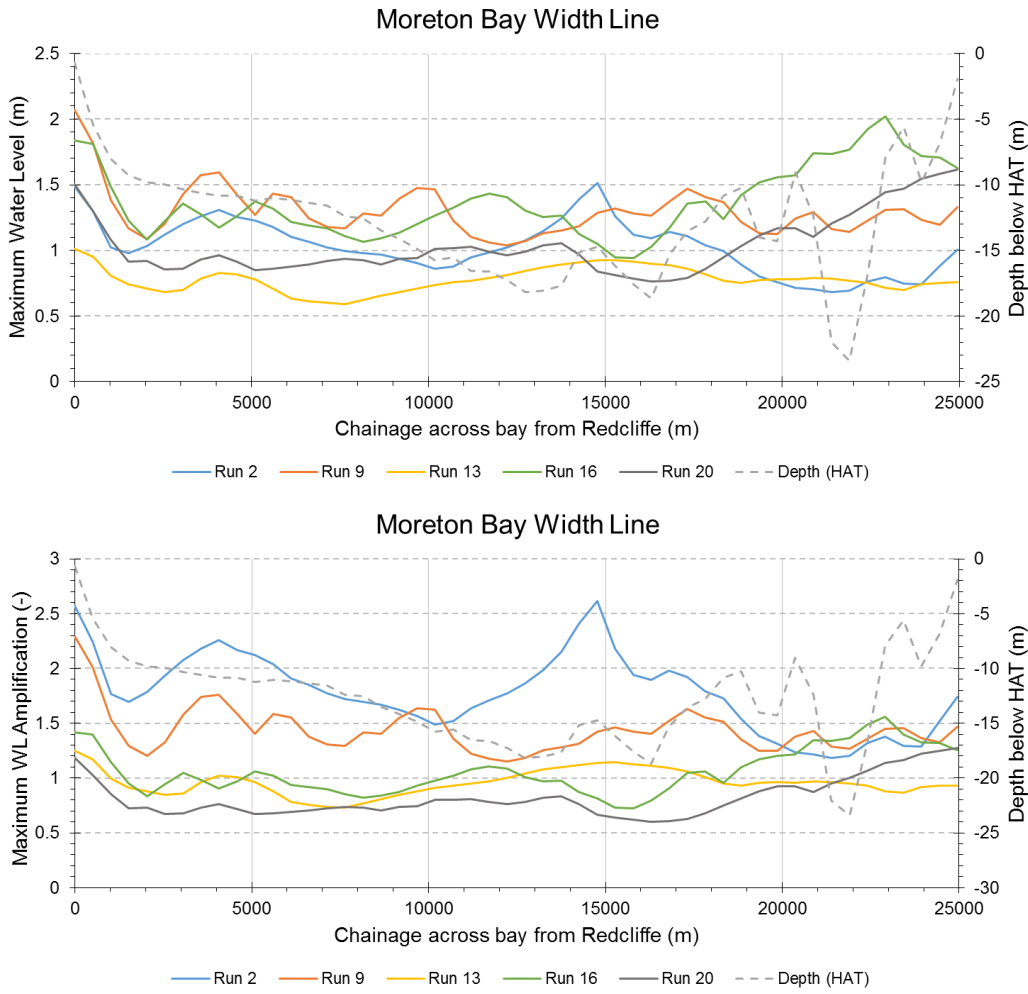


Figure 16 - Maximum water level (top) and amplification factor across the width of Moreton Bay (yellow line in Figure 14).

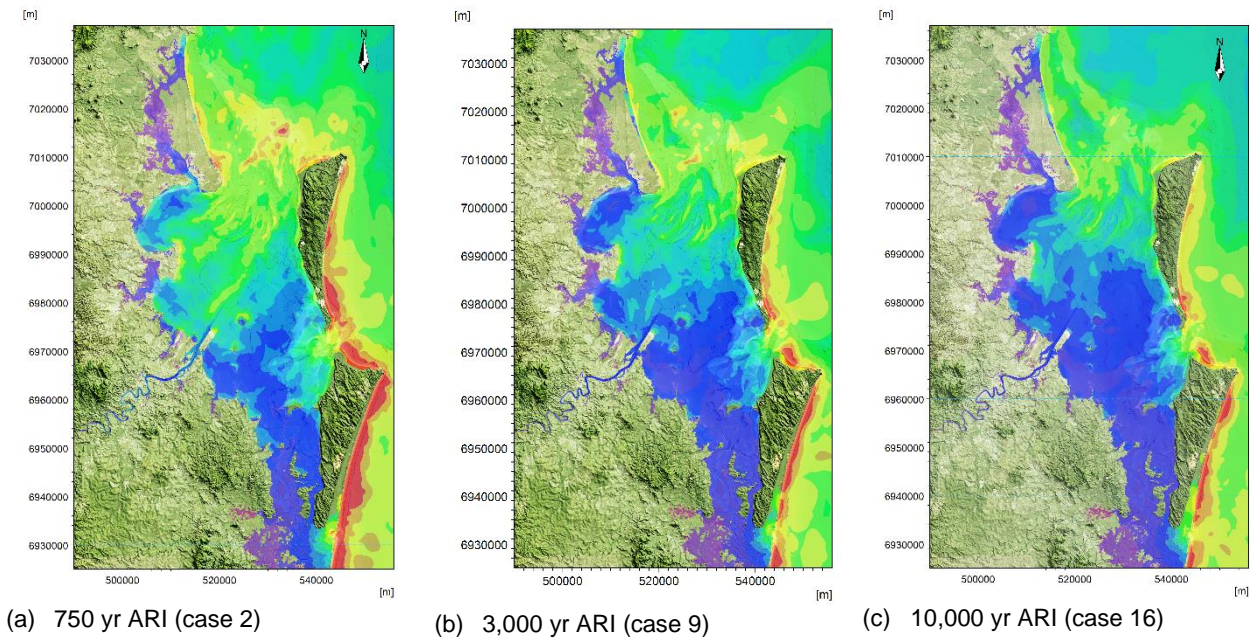


Figure 17 - Variation in amplification factor across ARI for events from Kermadec-Tonga.

### 8.1.3 Maximum Currents

Appendix F (refer Table 7) provides maps of the cell centred maximum depth-averaged current speeds for the worst case scenario of each ARI at HAT, being events from the Kermadec-Tonga subduction zone. Depth-averaged currents are greatest along the northern side of both Moreton and North Stradbroke Island, as well as the complex entrance shoals across North Passage, South Passage and Jumpinpin Channel. High current speeds are also seen along the ocean sides of North Stradbroke Island and Moreton Island. At these locations, depth averaged current speeds can reach up to 7 m/s for the 750 year ARI, and 8 m/s for the 10,000 year ARI. Current speeds within Moreton Bay and within the rivers and tributaries are lower, ranging from 0.2 m/s to 3.0 m/s for both the 750 year and 10,000 year ARI. The largest currents occurring along the Redcliffe Peninsula (refer Figure 12), and within the entrances to the canal estates at Scarborough and Raby Bay. Maximum currents within the Brisbane River are consistently in the order of 0.5 metres per second.

Areas identified as having a higher nearshore hazard (in terms of depth average current speeds) are in decreasing order of magnitude:

- Moreton Island (north side);
- North Stradbroke Island (north side);
- Jumpinpin Channel entrance;
- North Stradbroke Island (ocean side);
- Moreton Island (ocean side);
- North Passage, South Passage and Jumpinpin Channel sandbanks;
- Bribie Island (ocean side);
- Amity Point;
- Bulwer;
- Redcliffe Peninsula;
- Cowan Cowan;
- Brighton to Fisherman Island;
- St Helena Island;
- Beachmere;
- Peel Island; and
- Wellington Point.

### 8.1.4 Arrival Times

Arrival times depend on the distance the tsunami needs to travel from its generation. As tsunamis travel as shallow water waves across the open ocean, it is expected that arrival times will be similar at a given location for events from the same subduction zone, with some variations to account for differences in the particular fault zone location. Tsunamis will reach the ocean side of Moreton and North Stradbroke first, and will slow down as they enter the shallower Moreton Bay. Cape Moreton is the first location to be impacted, due to the continental shelf being the narrowest at this location.

As mentioned in Section 8.1.1, arrival times within the bay will depend on the proximity of the site of interest relative to the three main entrances. Appendix E provides the arrival times of the leading wave for a number of locations and subduction zones. The tables have been categorised into broad regions: ocean side; Moreton Bay; Brisbane River; and Pumicestone Passage. In general, events from the New Hebrides have the shortest arrival time of just over four hours after the earthquake, with events from South America arriving much later at over 18 hours.



Another way to examine this data is to consider the time differences relative to first arrival within the study region, thereby removing variations associated with trans-Pacific travel times. By calculating the travel time relative to arrival times to Cape Moreton, there is much less variation for a particular site for all events (refer Table 9), giving an indication of expected arrival times once the tsunami first reaches the coast. In general, once the tsunami reaches Cape Moreton, it will take between 1 and 1.5 hours for the tsunami to reach the mainland within the bay, and about 2.5 hours to reach Indooroopilly within the Brisbane River.

The tsunami waves generated from Kermadec-Tonga for water level HAT Bay over all ARI for a point located offshore Moreton Island (longitude 153.45° east, latitude 27.14° south) at a depth of 22.1 m is shown in Figure 18. It is seen that the leading wave is not necessarily the wave with the highest amplitude, and that larger waves can potentially arrive several hours after the initial wave.

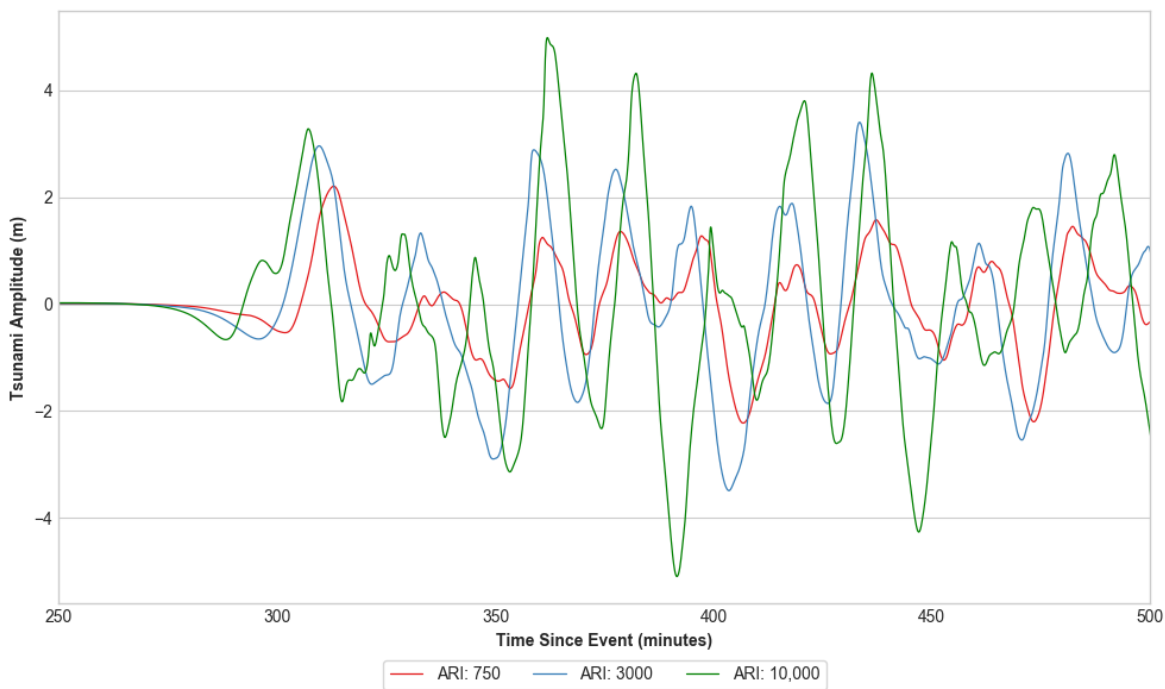


**Figure 18 - Kermadec-Tonga wave heights by ARI at a location offshore Moreton Island for tide level HAT Bay**

**Table 9 - Arrival times after arrival at Cape Moreton.**

Region	Location	Arrival time (hrs:min)	
		Average	Std Deviation
Ocean side	Amity	0:13	0:03
	Blue Lagoon Campsite	0:00	0:00
	Caloundra	0:24	0:01
	Jumpinpin	0:09	0:04
	Moffat Beach	0:22	0:01
	Shelly Beach	0:22	0:01
	South Morton Island Outside	0:04	0:01
	South Stradbroke Island	0:06	0:04
	Woorim	0:37	0:00
Moreton Bay	Beachmere	1:18	0:02
	Bongaree	1:01	0:02
	Brighton-Sandgate	1:27	0:00
	Brisbane Airport	1:23	0:01
	Bulwer	0:27	0:02
	Cleveland	1:06	0:05
	Clontarf	1:23	0:01
	Deception Bay	1:28	0:01
	Dunwich	0:49	0:07
	Goodwin Beach	1:08	0:02
	Manly	1:17	0:02
	Pine River	1:38	0:01
	Redcliffe	1:10	0:02
	Redland Bay Victoria Point	1:18	0:06
	Scarborough	1:13	0:03
	South Bay Islands	1:18	0:06
	South Morton Island Inside	0:20	0:02
	Wellington Point	1:16	0:03
Brisbane River	Port of Brisbane	1:16	0:02
	Newstead Park	1:50	0:02
	Kangaroo Point	2:00	0:02
	St Lucia	2:20	0:02
	Indooroopilly	2:37	0:02
Pumicestone Passage	Pumicestone Passage	1:05	0:03
	Donnybrook	1:47	0:05
	Golden Beach	0:32	0:00
	Pelican Waters	0:44	0:02

## 8.2 Location Specific

Below are specific comments that relate to particular areas within the study domain. Note that inundation maps provided in Appendix G (refer Table 7) are for the extreme upper-limit of the modelled scenarios for each ARI.

### 8.2.1 Southern Moreton Bay Islands

Russell Island, Karragarra Island, Lamb Island and MacLeay Island do not experience any inundation for MSL scenarios for all ARI. Inundation does occur to coastal bordering properties for HAT scenarios with little variability between ARI. The low variability in wave heights across ARI within Moreton Bay is due to the attenuation of wave energy entering the bay (see Sections 8.1.1 and 8.1.2), suggesting that increased inundation extents for HAT scenarios are mainly a result of increased water levels and not increased wave heights (this is discussed in Section 9.2).

### 8.2.2 Redland Bay and Victoria Point

Model results show minimal inundation occurring for coastal properties around Redland Bay and Victoria Point for MSL scenarios, though there is a small land hazard at the numerous marinas and boat ramps in this region experiencing some inundation. Locations such as the Redland Bay Marina, Bay Islands Vehicle Ferry jetty, and the boat ramp and carparks situated on the coast at Victoria Point Reserve show risk of inundation at MSL increasing in severity for higher ARI. This hazard is further increased for HAT scenarios with inundation occurring to coastal bordering properties for all HAT scenarios. Current speeds are generally below 0.5 m/s throughout the region but increase to 1.2 m/s around Victoria Point for HAT scenarios.

### 8.2.3 Manly to Raby Bay

From Manly to Raby Bay, model results show minimal inundation for MSL scenarios across all ARI. The more exposed Stradbroke Ferries, Old Cleveland Lighthouse, Wellington Point Recreation Reserve and Norfolk Point show some risk of inundation to the boat ramps and car parks with extents increasing for higher ARI. Within the canals at Raby Bay there appears to be small levels of inundation to these properties and some amplification of water levels within the Columbus Canal.

Inundation extents increase for HAT scenarios with little variability between ARI showing inundation occurring to coastal bordering properties and to wetlands along Tingalpa Creek and Hilliards Creek. The level of amplification within Columbus Canal, as well as within the Manly Boat Harbour, is increased for HAT scenarios and current speeds increase at these entrance ways reaching 2.5 m/s at 10,000 year ARI.

### 8.2.4 Brisbane River

Modelling results for the Brisbane River suggest small amounts of inundation to properties along the river with no variability to the inundation extents between MSL and HAT scenarios, and across all ARI. This is due to the limited increases in maximum water level with increasing ARI. Maximum tsunami amplitudes during the 750 year ARI Kermadec-Tonga event at MSL (run 1) shows very little attenuation up to St Lucia, with amplitudes ranging between 0.4 and 0.5 m. By comparison, the Kermadec-Tonga 10,000 year ARI event at HAT (run 16) produced amplitudes of  $0.6 \pm 0.05$  m within the river up to St Lucia. Current speeds in the river range from 0.3 to 0.8 m/s for all modelled water levels and ARI, with some increase at tributary entrances up to 1.2 m/s for all ARI.

It is noted that the modelling is based purely on tsunami propagation and so does not include the effect of tidal or freshwater currents.

### **8.2.5 Port of Brisbane and Brisbane Airport**

There is no significant inundation to the Port of Brisbane or Brisbane airport for MSL scenarios for all ARI. HAT scenarios do not cause an increase in inundation at the port, but do increase inundation extents to low-lying areas around the airport. Mostly this is limited to non-infrastructure areas along Kedron Brook, but there is some risk of inundation occurring to the north-eastern runway and the northern section of the Luggage Point Sewage Treatment Plant during HAT scenarios. Current speeds around the port reach 1.5 m/s for all ARI.

### **8.2.6 Brighton to Nudgee**

From Brighton to Nudgee inundation is minimal for MSL scenarios across all ARI, generally not effecting any coastal properties. Areas that show small amounts of inundation include the Queensland Cruising Yacht Club and nearby Allpass Parade, and along the Sandgate-Brighton Foreshore.

Inundation extents are significantly increased for HAT scenarios with little variability between ARI. Inundation occurs to all of Nudgee Beach, Boondall Wetlands, Nudgee Golf Course, Queensland Cruising Yacht Club, Sandgate Golf Club and properties on Palm Avenue on the golf course side, properties along Cabbage Tree Creek, numerous properties between the Sandgate–Brighton Foreshore to Beaconsfield Terrace and Brighton Terrace, Decker Park and Brighton Park. Overland current speeds at these inundated locations can exceed 1 m/s (up to 2 m/s on the foreshore) creating a land and marine hazard for events occurring on higher tide levels.

### **8.2.7 Pine River**

No inundation is seen to properties along the Pine River for MSL scenarios across all ARI within the model extent. Inundation occurs for HAT scenarios with low variability between ARI. Properties along Dohles Rocks Road, Deep Water Bend Reserve and sections of the Boral Quarry experience inundation, as well as the uninhabited Tinchi Tamba Wetlands Reserve.

### **8.2.8 Redcliffe Peninsula**

Although the eastern coastline along Redcliffe and Scarborough experience the highest waves within Moreton Bay, with wave amplitudes exceeding 2 m for all scenarios, the high topographic relief limits any significant inundation occurring for MSL scenarios. Though there is a considerable land and marine hazard in this area due to the exposure of numerous beaches on the eastern coastline to large waves and currents speeds exceeding 2.5 metres per second. The jagged and steep coastline along the eastern Redcliffe Peninsula creates a number of coastal trapped edge waves at particular harmonics that result in considerable longshore variation in maximum water levels (refer Figure 11).

Wave energy is reduced on the north-western side of Scarborough and Newport limiting inundation within the Scarborough Marina and to some properties situated in the Newport canals.

The entrance to the marina and the canals are also areas of strong currents, reaching 3 m/s within the marina entrance. Significant energy dissipation occurs at the entrance to the canal estate at Newport such that maximum water levels within the estate are limited to between 0.2 and 0.4 m for all events. Mesh resolution and interpolation schemes within the modelling software has resulted in

artificially shallow sections in these canals for the MSL cases that has limited inundation. The HAT scenarios are considered a better representation of inundation within the canal estate.

HAT scenarios increase the severity of the land and marine hazard, and cause significant inundation to properties bordering the eastern coastline, including the popular Suttons Beach Park, Settlement Cove Lagoon, and across Redcliffe War Memorial Park into Humpybong Park. Increased inundation extents occur at the Scarborough Marina, extending to properties on Reef Point Esplanade and Second Avenue, Endeavour Esplanade, and more properties within the Newport canals. Low-lying areas off Hays Inlet Conservation Park and the Nathan Road Wetlands also experience inundation such as The Village at Redcliffe and the Redcliffe Aerodrome.

Although the detached breakwater at Redcliffe may provide some protection from short period wind waves, modelling indicates that it will not provide protection from tsunamis, with both high amplitudes and strong currents developing around the structure (refer Section 9.5).

### **8.2.9 Deception Bay and Beachmere**

Inundation for Deception Bay and Beachmere is very minimal for MSL scenarios across all ARI, effecting some coastal bordering properties in Beachmere along Biggs Avenue. For HAT scenarios there is no variability between ARI for southern Deception Bay, with inundation occurring to coastal properties, particularly to properties along the culvert between the Esplanade and Captain Cook Parade and to the Palm Lake Resort. Properties bordering the Deception Bay Conservation Park and the Caboolture River are inundated, such as the Uhlmann Road Public Boat Ramp and properties at Timothy Esplanade. Along the Beachmere foreshore, inundation is seen to coastal bordering properties, with extents reaching inland to Trevor Street and Apollo Crescent in the south, and to Bishop Road in the north. Properties near to the Beachmere Conservation Park and the Palm Lake Resort Beachmere Sands are also at risk of inundation during HAT scenarios.

### **8.2.10 Godwin Beach and Sandstone Point**

For MSL scenarios across all ARI there is no inundation to properties at Sandstone Point and Godwin Beach. Some inundation does occur to coastal properties south of Godwin Beach at Bayside Drive. Inundation extents increase for HAT scenarios to more properties at Bayside Drive and to numerous properties at Godwin Beach reaching inland to Georgia Street. The high topographic elevation of the Sandstone Point coastline mitigates inundation to properties within this area. At the entrance to Pumicestone Passage, the Spinnaker Sound Marina and surrounding properties, such as the Silver Shores Caravan Park, are inundated during HAT scenarios and current speeds through the marina entrance exceed 1.2 metre per second.

### **8.2.11 Pumicestone Passage (South)**

There is no inundation to properties along Pumicestone Passage for MSL scenarios for all ARI. Inundation occurs for HAT scenarios to properties along Pumicestone Passage at Bongaree, with extents reaching inland to Fifth Avenue and Bestman Avenue. Inundation also occurs to properties along Sylvan Beach Esplanade at Bellara, Solander Esplanade at Banksia Beach, properties within the canal areas, Toorbull, Meldale, and Donnybrook. Current speeds are generally below 0.6 m/s in Pumicestone Passage with increases at tributary and canal entrances up to 2 metres per second. Strong currents of up to 5 m/s develop at the northern entrance.

### 8.2.12 Bribie Island

Bribie Island is a popular recreational beach and camping area. The ocean side of Bribie Island has greater exposure to tsunami waves (maximum water levels of up to 5 m) that create both a land and marine hazard, with the marine hazard being greatest in the vicinity of Woorim. When considering MSL scenarios, inundation is limited mostly to the beach for the 750 year ARI. Inundation extents increase for higher ARI with breaching of some gaps between coastal dunes, and complete inundation of the low-lying northern end of Bribie Island for 3,000 and 10,000 year ARI scenarios. At Woorim, inundation is seen for coastal bordering properties at 3,000 year ARI, with inundation extents increasing to North Street for 10,000 year ARI.

HAT scenarios show complete inundation of north Bribie Island and to some coastal bordering properties in Woorim for ARI 750 years. The inundation extent significantly increases with increasing ARI, inundating beyond Arcadia Avenue, and Sixth Avenue at Woorim Beach, for the 10,000 year ARI. Current speeds exceeding 3 m/s for 750 year ARI and 5.5 m/s for 10,000 year ARI occur along the beach at Woorim for both MSL and HAT scenarios.

As discussed in Section 8.2.11, the hazard is greatly diminished for communities on the southern Pumicestone Passage side of Bribie (maximum water levels below 0.8 m), with minimal inundation.

In addition to the short-term impacts arising during the event, the complete inundation and overtopping of the northern Bribie may introduce long term morphological changes that could impact on coastal processes near Pelican Waters and Golden Beach.

### 8.2.13 Stradbroke Island

The ocean sides of North and South Stradbroke Island have the greatest exposure to tsunami waves ranging from 3 to 10 m, and being popular recreational areas create a land and marine hazard due to high wave heights and strong current speeds (see Section 8.1.2). Coastal dunes provide protection limiting the inundation extent beyond the beach. This is most effective on the northern stretch of the east beach on North Stradbroke where foredune elevations exceed 12 m AHD fronting Pleistocene and Holocene sand dune ridges reaching 200 m in height.

Low lying areas at the northern and southern ends of North Stradbroke Island, and the northern end of South Stradbroke Island are particularly susceptible to inundation. Foredune heights in these areas are typically below 6 m AHD, falling below 4 m AHD at locations between Amity Point and Point Lookout. Communities and camp sites within these low lying areas are susceptible to inundation for even the lower ARI and MSL events, especially the small community at Flinders Beach. At 750 year ARI, run-up levels reach 4.5 m, causing inundation to properties and campsites at Flinders Beach, and to properties along Dickson Way at Point Lookout. Run-up levels increase for higher ARI scenarios, reaching 6 m AHD between Amity Point and Point Lookout, and up to 9 m on the eastern beaches for the 10,000 year ARI scenario. At these ARI, substantial inundation of the coastline adjoining Jumpinpin Channel occurs (Figure 19), as well as complete inundation of the Flinders Beach community (Figure 20).

Current speeds between Point Lookout and Amity Point exceed 5 m/s in the nearshore and 1 m/s overland for 750 year ARI, increasing to 8 m/s and 3 m/s respectively for 10,000 year ARI. Inundation and run-up levels are higher for HAT scenarios at all areas described in MSL scenarios, increasing in severity for higher ARI.

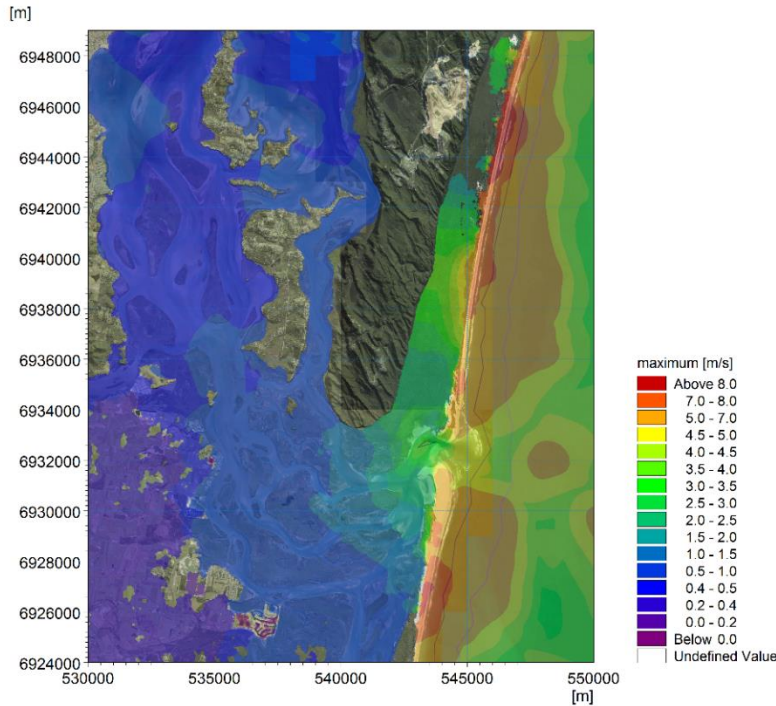


**Figure 19 - Inundation of southern Stradbroke Island during run 16 (Kermadec-Tonga, 10,000 year ARI).**

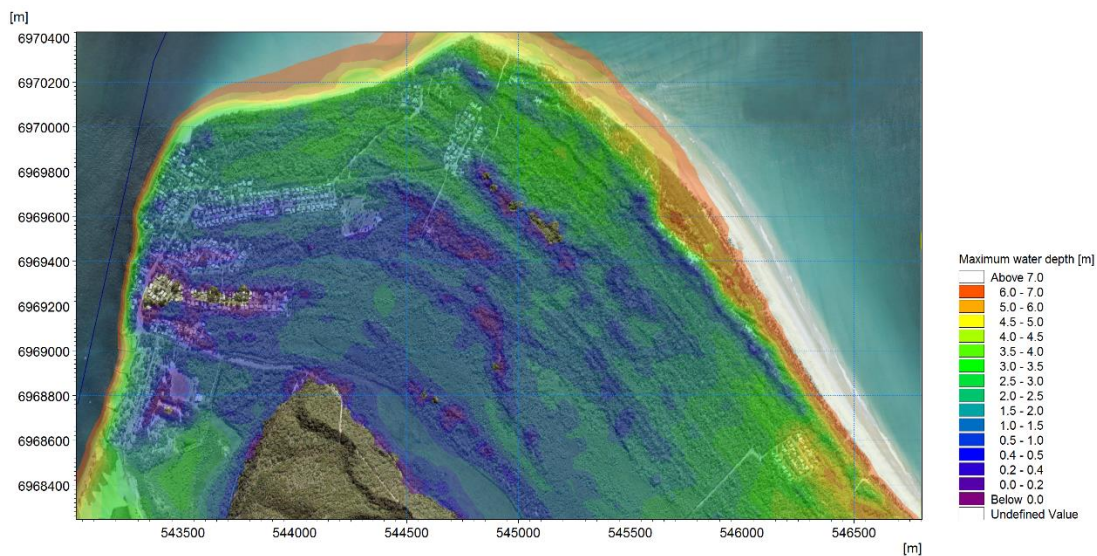


**Figure 20 - Inundation extent and water depths at Amity Point and Flinders Beach during run 16 (Kermadec-Tonga 10,000 year ARI at HAT Bay).**

The Moreton Bay side of North Stradbroke Island is exposed to much less wave energy with no inundation occurring at Dunwich for MSL scenarios across all ARI. Inundation does occur at One Mile Jetty, Bradbury’s Beach Camping Ground and properties along Flinders Avenue for HAT scenarios, with inundation extents increasing for higher ARI.

### 8.2.14 Moreton Island

Similar to North Stradbroke Island, the ocean side of Moreton Island has a greater exposure to tsunami waves creating both a land and marine hazard that may affect recreational areas for camping and beach 4WD activity. Coastal foredunes around 7 m AHD are backed by heavily vegetated Pleistocene and Holocene sand dune ridges exceeding 200 m AHD, providing protection



from inundation. Low-lying areas on the northern and southern ends of the island are more susceptible, experiencing inundation for MSL scenarios with extents increasing for higher ARI. HAT scenarios further increase these inundation extents.

Many camp sites are located in areas protected by high dune elevations, but those close to the beach or in areas of low dune elevation, are at risk with inundation to the beach for MSL and HAT scenarios increasing for higher ARI. At the Blue Lagoon Sunrover Campsite, dunes provide adequate protection for 750 year ARI scenarios but are exceeded for 10,000 year ARI MSL and HAT scenarios, inundating the campsite with run-up levels exceeding 10 m AHD. Current speeds range from 1 m/s at 750 year ARI up to 3 m/s at 10,000 year ARI on the beach fronting the campsite for MSL and HAT scenarios.

Communities on Moreton Island located on the bay side are protected due to the attenuation of waves propagating into the bay (see Section 0) and experience much lower maximum water levels and current speeds. No inundation occurs at Bulwer for MSL scenarios across all ARI, with small amounts of inundation to coastal bordering properties at Cowan Cowan and Tangalooma Resort. Inundation extents are increased for HAT scenarios, with little variability between ARI, also causing inundation to properties along the Strand at Bulwer. Current speeds range from 1 m/s at 750 year ARI to 3 m/s at 10,000 year ARI in the nearshore at these locations for both MSL and HAT scenarios.

### 8.3 Climate Change (Sea Level Rise)

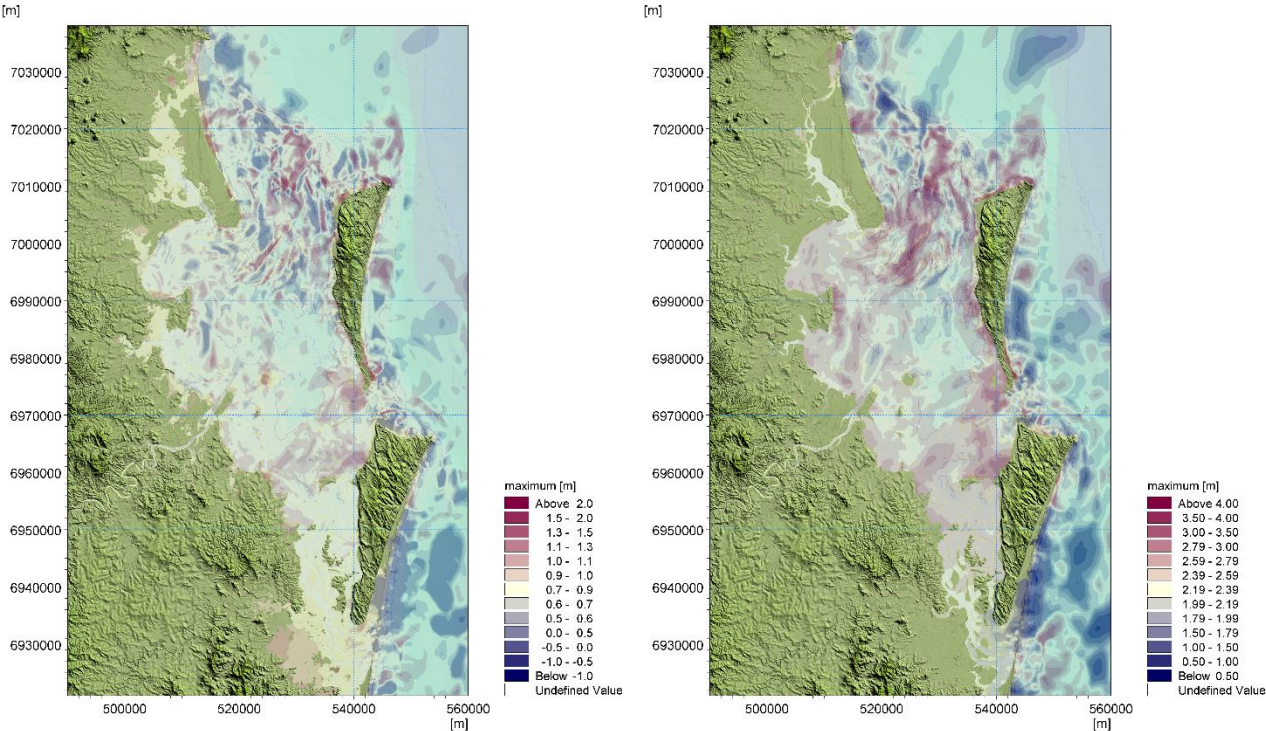
Although expected climate change outcomes relate to meteorological changes, the increased water level due to sea level rise (SLR) may increase tsunami amplitudes (see Section 9.2), and will make low-lying areas more susceptible to inundation.

To provide an indication of potential impacts associated with SLR, runs 16 and 17 representing the Kermadec-Tonga 10,000 year ARI event were repeated with a water level increase of 0.8 m (Table 5). Figure 21 shows the difference in maximum water elevation for run 18 (Bay HAT and SLR) compared to run 16 (Bay HAT) and run 15 (MSL). The scale bars are centred on the change in still water level (SLR for case 1 and SLR + HAT Bay for case 2) with a tolerance of  $\pm 0.1$  m (yellow). Red represents an increase in maximum water level and blue represents a decrease.

Outside the bay, there is a spread of increases and decreases, most likely contributable to changes in reflection patterns. Within the bay, increases in still water level equate to increased depth within the entrances and therefore less wave dissipation, resulting in more energy entering the bay. In general, the increases in maximum water level are mostly within 0.1 to 0.2 m for case 1, and 0.2 to 0.4 m for case 2. These increases are small in comparison to the change in still water level (0.8 m for case 1 and 2.29 m for case 2). This result is based on a static bathymetry. In reality, the sandbanks within these entrances will evolve over time so this result should be considered as conservative.

Figure 22 shows the increase in inundation extent for case 18 over case 16 (that is, an increase in SLR only). SLR does significantly increase the inundation occurring throughout some of the study region. Notably this is mostly limited to uninhabited low-lying areas off tributaries or within wetlands, though there are locations which experience greater levels of inundation than the extents identified in Section 8.2. These include Hemmant, Shorncliffe, Brighton, estates between Beachmere and Godwin Beach, Bongaree, Bellara and Dunwich. More detailed inundation maps are provided in Appendix I (refer Table 7).





(a) Difference Plot of maximum water level (Run 18 – Run 16)      (b) Difference Plot of maximum water level (Run 18 – Run 15)

**Figure 21 - Influence of SLR on maximum water level relative to HAT (left) and MSL (right) case for Kermadec-Tonga, 10,000 year ARI.**

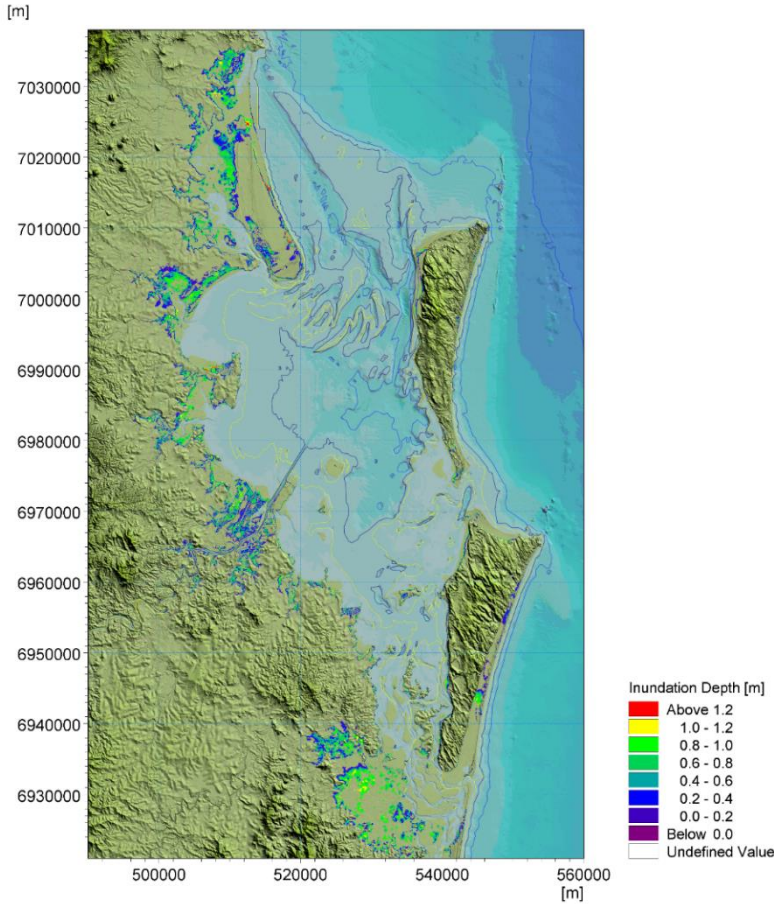


**Figure 22 - Increase of inundation extent for SLR condition (run 18 relative to run 16).**

## 9 Discussion

### 9.1 Updated PTHA – Comparison at Golden Beach

The original PTHA was developed in 2010. Over the past eight years, the science and knowledge regarding tsunami generation and propagation has developed rapidly. The occurrence of more events over this period has provided more insight and skill into modelling these hazards. The revised PTHA has drawn upon this knowledge to provide the best present understanding of tsunami hazard near the Australian coast.

Overlap in model domain between this study and the previous Stage 2 Sunshine Coast study (Boswood, 2013b) provides an opportunity to access differences in inundation extents arising from the revised PTHA boundary conditions at Golden Beach. Stage 2 modelled scenarios from the New Hebrides subduction zone using a HAT level of 1.18 m above MSL. This can be compared with scenarios within this study also from New Hebrides at the HAT ocean tide level of 1.15 m above MSL. Both studies considered the same ARI. Table 10 summarises similar events from both studies.

**Table 10 - Comparable model scenarios between Stage 2 study and Stage 3 study**

ARI	Stage 2			Stage 3		
	PTHA Event ID (previous version)	Max Amplitude (m)	Earthquake Magnitude (Mw)	Revised PTHA Event ID	Max Amplitude (m)	Earthquake Magnitude (Mw)
750	49501	0.48	8.3	3475	0.56	8.9
3,000	49907	0.94	8.8	9774	0.935	9.0
10,000	50127	1.53	9.2	9743	1.267	9.0

Model results show inundation levels at Golden Beach to be very similar between Stage 2 and Stage 3. The extent of inundation and the areas which show greater inundation are the same between both studies, and inundation extents increase with ARI at similar rates. The revised PTHA suggests an increase in the tsunami hazard from the Kermadec-Tonga subduction zone (see Section 7) which is included in this study. Modelled scenarios from Kermadec-Tonga result in greater inundation compared to scenarios from New Hebrides for the same ARI level. These results suggest that with the increase in tsunami hazard for the revised PTHA, re-evaluation of the Stage 2 Sunshine Coast study (Boswood, 2013b) may be warranted.

It is noted that this study relied on a draft version of the revised PTHA as of February 2018. Any changes to the hazard assessment in the final release of the PTHA may influence the above discussion.

### 9.2 Stage of Tide and Inundation

Modelling undertaken of three still water levels (SWL) allows us to consider the influence of the stage of tide on tsunami inundation for the study area. The distribution of maximum water levels of the same 10,000 year Kermadec-Tonga scenario over the different model SWL is shown in Figure 23. The histograms show a count of the maximum water level that occurs during the modelled scenario for each respective mesh element in the model. Mesh elements which did not experience any deviation in water level (threshold level below 0.01 m) are not included in each respective plot, resulting in a difference in the total amount of elements included in each histogram. Overland

elements that are not above this threshold can be considered to have not been flooded indicating no inundation.

For lower maximum water levels below 1.5 m (that is, below the maximum tide range) there is a noticeable difference in the number of flooded model elements at these levels between MSL and HAT. For values greater than 1.5 m the distribution across all the tide levels are similar. This is also seen in the spatial distribution of maximum water level for these scenarios (refer to the separate GIS Database), which show similar levels outside of Moreton Bay across all SWL, and increased inundation within Moreton Bay for higher water levels. Increases in SWL was also considered in the SLR example (Section 8.3), showing only small increases in wave amplitude within the bay compared to the large variations in SWL.

To further illustrate this point, Figure 24 shows a comparison of wave amplitudes at different SWL for a location offshore of Moreton Island (same as Figure 18) and inside Moreton Bay near South West Spit on the Central Banks (longitude 153.24° east, latitude 27.18° south, depth of 10.8 metres). The effect of the stage of tide on wave height is less noticeable outside of Moreton Bay. Within the bay there is greater variability in wave phase and wave heights, such that the tsunami at MSL has a phase lag and slightly reduced amplitude due to the reduced depths. Therefore, it can be concluded that the main factor contributing to increases in inundation is the stage of tide (1.49 m difference between MSL and HAT in the bay), contributing to increased tsunami inundation in low-lying areas. Although the tsunami amplitude is relatively lower in Moreton Bay, the higher water level slightly increases tsunami amplitudes within the bay, which will also contribute to the increased inundation.

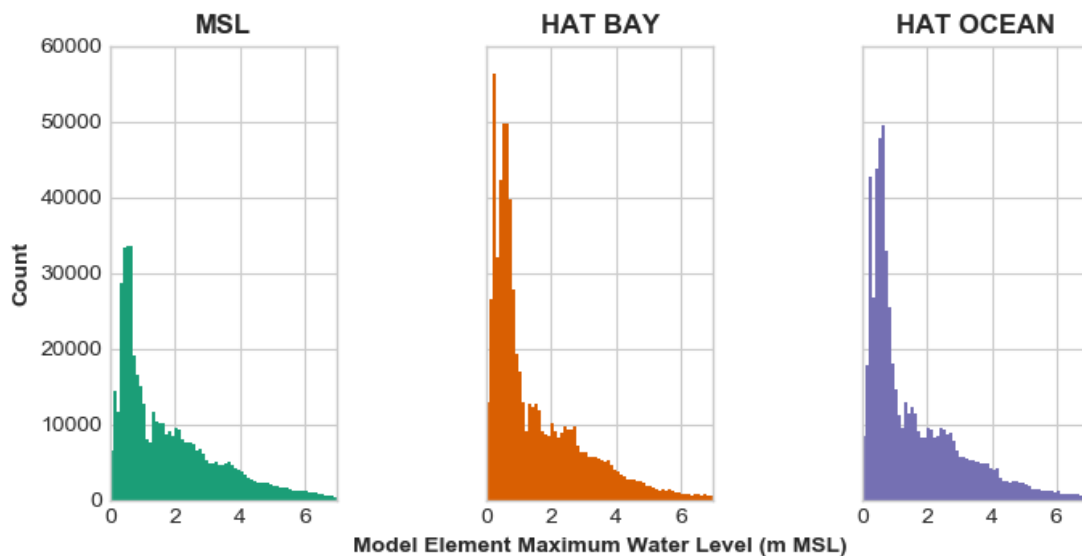


**Figure 23 - Kermadec-Tonga 10,000 year ARI (Event ID 34890) modelled maximum water levels by stage of tide**

Mofjeld (2007) examined the influence of tides on the maximum water level by superimposing theoretical tsunami wave time series based on an exponential decay coefficient of 2 days over a duration of five days (based on measurements within the Pacific Ocean), on tides typical for Oregon, USA. The results showed that for small tsunami amplitudes, the maximum water levels tend to occur near mean higher high water with little spread. As the tsunami increases, the maximum water level tends towards a limit of MSL plus the tsunami amplitude (for tsunami amplitude > tide range). Although the principle of an exponentially decaying tsunami time series may be applicable in the open Pacific Ocean, the nearshore tsunami time series in this study is

complicated by interaction of reflections, shelf trapped waves and coastal trapped waves. The approach undertaken in this study is considered to provide a conservative result.

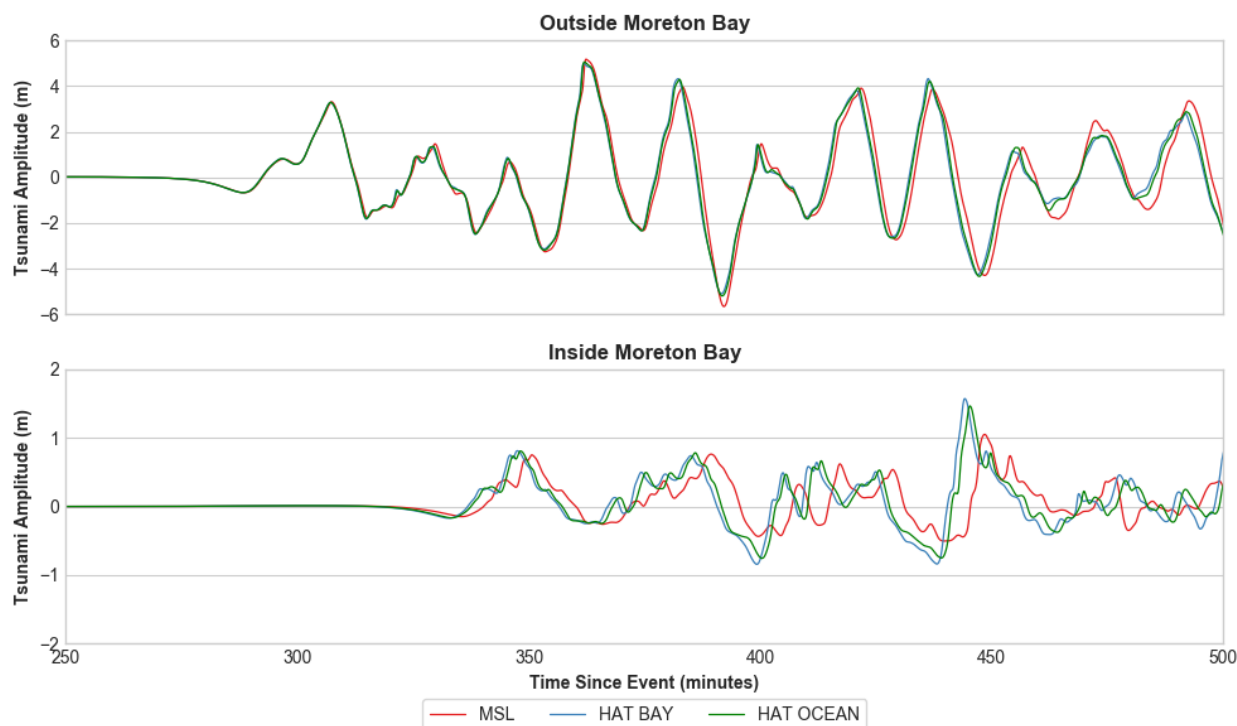


**Figure 24 - Influence of stage of tide on tsunami amplitude for Kermadec-Tonga 10,000 year ARI (Event ID 34890)**

### 9.3 Offshore Boundary

The location of the offshore boundary has been based on the output locations from the draft revised PTHA. Stages 1 (Boswood, 2013a) and 2 (Boswood, 2013b) relied on the original TsuDAT product provided by GA (refer Section 5.2.3), which provided stage and momentum time series at the 100 m depth contour at MSL. The revised PTHA provides more flexibility of event output locations. For the current study, the 1000 m depth contour was considered given the close proximity of the continental shelf to Cape Moreton.

Examination of model results has shown the presence of shelf trapped waves, an example of which is provided in Figure A. 9 for run 9. In that example, a transient wave generated during a modelled 3,000 year ARI tsunami event is initially reflected off the Great Sandy National Park coast. As it nears the continental shelf, it is refracted back towards the coast to impact Bribie Island, some 120 km south of the initial reflection, producing the maximum water level at Bribie for that event.

Although the 1000 m depth contour allowed for the development of this phenomena, issues arose with downscaling as the finer model mesh created high irregularities along the boundary that were a source of instability and iterative adjustment. These irregularities are due to the numerous canyons that incise the continental slope, as shown in Figure 25.

To assure that these processes can develop within the model domain and to limit numerical instabilities, it is suggested that the offshore boundary for tsunami modelling within Queensland is situated offshore of the continental shelf. Similarly, the lateral boundaries should be of sufficient



distance away from the model domain to allow the development of shelf and coastal trapped transient waves.

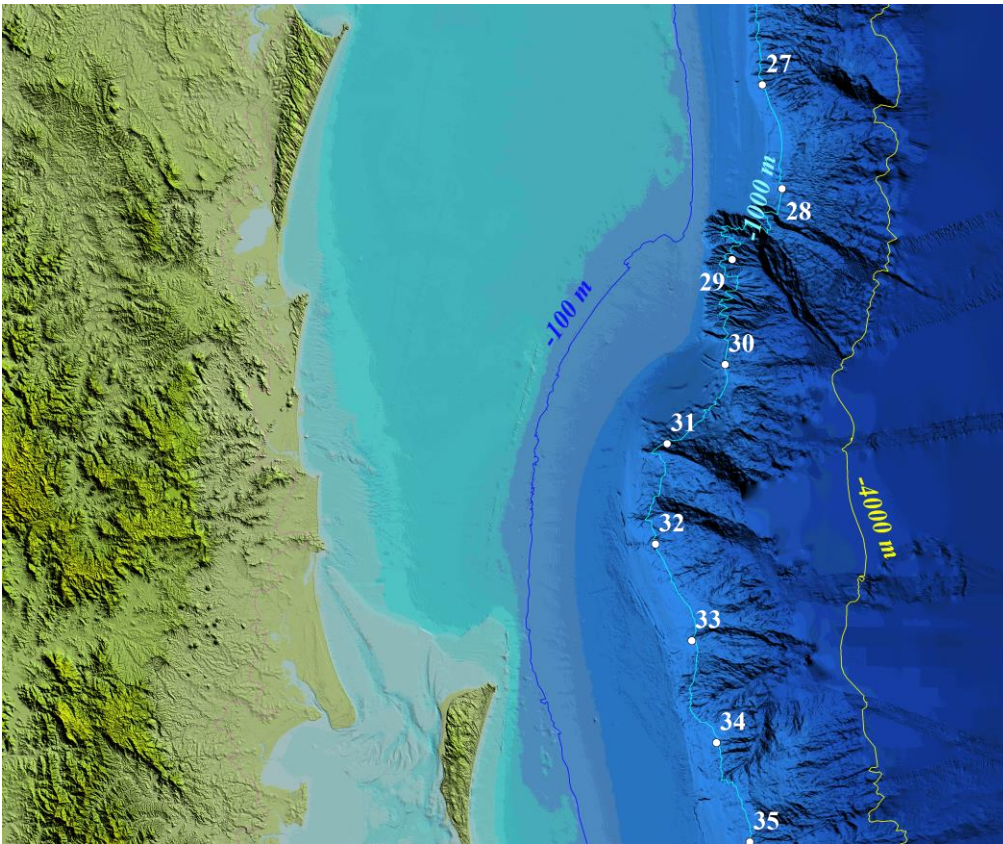


**Figure 25 - Continental shelf between Moreton Island and the Great Sandy National Park (dots represent PTHA points).**

## 9.4 Undular Bores (Short Waves)

During the 2004 Indian Ocean tsunami, media reports showed what appeared to be a series of waves approaching the coast of Thailand (refer to Figure A. 16). Research has shown that these shorter period waves are in fact riding on top of the underlying tsunami, and are produced when the front face of the tsunami wave becomes steep enough to disintegrate into an undular bore with short and steep transient waves of periods in the order of 10 to 15 seconds. Madsen et al. (2008) were able to reproduce this phenomena with the aid of a high order Boussinesq numerical model with a grid spacing of 10 metres. They also concluded that although these transient waves will have an impact on coastal structures, the run-up and inundation that occurs is a result of the underlying longer period tsunami.

The computational demand of such models precludes their use on a large scale. However, closer inspection of the time and line series from the modelled water levels can give an indication based on the steepness of the front face of the wave.

Figure 26 provides snapshots (in elapsed time) of tsunami wave profiles along a line through North Passage and offshore of Redcliffe. The profiles are complicated by the interaction of incident and reflected waves but as can be seen, the waves are asymmetric with steep front faces. It is possible that these conditions are conducive to the formation of undular bores.

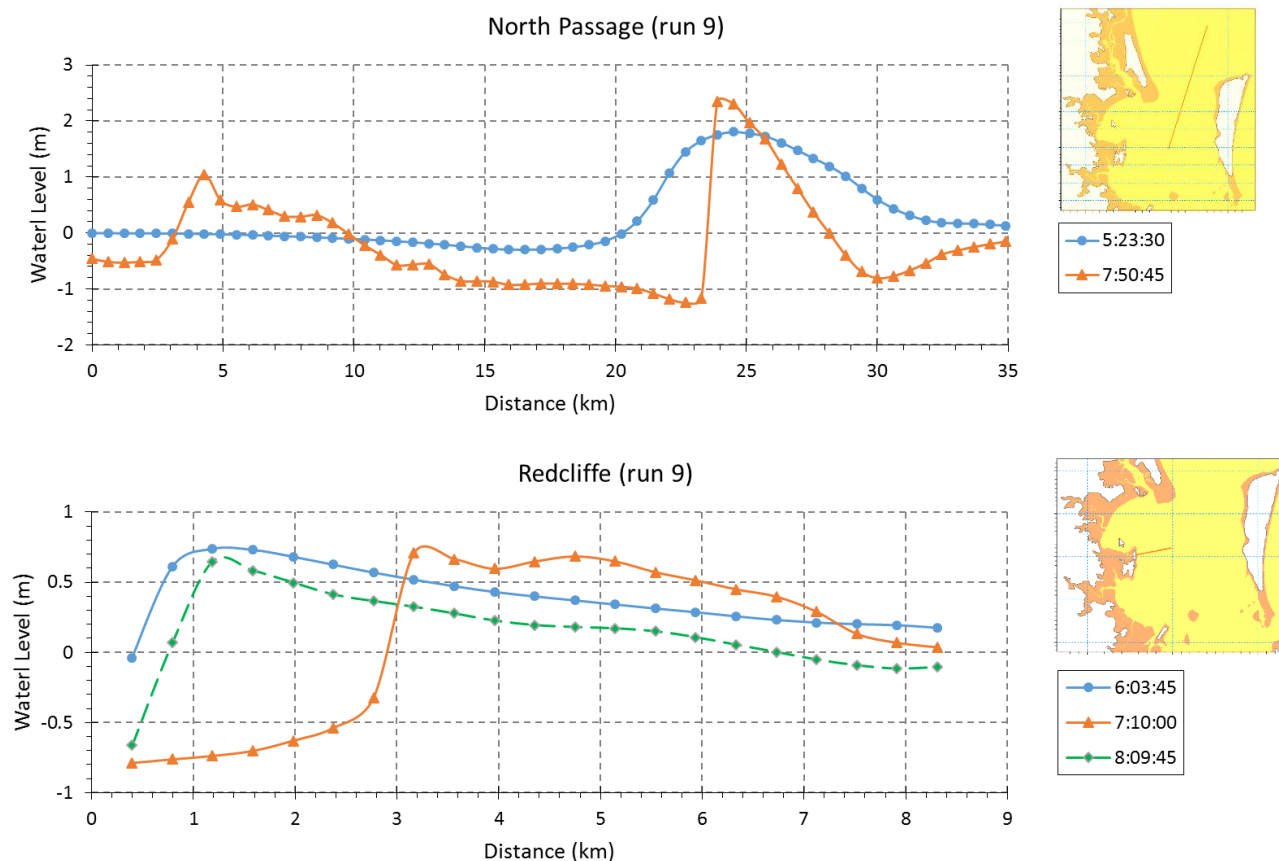


**Figure 26 - Tsunami wave profile snapshots during run 9 through North Passage (top) and off Redcliffe (bottom).**

## 9.5 Sub-grid Structures (Redcliffe Detached Breakwater Example)

Modelling is a balance between mesh resolution and computation times. Reducing the spatial distance between nodes by half will introduce four times more mesh elements and can significantly increase computational times. Coastal management structures such as detached breakwaters are designed to provide shelter from short period waves in their lee, thereby providing protection to vessels or the coastline. Murata et al. (2010) advise that small scale features such as detached breakwaters do not provide protection from tsunamis given their size is small relative to the tsunami wavelength, and their crests are typically too low to block tsunamis. Therefore their impact on inundation extents is limited. Mesh resolution within the study area was selected to replicate tsunami propagation characteristics to the coast, and inundation at a typical property block scale.

Mesh resolution off the coast of Redcliffe Peninsular is typically about 100 m, reducing to 30 m on the coastline. Therefore subscale size features such as the detached breakwater at Redcliffe Pier are not fully resolved. To test the assumption that sub-grid structures do not provide protection from tsunamis, an additional model run was undertaken for run 16 with a further refinement of the mesh in the vicinity of the Redcliffe Pier down to 20 to 30 m. As can be seen in Figure 27 and Figure 28, the detached breakwater provides little protection from tsunamis. In fact, the modelling indicates higher tsunami amplitudes and currents in the lee of the structure. This may be a factor of the structure's scale being much smaller than the tsunami wavelengths, or the presence of coastal trapped waves that are travelling parallel to the coast rather than onshore. However, the overall



inundation and maximum water levels at the coast are similar in both runs, supporting the use of the original mesh.

In any case, the modelling indicates that the offshore breakwaters at Redcliffe Pier pose a marine hazard and should be avoided during an event.

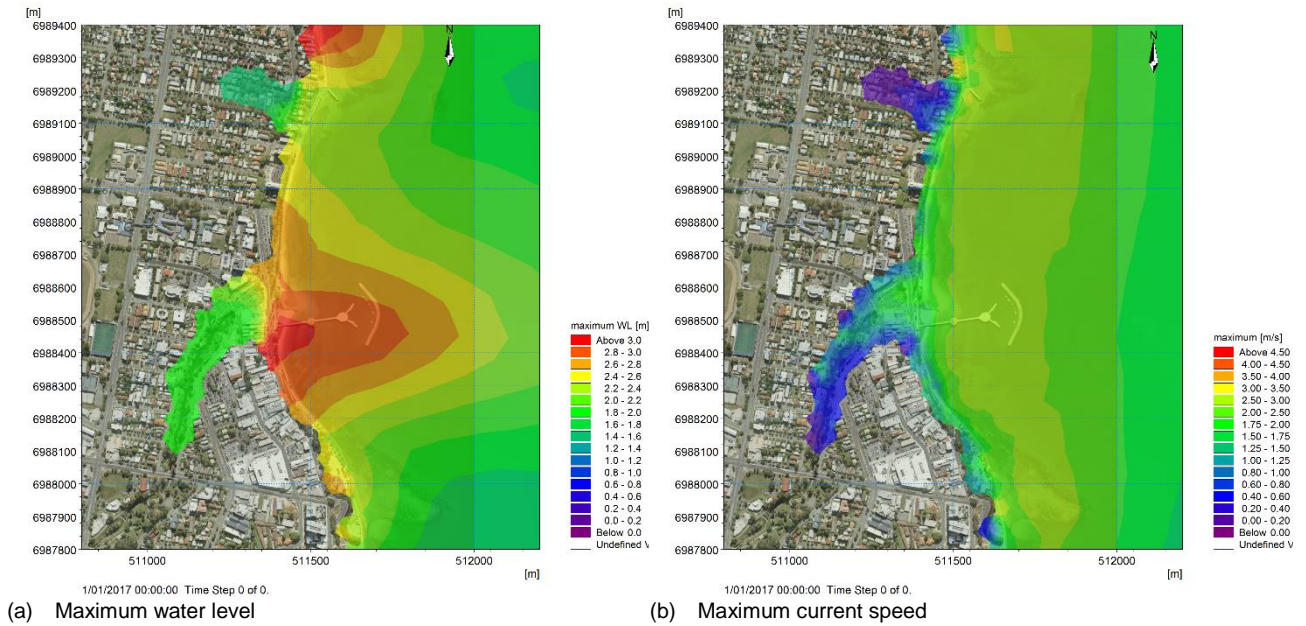


**Figure 27 - Maximum water levels and currents in the vicinity of the Redcliffe Pier for run 16 (Kermadec-Tonga, 10,000 year ARI).**

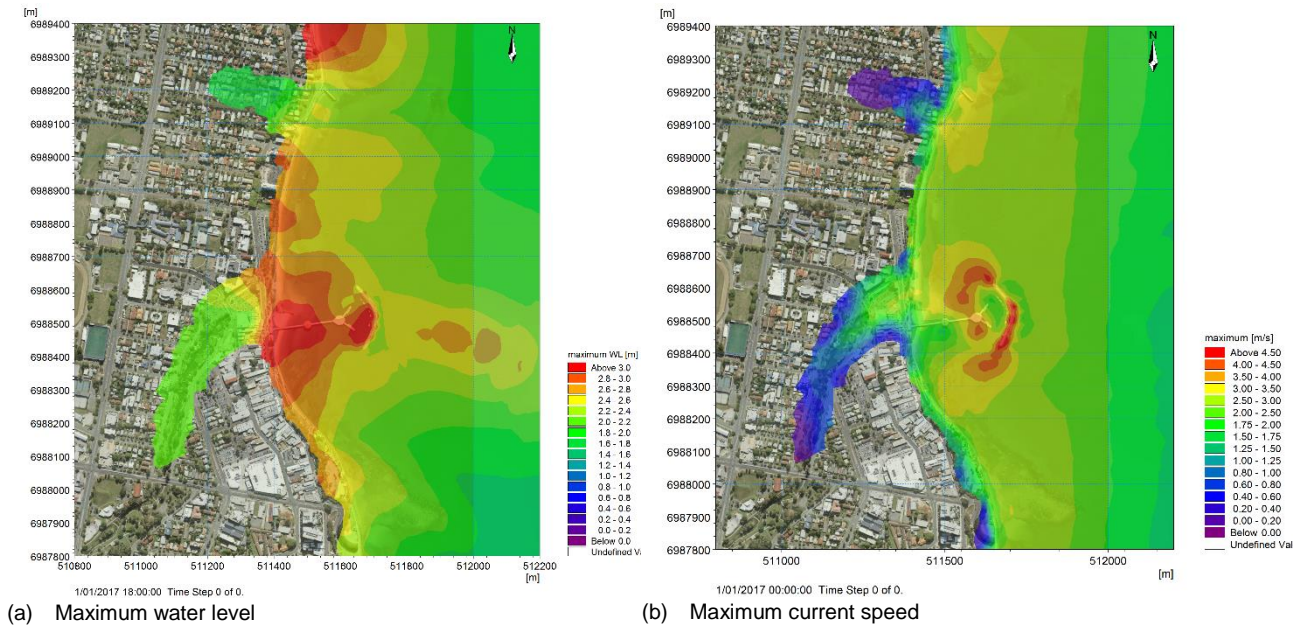


**Figure 28 - Maximum water levels and currents in the vicinity of the Redcliffe Pier for run 16 after mesh refinement (Kermadec-Tonga, 10,000 year ARI).**



## 9.6 Scour Implications

### 9.6.1 Entrance Shoals

The modelling approach adopted is based on a non-erodible seabed. Although this is consistent with approaches undertaken by others internationally, the strong currents identified in Section 8.1.3 within the South and North Passage have the potential to scour out the shallower sandbanks. As shown in Figure 29, these sandbanks can be less than 5 m in depth at MSL in some areas, particularly within South Passage. The extensive and complex sandbank patterns within these entrances are important controls for tsunami penetration within Moreton Bay.

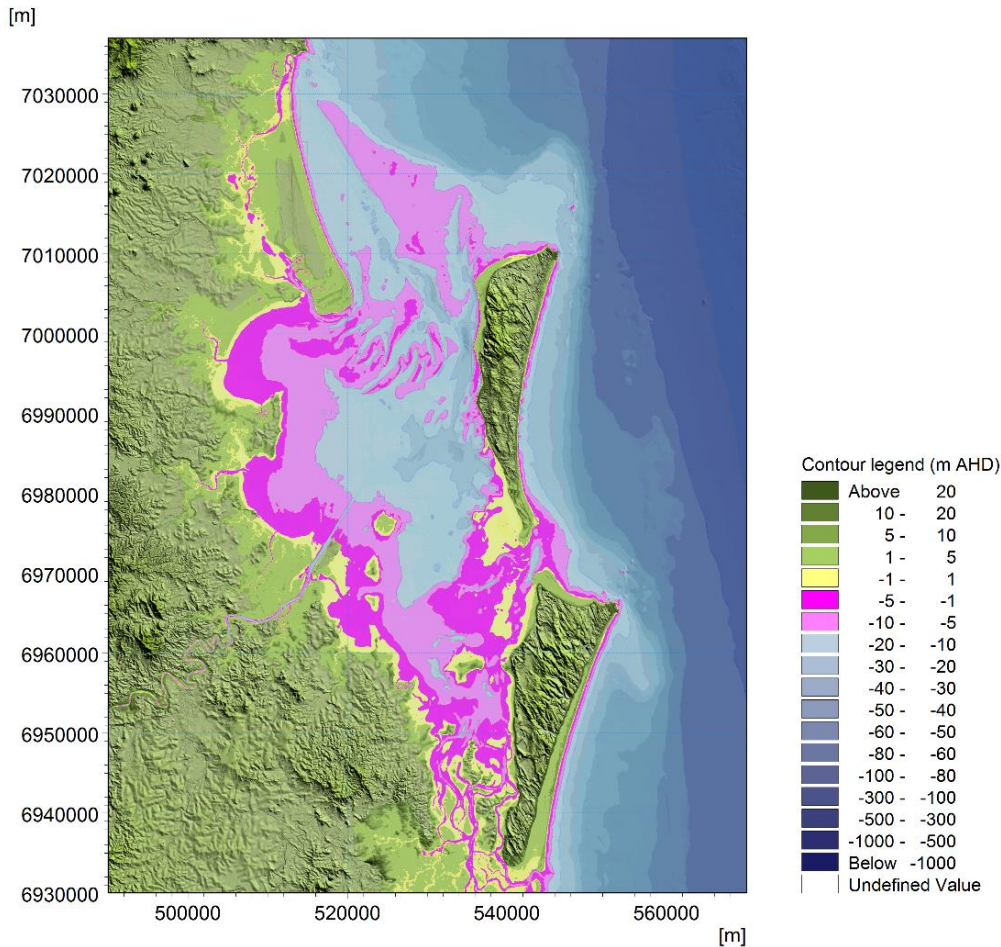


**Figure 29 - Shallow sandbanks within North and South Passage.**

Although the quantification of the level of scour is difficult to model with any certainty, and is a continuing field of research, the implications of potential scour on tsunami amplitudes within the bay has been investigated by assuming two scenarios based on the 10,000 year ARI Kermadec-Tonga event (run 16): instantaneous scour of the North and South Channels to RL -5 m AHD and RL -7 m AHD. The latter being consistent with the bathymetry adjacent to these shoals.

Figure 30 shows the resulting amplification (relative to the base condition) of the maximum water level for both scenarios. The greatest impact occurs in the southern region of the bay due to increased tsunami penetration through South Passage. South Passage is very shallow in some areas. The tsunami would have to remove 1,226 m<sup>3</sup> of sand to achieve the RL -5 m AHD elevation within South Passage. It is likely that some sand would be reworked by the event, but it is difficult to quantify.

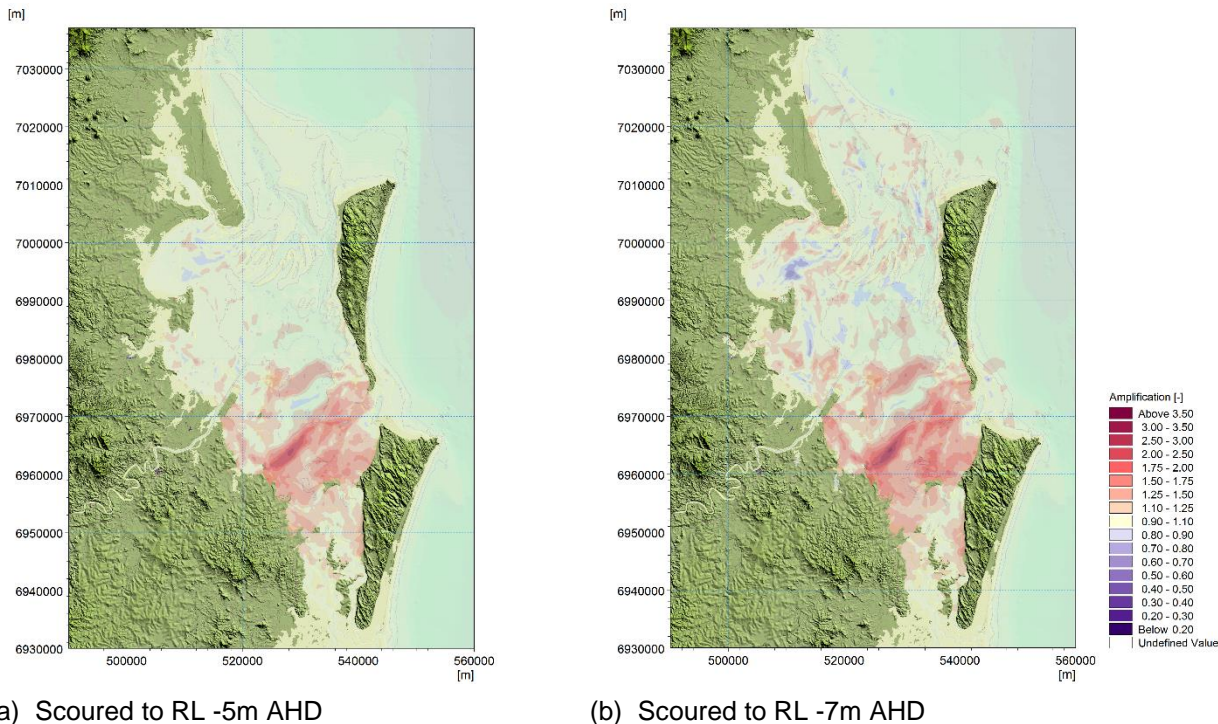


**Figure 30 - Amplification factor (relative to based condition, run 16) for two scour scenarios of North and South Passage.**

In the event of the first scenario occurring, there is potential for inundation to extend further inland, particularly to the south of the Brisbane River, as illustrated in Figure 31 for Manly and Wynnum.



**Figure 31 - Additional inundation extent and depths for Scenario 1 (scouring of North and South Passage to RL -5m).**

### 9.6.2 Anthropogenic Structures

There is limited published literature that quantifies scour depths associated with the interaction of tsunamis with structures such as sea defences (for example rock revetments or breakwaters) and bridge piers. This is complicated by the lack of field data to inform research.

Traditional design of bridge piers is based on freshwater flooding. TMR (2013) provides design considerations for bridge scour from riverine flows, which takes into consideration a number of factors including shape and size of the pier, angle of attack, bed condition and mean velocity of the flow (known as the HEC-18 pier scour equation).

Literature dealing with scour from tsunami are concentrated to scour from overland flow during inundation. FEMA and NOAA (2012) provides approximate scour depths for various soil types based on the work by Dames and Moore (1980), which is reproduced in Table 11.

**Table 11 - Approximate scour depths as a percentage of flow depth (D) (reproduced from FEMA, 2012).**

Soil Type	Scour depth (% of D) (Shoreline Distance < 300 feet)	Scour depth (% of D) (Shoreline Distance > 300 feet)
Loose sand	80	60
Dense sand	50	35
Soft silt	50	25
Stiff silt	25	15
Soft clay	25	15
Stiff clay	10	5

The two primary bridges close to river entrances are the Sir Leo Hielscher Bridges on the Brisbane River, and the Hornibrook and Ted Smout Memorial Bridges at the mouth of North Pine River/Hays Inlet. Based on the HEC-18 equation, the scour for the 10,000 year ARI event (run 16) would range from 0.5 to 2.5 metres. It is difficult to ascertain the level of scour for a tsunami as the flow varies quicker than for a riverine flow, and reverses based on the stage of the wave. These numbers are therefore only indicative and should not be relied on. It should be noted that the piles for the Sir Leo Hielscher Bridges are driven 50 m below the river. The piles for the Ted Smout Memorial Bridge are bedded up to 36 m below the seabed.

The original Hornibrook Bridge deck has the lowest clearance being only approximately 4.5 to 6.4 m above low water. The 10,000 year ARI event (run 16) has a maximum water level at this bridge of 0.7 m above HAT, or 2.2 m above LAT.

Other structures at risk of scour and potential failure are coastline revetments and buildings with shallow foundations. Experiences from the 2004 Indian Ocean and the 2011 Great East Japan tsunami events have shown that as the tsunami overtops sea defences such as revetments, they can scour behind the structure causing failure. Houses can be damaged by impact forces, scour and liquefaction.



## 9.7 Community Vulnerability

Although a complete exposure, vulnerability and risk assessment is beyond the scope of this study, it is useful to examine metrics that would assist disaster managers in assessing their risk. The vulnerability of a community to tsunami hazard can be categorized into physical, social, economic, and environmental (UNESCO, 2015 and UNISDR, 2017). The physical aspects relate to factors such as human casualties, building damage and loss of infrastructure. The concept and quantification of vulnerability is well understood for other water hazards that occur more frequently such as riverine flooding and storm surge (refer Section A.5).

Research into vulnerability measures for tsunami hazard has mostly developed post 2004, but particularly following the 2011 Great East Japan tsunami. As such, the tsunami community is still in the early stages of understanding how to quantify the physical and social vulnerability. Building vulnerability research has focused on developing empirical damage or fragility functions (probability of exceeding a given damage state based on a measure of tsunami intensity) for a range of structure types and predefined damage states based on post event assessments and laboratory experiments. However, there is still a degree of uncertainty associated with the fragility estimations as well as variability for different locations, limiting their generic use (Charvet et al., 2015). This is affected by a number of factors including the current state of understanding of the primary tsunami intensity measures, variability in the classification and assessment of building type and damage state, variability in building quality, locality specific influences (bathymetry, topography, typology), incomplete field survey databases, and the statistical approaches adopted (Charvet et al., 2017). They also do not capture all failure mechanisms such as debris impact, foundation scour and liquefaction. Further information is provided in Section A.5.2.

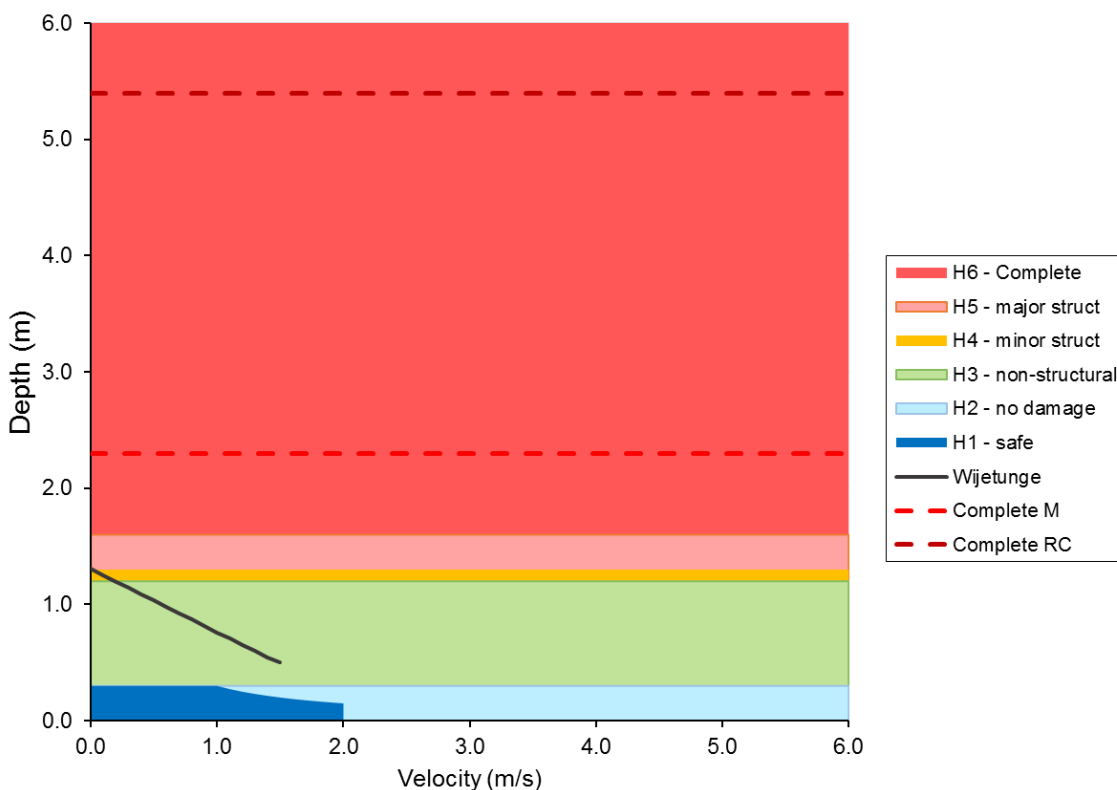


**Figure 32- Combination of general vulnerability curves for tsunami inundation.**

UNESCO (2015) provides some generic median damage states from Nanayakkara and Dias (2013) for single-storey buildings constructed from commonly used materials based on inundation

depth. Figure 32 summarises these based on the lower limits for timber structures. Complete damage for masonry (M) and reinforced concrete (RC) are also shown as lines. The figure also includes the human stability criteria from Wijetunge (2009), based on the experimental results of Takahashi (2005). Further detail is provided in Section A.5.2.

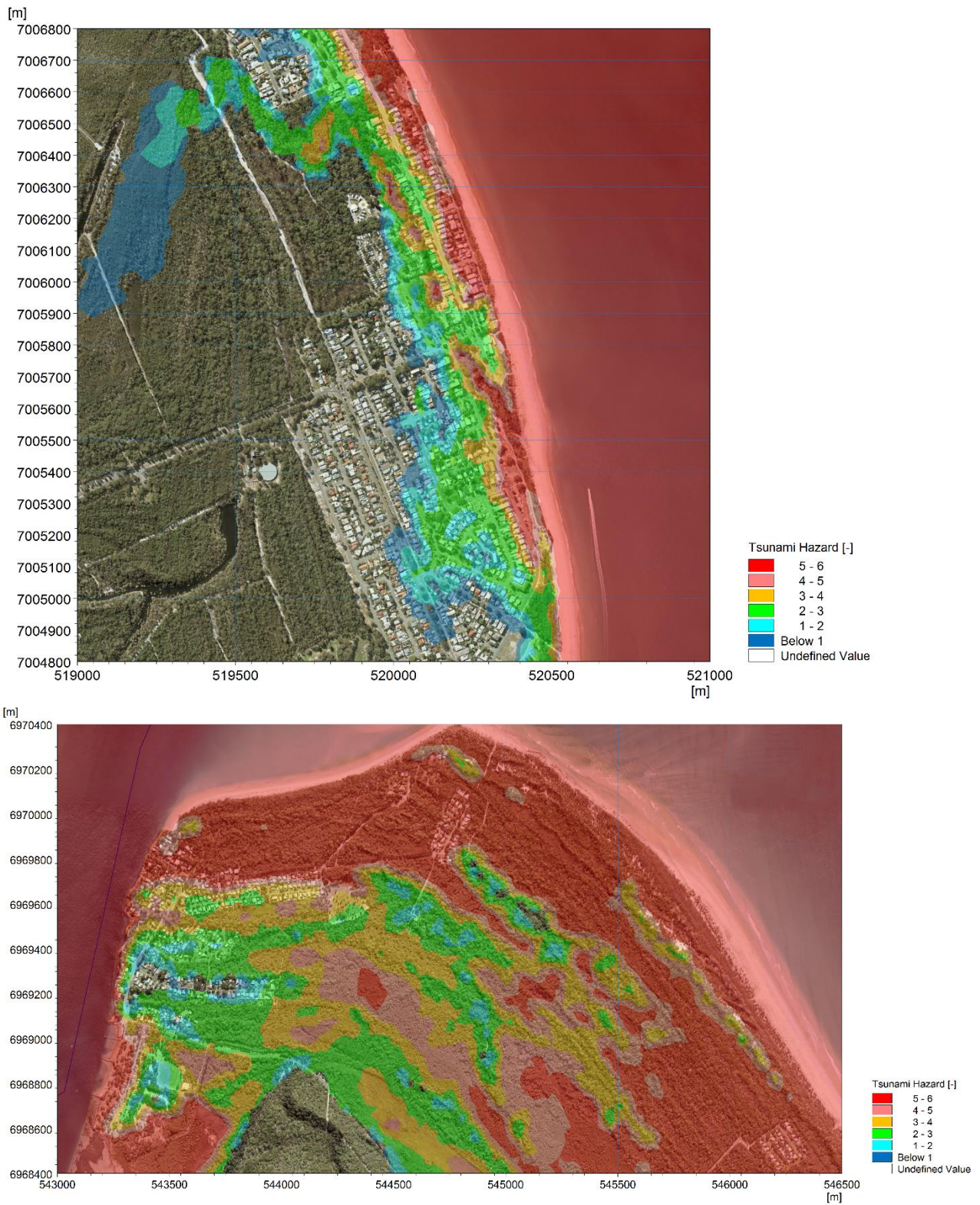


Figure 33 - Example of application of hazard levels for run 16 at Woorim (top) and Amity Point.

Figure 32 represents the median state based on data from Sri Lanka and Thailand during the 2004 Indian Ocean tsunami, as well as Samoa during the 2009 South Pacific tsunami. Therefore it may not be suitable for locations with different building standards and typology (refer Section A.5.2). However, it provides a general indication of potential vulnerability. Figure 33 demonstrates the vulnerability based on this criteria for run 16 at two of the higher hazard locations: Woorim and Amity Point.

Further research is required into developing tsunami vulnerability curves specific for the Australian built environment. Should overland flow velocity become an important variable, then a finer model mesh may be required to resolve velocity patterns around buildings.

## 9.8 Marine Hazard and Vulnerability

Although tsunami inundation is perhaps the most considerable and obvious risk to the public, there can still be significant damage to maritime facilities from events that do not pose an inundation threat. Within ports and marinas, maritime assets are vulnerable to significant damage from strong currents and associated drag forces (Lynett et al., 2014).

Lynett et al. (2014) undertook a review of recorded vessel damage against measured and modelled tsunami current speeds within ports and harbours predominantly in California following the 2010 Chile and 2011 Great East Japan tsunamis, to note distinct damage thresholds as summarised in Table 12. Further detail is provided in Section A.5.1.1.

**Table 12 - Marine facility damage classification from Lynett et al. (2014).**

Damage Index	Damage Type	Threshold Velocity (m/s)
0	no damage/impacts	<1.5
1	small buoys moved	<1.5
2	1–2 docks/small boats damaged and/or large buoys moved	1.5
3	Moderate dock/boat damage (<25% of docks/vessels damaged) and/or midsized vessels off moorings	1.5
4	Major dock/boat damage (<50% of docks/vessels damaged) and/or large vessels off moorings	3
5	Extreme/complete damage (>50% of docks/vessels damaged)	4.6

The above criteria was applied to the maximum current speeds for run 16 (refer Figure 34), showing the potential for extreme marine damage along the open coastline of Moreton and North Stradbroke Island.



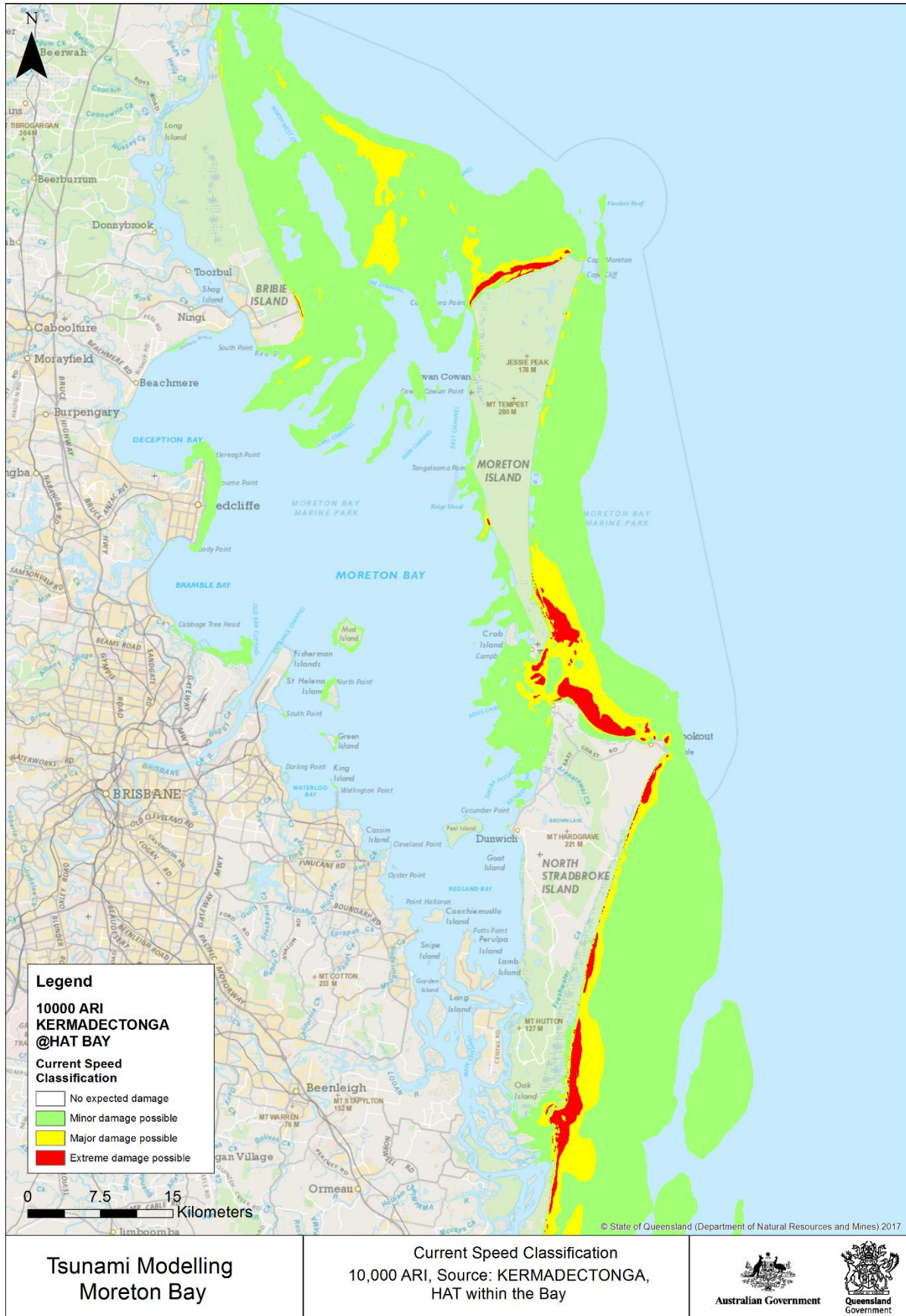


Figure 34 - Example of marine vulnerability for run 16, based on the criteria of Lynett et al. (2014).



## 10 Conclusion and Recommendations

The tsunami modelling undertaken has given a better understanding into tsunami propagation and potential inundation for Moreton Bay, including the identification of regions of higher hazard exposure. Although the mean recurrence intervals (ARI) selected are quite high, it is important to consider the confidence limits associated with these estimates. For example, the mean 100 year ARI event is about 0.3 m, but could also be between 0.1 and 0.5 metres. The upper limit being only seven centimetres below the mean 750 year ARI. Below are some key learnings from the study:

- Across all ARI, tsunami events generated from the Kermadec-Tonga subduction zone resulted in the most extreme wave amplitudes, current speeds and inundation levels for the modelled scenarios.
- The hazard is significantly greater on the ocean side of the islands that protect Moreton Bay, producing a significant marine and land hazard with maximum currents up to 8 m/s and maximum water levels up to 10 metres.
- Tsunamis propagate into Moreton Bay primarily through North and South Passage, and to a lesser extent through Jumpinpin Channel. Dangerous currents can develop along the numerous sandbanks and adjoining coastlines.
- The hazard is reduced within the Bay but still poses a threat, especially for the bay side of islands near North and South Passage, and the Redcliffe Peninsula where maximum water levels can reach 4 m and currents up to 3 metres per second.
- Arrival times are governed by the subduction zone from which they were generated. Those from the New Hebrides have the shortest arrival time of just over 4 hours, while events from South America arriving much later at over 18 hours.
- Once the leading wave reaches Cape Moreton, the additional time it takes to reach locations within the Bay is consistently between 1 and 1.5 hours, depending on the vicinity of the location with the three main entrances, and 2.5 hours to reach Indooroopilly within the Brisbane River.
- The first wave is not necessarily the largest. The largest wave may occur several hours after the leading wave reaches the coast.
- The stage of tide will significantly influence inundation within the Bay, with minimal inundation for tide levels below mean sea level.
- Strong currents and amplified water levels can develop around offshore protection structures, canals and marinas, providing little protection during tsunami events.
- Maximum water levels within the Brisbane River are consistent between ARI, ranging between 0.4 and 0.6 m with little attenuation up to St Lucia.
- Although not modelled, there is potential for shorter steep waves to travel on top of the underlying tsunami in areas where the tsunami wave steepens significantly (particularly close to the coast at Redcliffe and over the entrance sandbanks).
- Sea level rise associated with climate change may increase inundation extents within the Bay, which warrants consideration in vulnerability studies from climate change. The areas at most risk include Hemmant, Shorncliffe, Brighton, estates between Beachmere and Godwin Beach, Bongaree, Bellara and Dunwich. However, the actual impact will depend on the evolution and adaptation of the complex sandbanks throughout the North and South Passages, which was not considered in this study.

Based on the modelling undertaken, the areas identified as having a greater marine hazard (based on maximum water level and currents) are grouped below in decreasing order:

- Ocean side of North Stradbroke, Moreton and Bribie islands including Amity Point;
- North Passage, South Passage and Jumpinpin Channel;
- Bay side of Moreton Island and Redcliffe Peninsula;
- Entrances to canal estates and marinas;
- Brighton to Fisherman Island;
- Beachmere, Peel Island and St Helena Island; and
- Wellington Point to Raby Bay.

In general, the majority of the coastline will experience some inundation, especially at higher ARI and HAT levels. This may be restricted to the foreshore, with coastal properties in low lying areas being more susceptible at the higher tide levels. The communities identified as having a greater land hazard (based on inundation extent) are:

- Amity Point to Point Lookout;
- Woorim;
- Moreton Island Communities (Cowan Cowan, Tangalooma, Koorinal, and Bulwer);
- Brighton to Brisbane Airport;
- Redcliffe Peninsula;
- Beachmere and Godwin Beach;
- Russell, Macleay, Coochie, Peel and St Helena Islands;
- Bongaree; and
- Wynnum to Raby Bay.

The locations identified in the first two dot points above (as well as Cowan Cowan and Tangalooma) experience some inundation for the MSL cases, whereas the other locations are more exposed at higher tide levels.

The infrastructure at Port of Brisbane is situated at elevations that do not pose an inundation risk for the scenarios modelled. However, currents may pose a marine hazard. There is no significant risk to infrastructure at Brisbane airport for all MSL cases. However there is potential for inundation of the north-eastern runway and the northern section of the Luggage Point Sewage Treatment Plant during HAT scenarios. There is minor inundation along low lying areas adjacent to the Brisbane River, as well as a possible marine hazard from increased currents.

The draft revised PTHA draws upon an additional eight years of events, learnings, and scientific knowledge to provide the best present understanding of tsunami hazard near the Australian coast. A comparison of inundation extents from this study and the previous Stage 2 study for Golden Beach suggests that the revised PTHA increases the inundation hazard compared to the previous PTHA, due to an increased contribution to the hazard from the Kermadec-Tonga subduction zone. This suggests that a review of previous studies based on the original PTHA may be warranted, including those undertaken for the Sunshine Coast and Gold Coast. If these models are revised, it is also suggested that the offshore boundary be positioned offshore of the continental shelf to allow any shelf trapped wave processes to develop.

The developed overland DEM is a fixed bare earth model in that only ground points have been included, thereby removing all structures and vegetation. The influence of these features on inland inundation is introduced implicitly by the introduction of roughness factors. The DEM is also assumed to be static and non-erodible. Should a tsunami cause significant erosion of the dune system or entrance shoals to the bay, then the extent of inundation may differ to these model results. The hazard considered relates to potential inundation and broad-scale currents. There may be secondary impacts associated with the tsunami such as coastal erosion, which have not been addressed in this study.

The events selected represent the mean of the maximum water levels for the chosen ARI based on the draft revised PTHA as of February 2018. Higher levels can occur within the 95 per cent confidence limits. Also, any changes to the PTHA since February 2018 may influence the outcomes of this report. Disaster managers may wish to consider appropriate factors of safety in any decisions based on the information provided through this study.

Overall, the study provides planners and disaster managers with a better understanding of the potential tsunami hazard within Moreton Bay and neighbouring islands.

## 11 References

- Australian Bureau of Statistics (ABS), 2016. 2016 Census Data by Local Government Areas, URL: <http://www.abs.gov.au/>
- Beaman, R.J., 2010. Project 3DGBR: A high-resolution depth model for the Great Barrier Reef and Coral Sea. Marine and Tropical Sciences Research Facility (MTSRF) Project 2.5i.1a Final Report, MTSRF, Cairns, Australia, p 13 plus Appendix 1. Available at: [http://www.deepreef.org/images/stories/publications/reports/Project3DGBRFinal\\_RRRC2010.pdf](http://www.deepreef.org/images/stories/publications/reports/Project3DGBRFinal_RRRC2010.pdf)
- BMT WBM, 2014. Northern Moreton Bay Shoreline Erosion Management Plan Stage 1, Prepared for Moreton Bay Regional Council, Report R.B20080.001.03.Stage\_1.docx, May, p 129, URL: <https://www.moretonbay.qld.gov.au/nmbsemp/>
- BMT WBM, 2017. Brisbane River Catchment Flood Study Technical Summary Report - Hydrologic and Hydraulic Assessments, Report prepared for the State of Queensland (Department of Natural Resources and Mines), February, p 142.
- Boswood, P.K., 2013a. Tsunami Modelling along the East Queensland Coast, Report 1: Regional Modelling. Brisbane: Department of Science, Information Technology, Innovation and the Arts, Queensland Government, p 111.
- Boswood, P.K., 2013b. Tsunami Modelling along the East Queensland Coast, Report 2: Sunshine Coast. Brisbane: Department of Science, Information Technology, Innovation and the Arts, Queensland Government, p 96.
- Boswood, P.K., 2013c. Tsunami Modelling along the East Queensland Coast, Coasts and Ports 2013, Engineers Australia, Sydney, 13–15 November, p 7.
- Bricker, J.D., Gibson, S., Takagi, H., and Imamura, F., 2015. On the Need for Larger Manning's Roughness Coefficients in Depth-Integrated Tsunami Inundation Models. Coastal Engineering Journal, volume 57(2), June, p 13, <https://doi.org/10.1142/S0578563415500059>
- Bunya, S., Deitrich, J.C., Westerink, J.J., Ebersole, B.A., Smith, J.M., Atkinson, J.H., Jensen, R., REsio, D.T., Luettich, R.A., Dawson, C., Cardone, V.J., Cox, A.T., Powell, M.D., Westerink, H.J., and Roberts, H.J., 2010. A High-Resolution Coupled Riverine Flow, Tide, Wind, Wind Wave, and Storm Surge Model for Southern Louisiana and Mississippi. Part I: Model Development and Validation, Monthly Weather Review, Vol. 18, pp 345–377.
- Burbidge, D., Mleczko, R., Thomas, C., Cummins, P., Nielsen, O., and Dhu, T., 2008a. A Probabilistic Tsunami Hazard Assessment for Australia, Geoscience Australia Professional Opinion 2008/04.
- Burbidge, D., Cummins, P., Mleczko, R., and Thio, H., 2008b. A Probabilistic Tsunami Hazard Assessment for Western Australia, Pure and Applied Geophysics 165 (11), pp 2059–2088.
- Cardno, 2013. NSW Tsunami Inundation Modelling and Risk Assessment, Report prepared for the NSW State Emergency Service and the Office of Environment and Heritage, p 64.
- Charvet, I., Macabuag, J., and Rossetto, T., 2017. Estimating Tsunami-Induced Building Damage through Fragility Functions: Critical Review and Research Needs, Front. Built Environ., Vol 3(36), p 22, doi: 10.3389/fbuil.2017.00036.

- Charvet, I., Suppasri, A., Kimura, H., Sugawara, D., and Imamura, F., 2015. Fragility estimations for Kesenuma City following the 2011 Great East Japan Tsunami based on maximum flow depths, velocities and debris impact, with evaluation of the ordinal model's predictive accuracy, *Nat.Hazards* 79, pp 2073–2099, doi:10.1007/s11069-015-1947-8.
- Dames and Moore, 1980. Design and Construction Standards for Residential Construction in Tsunami-Prone Areas in Hawaii, prepared by Dames & Moore for the Federal Emergency Management Agency, Washington D.C.
- Davies, G., Griffin, J., Løvholt, F., Glimsdal, S., Harbitz, C., Thio, H.K., Lorito, S., Basili, R., Selva, J., Geist, E., and Baptista, M.A., 2017. A global probabilistic tsunami hazard assessment from earthquake sources, In: *Tsunamis: Geology, Hazards and Risks*, Geological Society, London, Special Publications, 456, <https://doi.org/10.1144/SP456.5>
- Department of Environment and Heritage Protection (EHP), 2013. Coastal Hazard Technical Guide, Determining Coastal Hazard Areas, Queensland Government, p 18.
- DHI, 2017a. MIKE 21 & MIKE 3 Flow Model FM, Hydrodynamic and Transport Module, Scientific Documentation, Mike Powered by DHI, October, p 64.
- DHI, 2017b. MIKE 21 & MIKE 3 Flow Model FM, Hydrodynamic Module, User Guide, Mike Powered by DHI, p 148.
- Environmental Protection Agency (EPA), 2007. Solomon Islands tsunami, Fact Sheet, FS 2007-2, May, p 3.
- FEMA and NOAA, 2012. Guidelines for Design of Structures for Vertical Evacuation from Tsunamis, Second Edition, FEMA P-646, April, p 174.
- Fountain, L., Griffin, J., Van Putten, K., Sexton, J., Nielsen, O., and Wilson, R., 2009a. Capacity building for tsunami planning and preparation: inundation models for the Gold Coast, Geoscience Australia Professional Opinion 2009/08.
- Fountain, L., Van Putten, K., Griffin, J., Hingee, M., Wilson, R., Burbidge, D., Sexton, J., Nielsen, O., and Mleczo, R., 2009b. A Nearshore Tsunami Hazard Assessment for Australia, Geoscience Australia Professional Opinion 2009/06.
- Geoscience Australia (GA), 2010. Tsunami Data Access Tool (TsuDAT) User Guide, Version 1.0, p 27.
- Geoscience Australia (GA), 2016. Intertidal Extents Model Confidence Layer, URL: <http://pid.geoscience.gov.au/dataset/100464>
- Geoscience Australia (GA), 2017. High-resolution depth model for the Great Barrier Reef – 30m, URL: <http://pid.geoscience.gov.au/dataset/115066>
- Hayes, G.P., Wald, D.J., and Johnson, R.L., 2012. Slab1.0: A three-dimensional model of global subduction zone geometries, *J. Geophys. Res.*, 117, B01302, doi:10.1029/2011JB008524.
- Horrillo, J., Grilli, S.T., Nicolsky, D., Roeber, V., and Zhang, J., 2014. Performance Benchmarking Tsunami Models for NTHMP's Inundation Mapping Activities, *Pure and Applied Physics*, July, p 16, DOI 10.1007/s00024-014-0891-y.

Intergovernmental Oceanographic Commission (IOC), 2016. Tsunami Glossary, Third Edition, Paris, UNESCO, IOC Technical Series 85. (English, French, Spanish, Arabic, Chinese) (IOC/2008/TS/85 rev.2).

Lynett, P. J., Borrero, J., Son, S., Wilson, R., and Miller, K., 2014. Assessment of the tsunami-induced current hazard, *Geophys. Res. Lett.*, 41, pp 2048–2055, doi:10.1002/2013GL058680.

Madsen, P.A., Fuhrman, D.R., and Schäffer, H.A., 2008. On the solitary wave paradigm for tsunamis. *J. Geophys. Res.*, Vol 113, C12012, p 22, doi:10.1029/2008JC004932.

Maritime Safety Queensland (MSQ), 2018. Queensland Tide Tables: Standard Port Tide Times 2018, Department of Transport and Main Roads, Queensland Government, p 129, URL: <https://www.msq.qld.gov.au/Tides/Tide-tables>

MLITT, 2012. Guide to determining the potential tsunami inundation, Seacoast Office, Water and Disaster Management Bureau, Ministry of Land, Infrastructure, Transport and Tourism, Version 2.0 (temporary translation), p 82.

Mofjeld, H.O., Symons, C.M., Lonsdale, P., González, F.I., and Titov, V.V., 2004. Tsunami Scattering and Earthquake Faults in the Deep Pacific Ocean, *Oceanography*, Vol 17(1), pp 38–46.

Mofjeld, H.O., González, F.I., Titov, V.V., Venturato, A.J., and Newman, J.C., 2007. Effects of Tides on Maximum Tsunami Wave Heights: Probability Distributions, *J. Atmos. Oceanic Technol.*, 24, 117–123, <https://doi.org/10.1175/JTECH1955.1>

Murata, S., Imamura, F., Katoh, K., Kawata, Y., Takahashi, S., Takayama, T. (eds), 2010. Tsunami: To Survive from Tsunami, *Advanced Series on Ocean Engineering*, Volume 32, World Scientific, p 302.

Nanayakkara, K.I.U. and Dias, W.P.S., 2013. Fragility curves for tsunami loading, *International Conference on Structural Engineering & Construction Management*, Kandy.

NOAA, 2018. Tsunami: The Tsunami Story (web page accessed 2018), URL: [https://www.tsunami.noaa.gov/tsunami\\_story.html](https://www.tsunami.noaa.gov/tsunami_story.html).

Power, W.L. (compiler), 2013. Review of Tsunami Hazard in New Zealand (2013 update), *GNS Science Consultancy Report 2013/131*, p 222.

Smagorinsky, J., 1963. General Circulation Experiment with the Primitive Equations, *Monthly Weather Review*, 91(3), pp 99–164.

Takahashi, S., 2005. Tsunami disasters and their prevention in Japan – Toward the performance design of coastal defences, *Proc International Symposium on Disaster Reduction on Coasts*, Monash University, Melbourne, Australia.

Transport and Main Roads (TMR), 2013. Bridge Scour Manual, Department of Transport and Main Roads, Queensland Government, March, p 114.

United Nations Office for Disaster Risk Reduction (UNISDR), 2017. Words into Action Guidelines: National Disaster Risk Assessment, 2. Tsunami Hazard and Risk Assessment, p 9.

UNESCO, 2015. Tsunami risk assessment and mitigation for the Indian Ocean; knowing your tsunami risk – and what to do about it, *IOC Manual and Guides No 52*, Second Edition, p 160.

Webster, M.A., and Petkovic, P., 2005. Australian bathymetry and topography grid, *Geoscience Australia Record 2005/12*, June, p 27, URL: <http://www.ga.gov.au/meta/ANZCW07030080022.html>

Wijetunge, J.J., 2009. Demarcation of High Hazard Areas Based on Human Stability Considerations in Tsunami Overland Flow, Engineer, Vol XXXXII (01), Institute of Engineers, Sri Lanka, pp 45-52.



## Appendix A – Tsunami Dynamics

### A.1 Introduction

To better understand tsunami hazard, this section will briefly describe the processes that influence tsunamis. In basic terms, a tsunami is a series of long period waves generated by a disturbance in the ocean water column arising from abrupt geophysical events. These disturbances are more likely from movement of tectonic plates along faults in the form of submarine earthquakes, but could also be from submarine landslides, volcanic eruptions or a possible meteorite strike (in the extreme). More than 80 per cent of the world's tsunamis were caused by earthquakes (IOC, 2016). The earthquake scenario is the focus of this report.

A simple analogy would be dropping a pebble in a pond. The pebble generates a deformation of the water surface. This in turn creates a wave or series of waves that radiate or spread away from the source in concentric circles of increasing circumference as they propagate away. As the circumference increases, the amplitude decreases or attenuates due to energy being transferred along the wave crest. In reality, tsunami generation is not a point source but a complex pattern of bed movements. The three main phases are tsunami generation, propagation, and run-up/inundation. These phases will be briefly described below.

The following discussion has attempted to keep the subject matter as basic as possible. However, the topic itself can be complex, and so there is a need to provide some technical content for completeness.

### A.2 Tsunami Generation

#### A.2.1 Earthquake

The main source of tsunamigenic earthquakes (that is, capable of generating tsunami) that have notable effects on Queensland come from the so called "Ring of Fire", also referred to as the circum-Pacific seismic belt. It is a collection of oceanic trenches, volcanoes and plate movements along the rim of the Pacific Ocean, and is responsible for about 70 per cent of the world's tsunamis (IOC, 2016). There are three types of plate boundaries: convergent boundaries (where two plates are colliding); divergent boundaries (moving apart); and transform boundaries (plates sliding horizontally past each other) (refer Figure A. 1). The oceanic crust of a convergent boundary is denser than the continental crust and will be thrust beneath the continental shelf to form subduction zones. Friction between the plates opposes movement until energy build up causes the plates to suddenly slip past one another, generating an earthquake. The surface where the slip occurs is referred to as the fault and energy radiates outward from the fault in all directions in the form of seismic waves that can last for minutes. The magnitude of the earthquake is related to the length of the fault and the amount of slip. The location or epicentre and time of initiation of the earthquake can be determined from triangulation of available seismogram recordings based on the primary (P-wave) and secondary (S-wave) waves (Kayal, 2006 and USGS, 2018a).

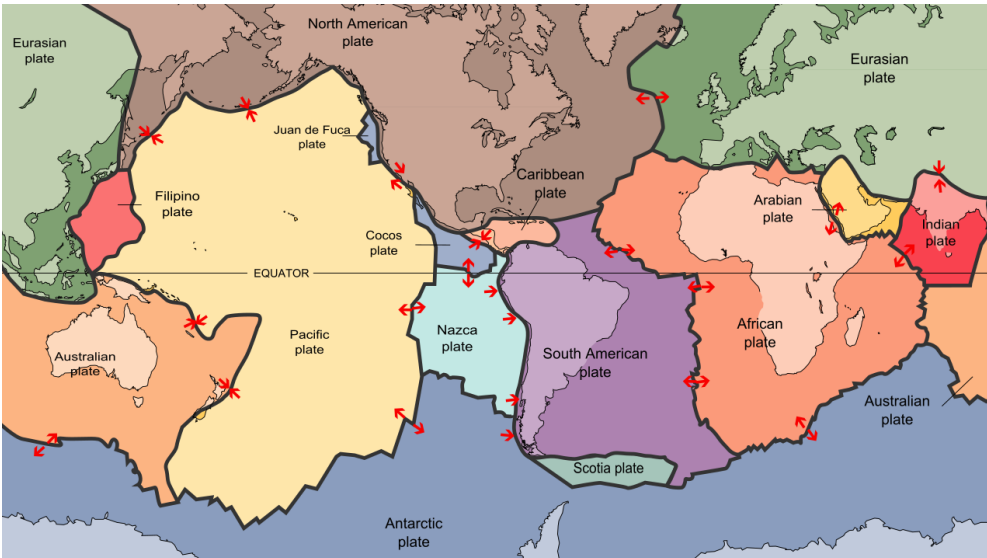
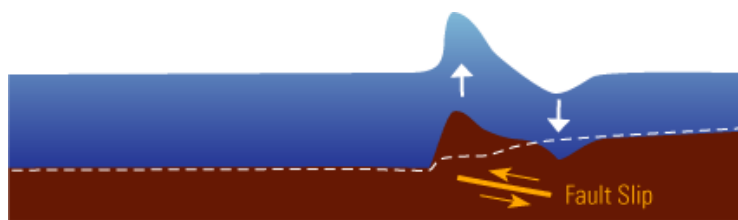


**Figure A. 1 - Tectonic plates** (source: <http://pubs.usgs.gov/publications/text/slabs.html>).

In general, a subduction zone slip results in the leading edge of the overriding plate (typically the continental plate) breaking free from its grip with the inducing plate, and to spring seaward. This generates a vertical rise in the full water column, which splits to propagate as a tsunami in all directions (refer Figure A. 2). Although the tsunami will propagate out in all directions from the generating area, the main energy propagation is generally orthogonal to the direction of the earthquake fracture zone (IOC, 2016).



(a) *Initiation of tsunami from seabed deformation.*



(b) *Tsunami wave splits and radiates out from subduction zone.*



(c) *Deep water wave travels faster, whilst shallow wave shoals.*

**Figure A. 2 - Tsunami generation (distorted scale)** (source: <https://walrus.wr.usgs.gov/tsunami/basics.html>)

As well as the uplift of the seabed, there can also be some subsidence of the overriding plate as shown in Figure A. 2. Communities that experience the tsunami on the continental shelf side (right in Figure A. 2) will experience a drawdown of the ocean prior to the tsunami reaching the coast. Communities to the left will not experience a drawdown prior to the tsunami. However, this is a simplified explanation, and a number of factors will influence tsunami generation.

A commonly adopted model for tsunami generation is to discretise the fault area into rectangular sub-faults. The deformation of the seafloor is then defined for each sub-fault by the use of a planar fault model (Okada 1985 and 1992), which considers parameters such as the depth below the seabed, orientation, and slip (Yamazaki, 2010). For specific events, tsunami waveform inversion analysis such as that proposed by Satake (1987) are used to estimate fault slip distribution (Adriano et al., 2018), as illustrated in Figure A. 3 for the 2016 Fukushima earthquake. The fault model as well as the initiation and rise time for each sub-fault are then used to determine the temporal and spatial seabed deformation, which is translated to sea surface displacement.

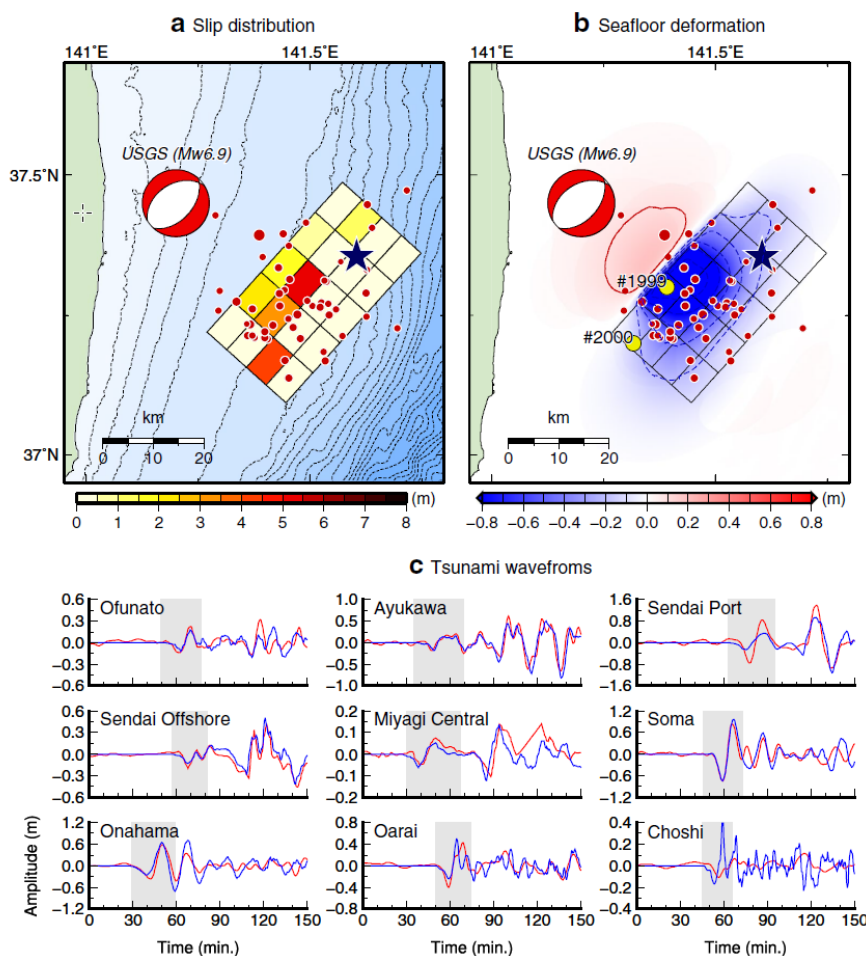


**Figure A. 3 - Slip distribution, seafloor deformation and resulting tsunami fit to measurements from an inversion analysis for the 2016 Fukushima Earthquake (Adriano et al., 2018).**

Tsunamis amplitudes are governed by the seabed deformation, whereas wave periods are determined by the fault area. Tsunamis have very long wavelengths of tens to hundreds of kilometres as the abrupt bottom movements that generated them have large horizontal scales (hundreds of kilometres). Multiple reflections and partial wave trapping, especially near the source, produce an extended wave train of many waves even though the original source was a single impulse. The latter waves in a tsunami wave train form very complicated patterns in which it is difficult to determine the relationship of a latter wave to the initial source. Hence, only the

observations of the first few waves at a site are used for comparison with model simulations and estimation of the earthquake source parameters, (Mofjeld et al., 2004).

## A.2.2 Landslide

Although not considered in this study, an introduction into tsunami generation would not be complete without mentioning tsunamis generated from landslides. Submarine landslides can occur on continental slopes and are similar to those that occur on land. They can be triggered by earthquakes. The tsunami that devastated Papua New Guinea in 1998 was much greater than expected for the magnitude 7 earthquake that preceded it. A subsequent seafloor survey indicated that a submarine landslide may have been triggered by the earthquake (González (1999), Synolakis et al. (2002), Bernard et al. (2006), and Tappin et al. (2008)), resulting in the unusually high tsunami waves.

The earthquake triggers a mass of seabed to break away and travel down the continental slope by gravity. As with earthquake generated tsunami, this in turn generates a movement in the column of water above the slide. The tsunami that is generated is related to a number of factors such as the dimensions of the failed mass and the speed and distance this mass travels down the slope. The closer the landslide speed is to the wave speed, the larger the tsunami (Geist et al., 2009). The impact zone of a tsunami generated by submarine landslide is typically more localised than that generated by earthquakes. As the continental shelf can be narrow, the land adjacent to the landslide may be impacted by powerful tsunamis with little warning. The Papua New Guinea event produced runup heights of over 10 m for a 25 km stretch of coastline, killing over 2,100 people (Synolakis et al., 2002). The tsunami will also travel offshore. Refraction processes as well as coastal and shelf trapped waves may result in tsunamis being felt at further distances for an extended duration. However, the largest waves will occur along the coastline within the immediate vicinity of the landslide.

Geist et al. (2009) found that for continental slope landslides, frequency dispersion and nonlinearity are important in modelling tsunami evolution. They modelled the Currituck landslide in North America with a 1D high resolution model based on the fully nonlinear Boussinesq equations, to show the formation of short period fission waves riding on the tsunami (discussed further in Section A.4) before it breaks into a tsunami bore.

## A.3 Tsunami Propagation

### A.3.1 Transoceanic Propagation

The resulting earthquake-generated tsunami propagates as a set of waves whose energy is concentrated at wavelengths corresponding to the earth movements (~100 km), at wave heights determined by vertical displacement (typically <1 m), and at wave directions determined initially by fault shape and orientation, and later by the adjacent coastline geometry. Because each earthquake is unique, every tsunami has unique wavelengths, wave heights, and directionality (NOAA, 2018a).

As the displacement occurs through the entire water column, and wave lengths are much greater than depth, the tsunami behaves as a shallow water wave even in deep water. From shallow water wave theory, the speed of the tsunami can be calculated from:

$$c = \sqrt{gD}$$

Equation A.1

Where  $c$  is the wave celerity (m/s),  $g$  is the acceleration by gravity (about  $9.81 \text{ m/s}^2$ ) and  $D$  is depth (m). This means that the tsunami in deep water can travel very fast (in the order of 600–800 km/hr in 3,000–5,000 m depth).

The wave period is generally in the range of 5 to 40 minutes. If the wave has to travel considerable distances, the shorter period wave energy will dissipate more. Therefore, the period of the tsunami increases with distance travelled. Periods of up to one hour were observed at Japan following the Great Chilean Earthquake of 1960 (Murata et al., 2010).

As the waves propagate away from the source in deep water, they also spread (as in the pebble analogy), causing some attenuation. As tsunamis are sensitive to water depth variations at all ocean depths, submarine features will influence the wave train. Wave refraction (described below) will occur at all depths. Linear features such as such as escarpments and ridges can act as wave guides, redirecting and concentrating wave energy. Other features such as seamounts can scatter wave energy. Basically, submarine features that extend to within 500 m depth can cause significant wave scatter (Mofjeld et al., 2004). Mofjeld et al. (2000 and 2001) mapped the distribution of a scattering index within the Pacific Ocean. They found that the southwestern Pacific exhibits the highest density of significant scatter features, which includes Australia, such that any tsunami within this region will experience strong scattering with a tendency to become trapped.

In addition to the above processes, oceanic islands will reflect and scatter wave energy. These processes tend to complicate and extend the tsunami wave train as it approaches the Australian continental slope. At this stage, amplitudes are relatively small and so may go unnoticed by a ship.

### A.3.2 Continental Shelf Propagation

As the tsunami reaches the continental slope, the depth can change drastically and abruptly compared to the long wavelength. In general, the tsunami may experience the same processes to that of short period waves, not limited to attenuation, shoaling, scattering, focusing, diffraction, reflection, and resonance, but at a larger scale. The more significant processes will be briefly described below.

#### A.3.2.1 Refraction, Shoaling and Reflection

As the tsunami approaches shallower water it will slow down, thereby adjusting direction such that the crest will tend to become more parallel with the contours (known as refraction). As the wave slows down, the amplitude will increase (shoaling). For steep coastlines (narrow continental self), such as South-east Queensland, the tsunami amplitude can increase considerably as there is less dissipation as the wave approaches. In areas where there is a wide and shallow continental shelf, or fringing reefs, the wave may dissipate. However, the wave may again increase as it reaches the shoreline due to shoaling. A first approximation of the shoaling wave height from linear wave theory, is Green's Law (Synolakis and Skjelbreia (1993), Geist (1998), Truong (2012), and Bryant (2014)):

$$\frac{H_1}{H_o} = \left[ \frac{d_o}{d_1} \right]^{1/4}$$

Equation A.2

Where  $H_1$  is the wave height at the intermediate depth,  $d_1$  and  $H_o$  is the deep water wave height at depth  $d_o$ .

As the tsunami approaches the coastline, it is influenced by coastal features and nearshore bathymetry. Refraction can focus energy on particular features such as prominent headlands or diverge energy such as the back beach of an embayment. Complex bathymetry may also cause crossing (superposition) of waves, generating localised amplification. Another feature of tsunami is they can reflect off the coastline. Unlike short waves, which steepen, break and dissipate on beaches; the length to wave height ratio of tsunamis rarely steepens to breaking point. The tsunami approaches the coast without breaking. Energy is transferred to run-up (refer next section) and reflections. If the coastline is of steep rocky headlands, the reflection will be more pronounced. The reflected wave can then be redirected by refraction and again returns to the coast (Murata et al., 2010). This can occur in V-shaped bays, resulting in higher than expected tsunami heights at the back beach as demonstrated in Figure A. 4. There is also potential for amplification within bays should the period of the tsunami be close to a harmonic of the natural period of the bay. If the tsunami travels along a solid surface such as a rocky headlands, Mach-stem waves may occur, greatly amplifying the tsunami against the steep surface (Bryant, 2014).

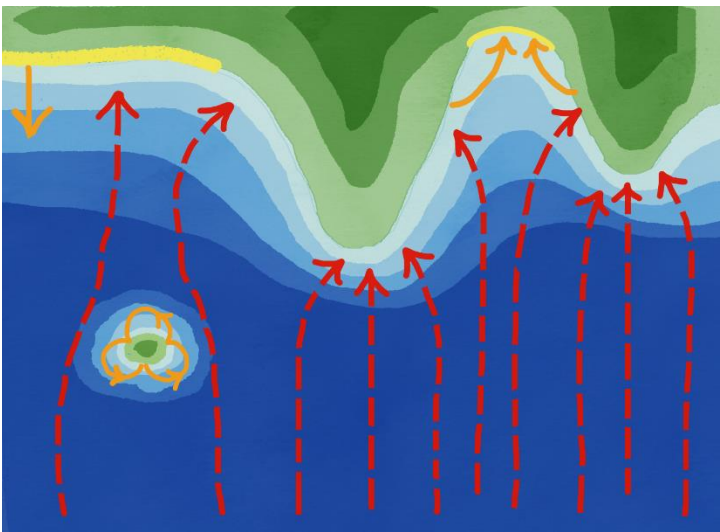


**Figure A. 4 - Schematic representation of refraction (red) and reflection (orange) of a tsunami. The curving near the islands is an indication of diffraction.**

#### A.3.2.2 Trapped Waves

A trapped wave is a wave that becomes bound by a particular feature, whether it be the coastline (coastal trapped waves), or the abrupt change in bathymetry (shelf trapped waves). For steep continental shelves where there is an abrupt change in depth over a length scale that is shorter than the tsunami wavelength, there can be partial reflection of the tsunami as it approaches the shelf, and then a further reflection from the coast. This bouncing back and forth is called shelf trapping (refer Figure A. 5). This process can also occur due to refraction when the tsunami is reflected at an angle to the coast. As the oblique reflected wave reaches the shelf, the rapid depth changes on the continental slope can cause the wave to refract back further along the coast in a leapfrogging pattern (a pattern analogous to skipping a pebble across the water surface).

Coastal trapped or edge waves are surface gravity waves that are trapped against a rigid body (the coastline) by refraction. In the offshore direction, the wave height diminishes rapidly, depending on the wave length and mode. The fundamental mode ( $n = 0$ ) producing an exponential decay offshore. Figure A. 6 provides an example of the theoretical profile of the first four modes based on the theory provided in Mei et al. (2005) and González et al. (1995), and in three dimensions in Figure A. 8, while Figure A. 7 shows modelled wave profiles off the coast of North Stradbroke Island for a hypothetical event originating from the Kermadec-Tonga subduction zone.



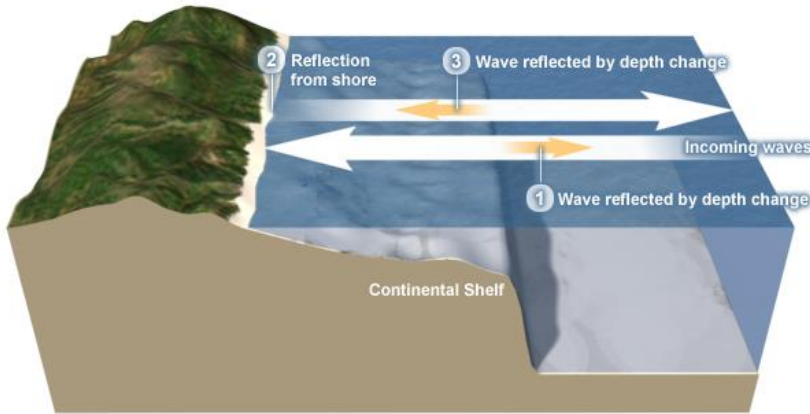


**Figure A. 5 - Shelf trapping mechanism (source: COMET® Website at <http://meted.ucar.edu/> of the University Corporation for Atmospheric Research (UCAR)).**

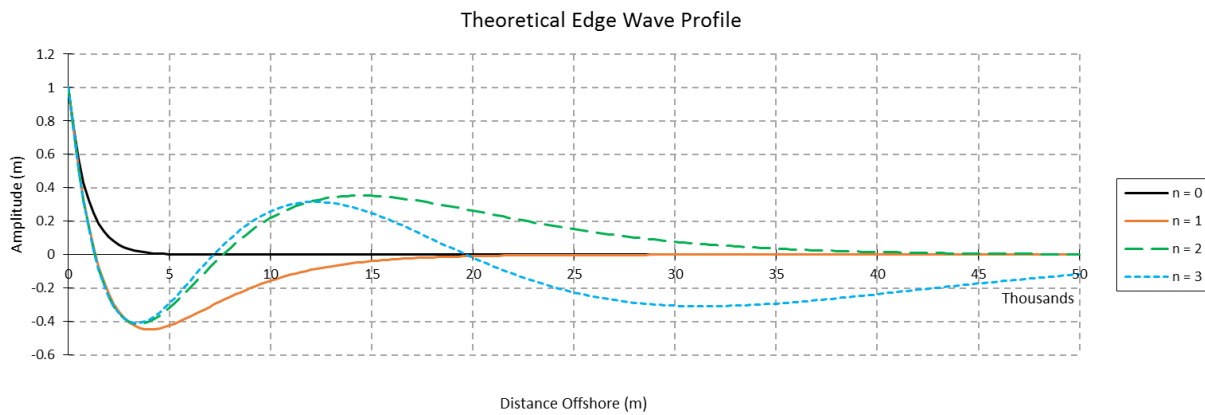


**Figure A. 6 - Theoretical edge wave offshore profile for the first four modes (n = 0 to 3) of a long wave (Amplitude = 1m, Period = 10 min).**

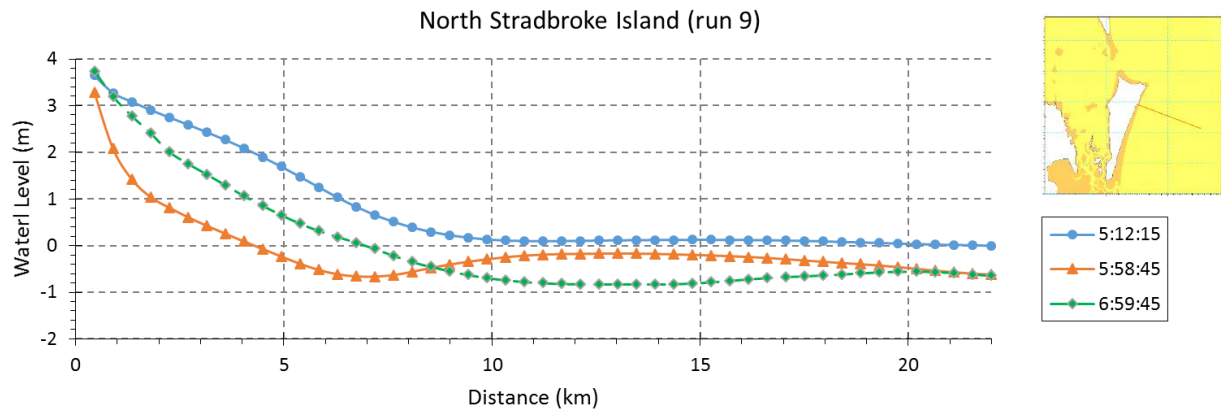


**Figure A. 7 - Modelled coastal trapped wave profiles generated off North Stradbroke Island by a hypothetical 3,000 year ARI event from the Kermadec-Tonga subduction zone (times given in hr:min:sec after initial generation).**

Coastal trapped waves can be described as either standing (stationary in space, but oscillating in time) or progressive (moving along the coastline). However, the progression of these waves is greatly affected by the complexity of the coastline. Progressive edge waves can be steered or guided by sudden drop-off in bathymetry such as the continental shelf.

Coastal and shelf trapped waves have been found to be important phenomena in understanding tsunami hazard along the coastline. The trapped and incident wave can interact, such that the wave train will be complex, of longer duration, and vary along the coast. More importantly, the constructive interaction between edge waves and the non-trapped modes of the tsunami can produce higher than expected secondary waves and associated run-up (Geist, 1998). The literature refers to two broad conditions of exciting trapped waves: those excited by tsunamigenic earthquakes on the continental shelf close to the coastline; and those excited from scattering of the incident tsunami from offshore sources by irregular coastlines.

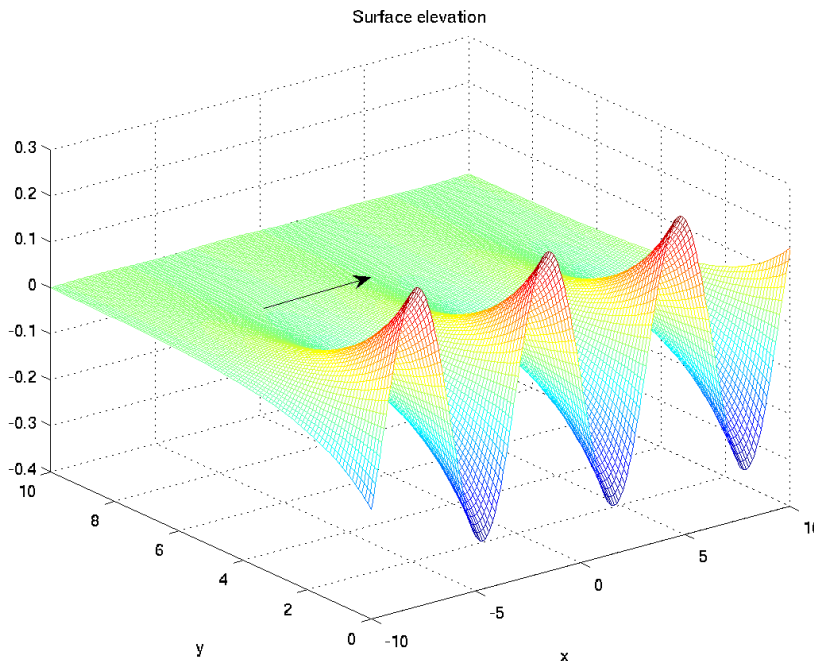


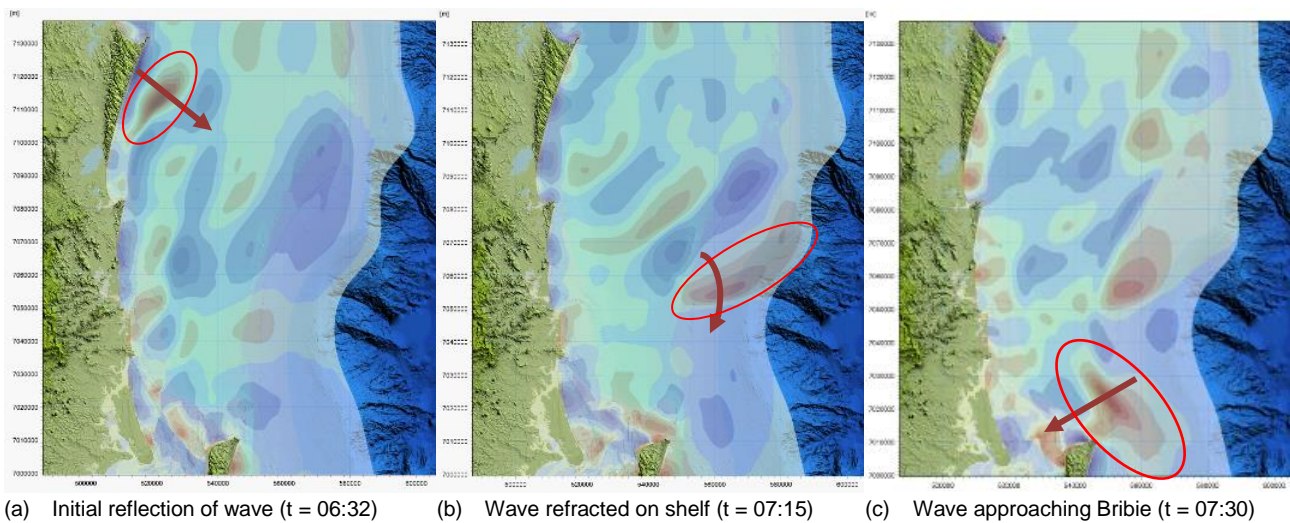
**Figure A. 8 - Three dimensional profile of edge waves propagating in the x direction, being the coastline**(Source: [https://en.wikipedia.org/wiki/Edge\\_wave](https://en.wikipedia.org/wiki/Edge_wave)).

Trapped edge waves excited from tsunamigenic earthquakes generated on shelves have been documented by González et al. (1995) when they analysed data captured during the April 1992 Cape Mendocino tsunami, which generated both incident and trapped edge waves along the Californian and Oregon Coast from a nearfield earthquake. They found these waves were of the fundamental mode (that is, exponential decay offshore); propagate much slower than the incident tsunami waves, and can travel long distances along the coast. Rabinovich et al. (2006) found the presence of trapped edge waves during the June 2005 tsunami generated by an earthquake offshore of California. The excitation of trapped edge waves from shelf generated tsunamis was also found by Neetu et al. (2011) following a reanalysis of the 1945 tsunami that impacted the Makran coast. They also found that these modes can be trapped in the alongshore direction due to longshore variations in shelf width. Yamazaki and Cheung (2011) modelled the 2010 Chile earthquake that occurred offshore of the central Chile coast to find that the continental shelf slope refracts and traps the radiated energy initially as progressive edge waves on the shelf. Reflections between headlands and the shelf generated a number of standing waves along the coast.

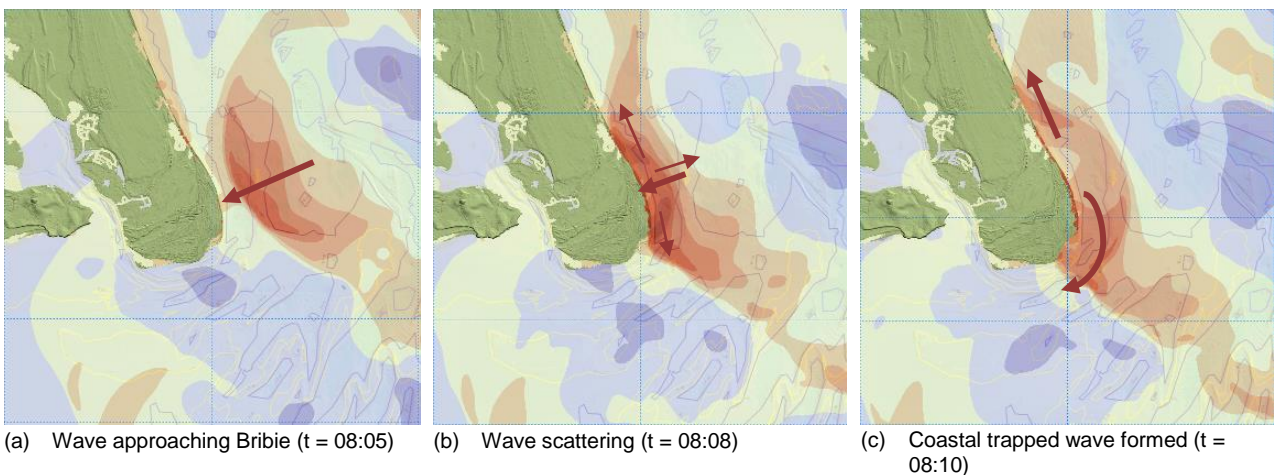
Fuller and Mysak (1977) demonstrated theoretically that trapped edge waves can be generated on a shelf with a straight coastline with small irregularities, due to energy transfer from scattering effects. They also indicated that the amplitude of trapped edge waves excited by a tsunami is about 70 per cent of the incident amplitude and that they slowly attenuate from scattering along

irregular coastlines. The presence of edge waves from tsunami generated offshore can be found in references that also discuss resonance as discussed in the following section.

Figure A. 9 demonstrates a shelf trapped transient wave generated during a modelled 3,000 year average recurrence interval (ARI) tsunami event on the south east Queensland coast. The wave is initially reflected off the Great Sandy National Park coast. As it nears the continental shelf, it is refracted back towards the coast to impact Bribie Island, some 120 km south of the initial reflection. As the wave reaches the Bribie coast, it splits to propagate along the coast in both directions as a coastal trapped wave (Figure A. 10). The combination of the trapped and incident waves resulted in the highest water level at Bribie for this event, about 207 minutes after the leading wave (Figure A. 11). Abraimi (2014) observed a similar phenomenon when analysing the results of modelling the 2010 Chilean Tsunami on the central Chilean coast.

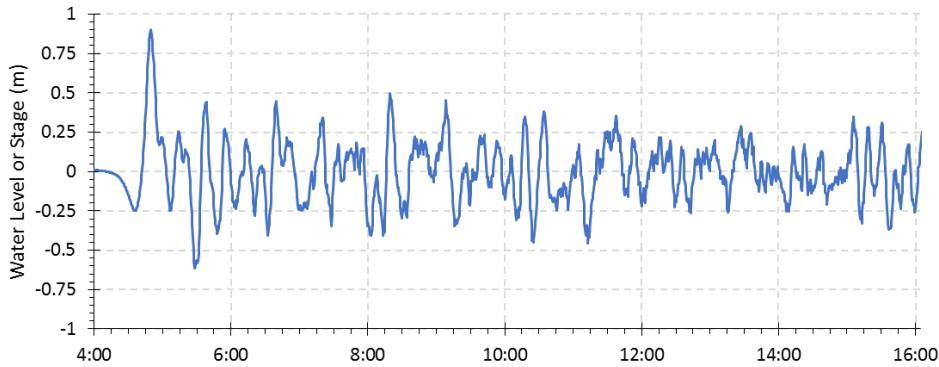
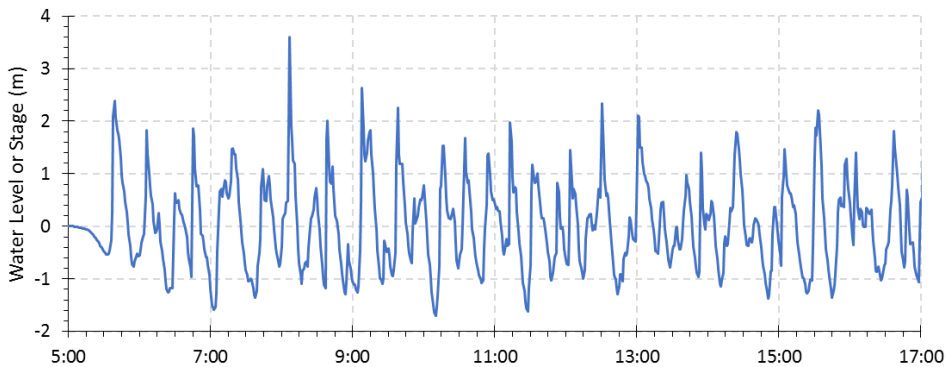


**Figure A. 9 - Shelf trapped wave along south east Queensland coast (3,000 year ARI event). Arrows indicate direction. Dark red shading represents 4 m. Time is elapsed time in hours:minutes.**



**Figure A. 10 - Coastal trapped wave example for Bribie Island, Queensland. (3,000 year ARI event). Arrows indicate direction. Dark red shading represents 4 m. Time is elapsed time in hours:minutes.**

(a) Boundary condition at defined hazard point (3000 year ARI event, depth = 1000m)

(b) Southern Bribie Island (3000 year ARI event, depth  $\approx$  5m)**Figure A. 11 - Time series of tsunami near the coast of Southern Bribie Island (3,000 year ARI event).****A.3.2.3 Standing Waves and Resonance**

Standing waves is the name given to the combination of two waves travelling in opposite directions at particular periods and timing that their interference creates the appearance of a wave where the crest appears to be stationary. For tsunami, the two waves will be the incoming wave and the reflected wave. Standing waves occur when the wave period (or frequency being the inverse of period) matches a natural period of the water body. In simple terms, when the wave period (or wave length) of the arriving tsunami matches a harmonic (an integer fraction) of the natural (or eigen) period (or length) of a water body (such as the length of a bay), a standing wave is generated that can amplify the tsunami height. A standing wave is the combination (or superposition) of the incident wave and a reflected wave (refer Figure A. 12). If the wave length is an integer factor of the overall length, the reflected and incident wave will combine to form nodes and antinodes in the spatial domain. The nodes are where the two waves are out of phase and so cancel each other out. The water level at nodes will be minimal due to destructive interference. The antinodes are where the two waves are in phase and the amplitude will be at a maximum due to constructive interference.



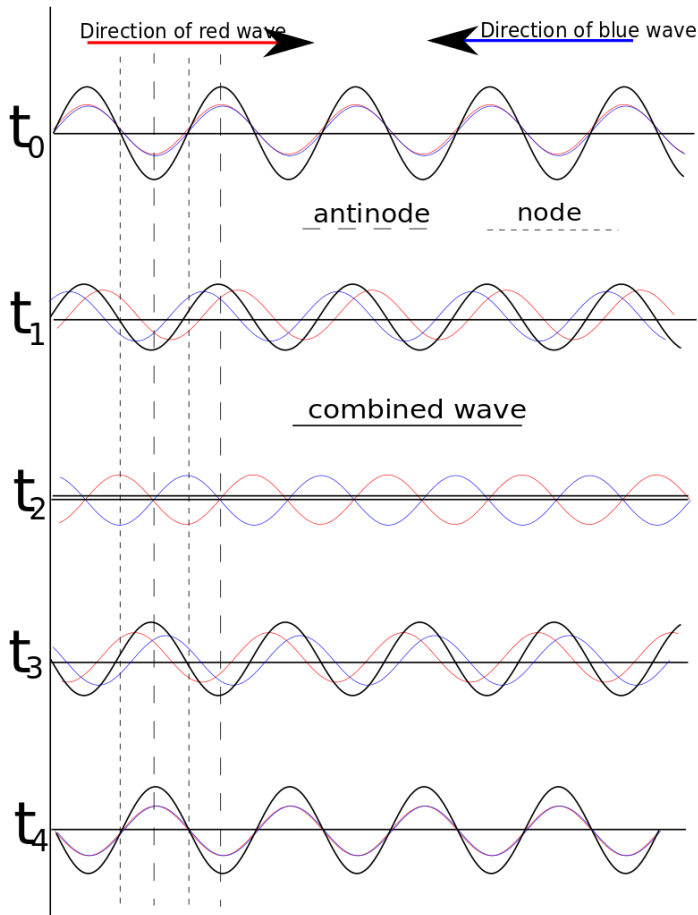


**Figure A. 12 - Standing wave example caused by an incident (red) and reflected (blue) wave (Source: [https://en.wikipedia.org/wiki/Standing\\_wave](https://en.wikipedia.org/wiki/Standing_wave)).**

The fundamental mode (also referred to as the zero mode or first harmonic) is the simplest mode and is the most commonly seen as it is subject to the least energy dissipation because they involve smaller velocities for a given amplitude (Nielsen, 2012). The wave length required to generate the fundamental node depends on the end conditions. For a simple condition of a semi-enclosed basin, the node will appear near the entrance. Therefore the fundamental mode will occur when the basin is a quarter of the wave length. The wave period can then be calculated with consideration of wave celerity (Equation A.1) giving (Bryant, 2014):

$$T_s = \frac{4L_b}{\sqrt{gD}}$$

Equation A.3

Where  $L_b$  is the length of the basin and  $T_s$  is the wave period required to initiate seiching. For an edge wave, the wave length is along the coast with nodes at either end. The fundamental mode will occur when the length between nodes is half the wavelength. In reality, the wave lengths required to generate the modes will be more complicated due to factors such as irregular coastlines, partial reflections, oblique waves, and irregular wave conditions to name a few. As the tsunami wave train consists of many waves over a wide range of wave periods, it is possible that this phenomena can occur and be excited at a number of modes.

Resonance is always associated with standing waves. To understand resonance, let us consider a wave entering a harbour. Reflections will cause the water level to oscillate after the passage of the wave, which will decay rapidly. However, if the wave frequency matches the natural frequency of



the harbour, then the waves will continue to oscillate for some considerable time (or resonate). The natural frequency being the frequency at which the harbour tends to oscillate in the absence of any driving or damping force.

If the external wave is a series of waves at the natural period, then each successive wave will add energy to the harbour oscillation which may grow larger than any individual wave in the original wave series. Resonance can appear in everyday life. The coffee in your cup that spills when you increase your walking pace is resonance caused by your motion matching the natural period of the cup. Resonance is a known issue for ports and harbours (referred to as a seiche), and can cause significant damage to moored vessels. Given the wavelength of tsunamis can still be tens of kilometres in the nearshore, the phenomena can also occur at larger scales such as bays and even the continental shelf.

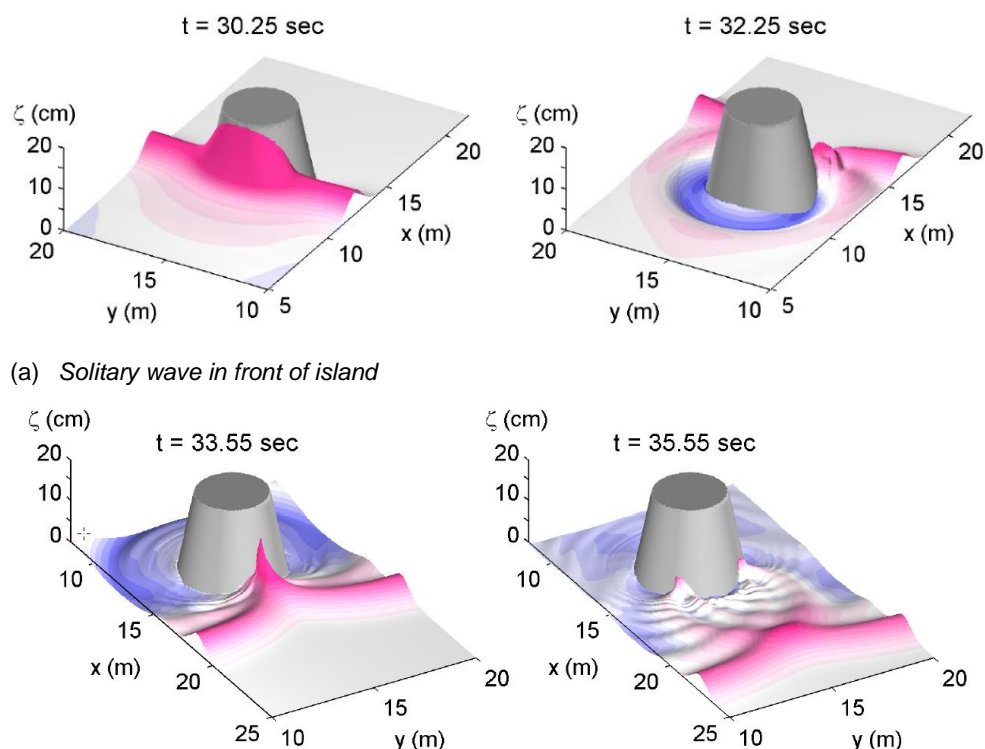
The presence of shelf resonance has contributed to unusually high tsunami wave heights at: Hawaii (Munger and Cheung, 2008) and Crescent City (Horrillo et al., 2008) from the 2006 Kuril Islands tsunami; the American Samoa from the 2009 Samoa tsunami (Roeber et al., 2010); and the Chilean coast following the 2010 Chilean earthquake (Yamazaki and Cheung, 2011). In these examples, standing edge waves resulted in a spatially and temporally complex tsunami patterns that would not be explained by solely examining the leading tsunami wave.

#### **A.3.2.4 Obstructions and Islands**

Obstructions such as islands, peninsulas or capes, may cause the tsunami to circle around to the back of the obstruction with reduced amplitude (referred to as diffraction). The obstruction must be significant enough in size to be felt by the long period tsunami. Murata et al. (2010) suggests the obstruction needs to exceed 500 m to have a notable influence.

For short period wind waves, the process of diffraction around islands has been known to produce a region of calmer water (known as the shadow zone) in the lee of the obstruction (such as islands) which may offer protection to the mainland coastline directly behind the obstruction. This concept has been utilised by coastal engineers through the design of detached offshore breakwaters as a coastal defence approach.

The behaviour of tsunamis around features such as islands can be quite different. The combination of refraction and edge waves can cause the wave to wrap around the island to reunite on the leeward side, such that the run-up levels can be as high as on the exposed side (Murata et al., 2010 and Wong et al., 2008). Yamazaki (2010) examined this phenomena by numerical modelling of a solitary wave approaching a conical island and compared the results against physical model results (Figure A. 13). Stefanakis et al. (2014) undertook 200 simulations of an idealised conical island in front of a coastline. They found that unlike short period waves, tsunamis tend to wrap around the island and form a focusing lens of energy on its lee side, amplifying wave heights on the mainland behind the island. Rasyif et al. (2016) examined the influence of small islands on tsunami propagation on the Sumatran coast by numerical modelling of three actual events and three hypothetical cases. The report found that under certain conditions (that is, the tsunami propagates from both sides of the island), the tsunami will focus on the lee of the island and amplify the tsunami on mainland communities behind the island.



(a) Solitary wave in front of island

(b) Solitary wave in lee of island

**Figure A. 13 - Solitary wave wrapping around idealised conical island (Yamazaki, 2010).**

### A.3.2.5 Ports and Marinas

Because of the long length scale of tsunamis even on the coast, small structures such as marinas and detached breakwaters for coastal erosion works have little influence on wave attenuation, unless their crest is above the tsunami run-up height. Under these conditions, there will be very strong currents at the openings. For ports and marinas, strong currents can develop as well as circulation systems. As flows accelerate around port structures, boundary shear leads to flow separation that can create transitional turbulent structures. These structures are referred to as coherent eddies or turbulent coherent structures (Borrero et al., 2015) and at first glance can be misconstrued as whirlpools.

### A.3.2.6 Wave Characteristics

The theory of waves is a complex subject and will not be discussed in any detail. Some of the more common terminology will be provided. The description of the tsunami wave form relates specifically to the leading wave, being the initial impulse of the tsunamigenic earthquake. Subsequent waves are a result of the processes mentioned earlier. In the deep ocean, the wave train follows an exponentially decaying envelope with the leading wave much larger than subsequent waves (Geist, 2009). As the tsunami approaches the coast, the wave form becomes more complex with no discernible characteristic envelope. However, there has been analytical work undertaken in describing the run-up (described below) in relation to the shape of the leading wave. Early work considered the leading wave as a solitary wave (being the infinite wavelength limit of cnoidal waves). Madsen et al. (2008) examined the solitary wave and concluded that it is not applicable for long waves on a sloping bottom. Tadepalli and Synolakis (1994) introduced the concept of the N-wave (in analogy to dipole waves in gas dynamics – Synolakis and Bernard, 2006) to describe analytical wave run-up from tsunami. They consider two forms: leading depression N-waves (LDN), being a drawdown of the ocean before the tsunami hits the coast, and leading elevation N-waves (LEN). These different wave profiles depicted by these theories are depicted in Figure A. 14.

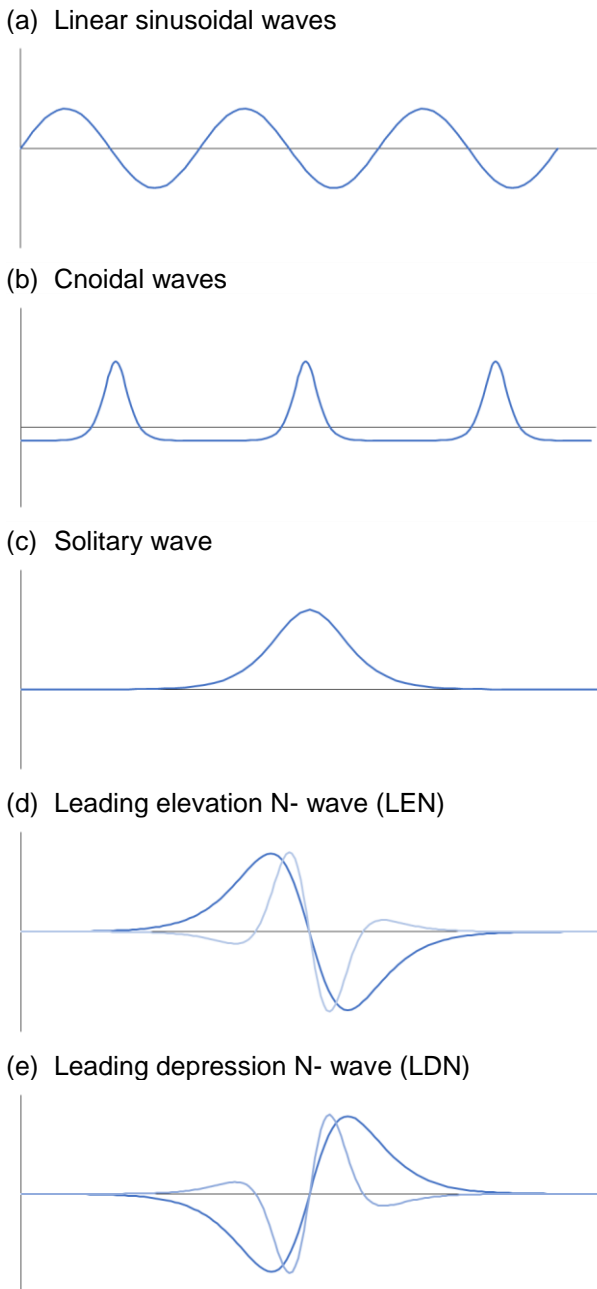


**Figure A. 14 – Different nonlinear wave theories adopted in literature to describe the leading tsunami wave. The first plot is based on linear wave theory provided as a reference. The lighter of the lines in the last two plots are double N-waves.**

In deep water, tsunami can be described by linear wave theory (assuming small amplitude, homogenous and incompressible fluid). For depths of less than about 50 m, it is suggested that nonlinear wave theory applies (Geist, 1998), as the waveform will change with time. Cnoidal waves are considered nonlinear waves. Therefore, numerical modelling within the coastal region should be undertaken with models based on the nonlinear shallow water equations (NLSWE) or Boussinesq equations.

Tsunami are generally described by the amplitude (height of the crest above the mean water level) and period (time between successive crests). However, the wave train will consist of numerous waves of varying amplitude and period. Short wave statistics can be used to describe the wave

train in terms of wave height (crest to trough height, approximately twice the amplitude) and period. Some common parameters include significant wave height ( $H_s$  being the average of the highest one-third of wave heights), root-mean-square wave height, peak period ( $T_p$  being the period corresponding to the peak spectral energy) and the zero up-crossing period ( $T_z$  being the average period based on the time each wave rises above the mean water level).

The water level at a particular moment in time is sometimes referred to as the stage.

All of the processes previously mentioned add to the complexity and length of the tsunami wave train. A tsunami event can therefore last for several hours, and the first wave may not necessarily be the largest. However, IOC (2016) suggest that the largest wave is usually one of the first five waves. As mentioned earlier, all these processes and their complex interactions will decrease the reliability of modelling the longer wave train.

#### **A.3.2.7 Tsunami and Tides**

The tide range in the open ocean is small relative to the depths (typically less than one metre). As the tides travel across the Australian continental shelf, amplification occurs. The largest tide ranges within Queensland occur around Central Queensland, with the highest documented tide range 9.1 m at McEwen Islet (MSQ, 2017).

Traditionally to minimise computation times, tsunami forecast and hazard modelling have decoupled the tides, adopting a constant level of Mean Sea Level (MSL). Mofjeld et al. (2007) examined the influence of tides on the maximum water level by superimposing theoretical tsunami wave time series based on an exponential decay coefficient of two days over a duration of five days (based on measurements within the Pacific Ocean), on tides typical for Oregon, USA. Maximum envelopes of tide plus tsunami were calculated by stepping the tsunami time series through a full year of tides representing an average year during the 18.6 year tidal cycle. The results showed that for small tsunami amplitudes, the maximum water levels tend to occur near mean higher high water (MHHW) with little spread. As the tsunami increases, the maximum water level tends towards a limit of MSL plus the tsunami amplitude (for tsunami amplitude > tide range), and the probability density function approaches that of the tides.

Although the principle of an exponentially decaying tsunami time series may be applicable in the open Pacific Ocean, the tsunami time series on the Australian continental shelf will be further complicated by the processes discuss above such that the largest wave my occur several hours after the onset of the leading wave. This is not discussed in the paper but it is possible that a tsunami time series with large amplitudes persisting for some time may increase the limit from MSL to a tidal plane above MSL.

## **A.4 Tsunami Run-up/Inundation**

The behaviour of tsunamis as they reach the coast is different to the behaviour of wind waves (refer Figure A. 15). Short period wind waves will continue shoaling until their steepness causes the wave to break. The broken bore will then continue to wash up the beach until its energy has been dissipated (referred to as the swash zone). The vertical height that is reached above the still water level is referred to as the run-up. The run-up depends on wave characteristics and beach slope. The particle motion within wind waves is orbital, becoming more elliptical in shallow water. Depending on wind wave and bathymetry characteristics within the surf zone, current patterns can develop including undertow, rip currents, and longshore currents.

With tsunamis, the wave length even in very shallow water can still be in the order of kilometres. Bryant (2014) describes that the wave form close to shore appears similar to either Stokes or  $N$ -

waves. These waves typically do not break, unless they are very large. Instead, they can appear as a fast moving tide or surge. The leading edge of some may decay into one or more bores or solitons (Bryant, 2014), and can appear like a fast moving tidal bore. The flow is horizontal in pattern (more like a river flow) and can be very strong and turbulent. The momentum of these waves can push water much further inland than wind waves at rates of 5 to 8 m/s (Bryant, 2014), and the currents can be too strong for a person to remain upright.

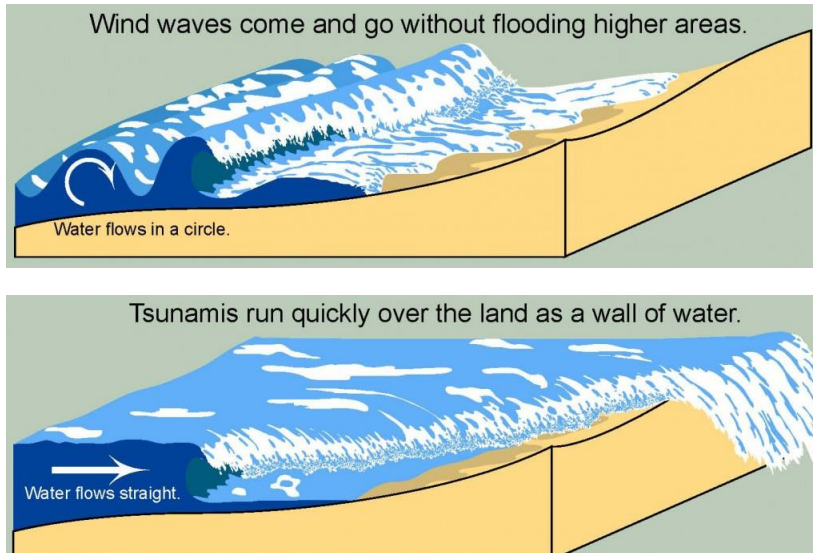


**Figure A. 15 - Differences between wind waves and tsunami at the coast. (source: <http://earthweb.ess.washington.edu/tsunami/>).**

Madsen et al. (2008) investigated the use of solitary waves to model tsunamis, and in doing so, examined some characteristics of long waves as they approach the coastline. With the aid of a high order Boussinesq numerical model based on Madsen et al. (2006), they concluded the following:

1. In general, there is insufficient distance for tsunamis to generate solitons in the ocean or continental shelf.
2. During shoaling from deep to shallow water, wave asymmetry will increase (seen as steepening of the leading face of the wave), whereas skewness remains low.
3. With decreasing water depth, nonlinearity grows rapidly while the effects of dispersion reduces. Nonlinear shallow water equations (NLSWE) provide a good approximation of this process.
4. As the wave propagates close to the beach, the front face of the wave may become steep enough to disintegrate into an undular bore with short and steep transient waves of periods in the order of 10 to 15 seconds riding on top of the tsunami. This process explains the observed short period waves during the 2004 Indian Ocean tsunami (Figure A. 16). Dispersion now becomes important and nonlinear dispersive models such as Boussinesq models are required to model this phenomenon. Although the NSWE may indicate this process due to numerical dispersion.
5. Even on a flat, shallow, and wide shelf, the asymmetry of the waves will continue to grow until the front face steepens to the point that undular bores develop.
6. Typically the bores develop close to the coast and hence do not have sufficient time or travel distance to develop leading solitons.
7. Wave breaking that is observed during events is typically related to the short period bores, and not the underlying tsunami.



8. Although these transient waves will have an impact on coastal structures, the run-up and inundation that occurs is a result of the underlying longer period tsunami.
9. Constant depth theory for cnoidal or solitary waves cannot be applied to approximating long waves on sloping bottoms.



(a) Undular bores riding on the underlying tsunami which is not apparent in the photo due to its gentle slope.



(b) Close up of approaching bores.

**Figure A. 16 - The 26 December 2004 Indian Ocean tsunami approaching the North Beach of the island Koh Jum, off the coast of Thailand. Photo taken from the top of Mt Pu (Copyright Anders Grawin. Reproduced from <http://www.kohjumonline.com/anders.html> with permission).**

For sloping topography, the inundation extent will be defined by the run-up limit. Murata et al. (2010) suggests that run-up will be greater on a gentle slope. For regions where there is a beach of uniform slope followed by a flat coastal plain, the momentum of the tsunami will travel further inland until friction overcomes it. For regions where the inland region slopes downward (such as behind dunes) the tsunami may accelerate with increased velocity. For both of these cases, tsunami velocities are slow to dissipate.

Extreme events have been known to destroy buildings, infrastructure and stripping vegetation, moving several kilometres inland (inundation extent). With such devastating events, like the 2004 Indian Ocean tsunami, a booming roar can be heard as the tsunami approaches (UNESCO/IOC,

2010). Circulation patterns can develop along the coast such as large eddies. As the trough of the wave approaches, the water level can recede rapidly generating strong offshore currents that wash obstacles out to sea.

Of course the ability to inundate depends on a number of factors including tsunami height and period, stage of tide, height of any barriers (such as seawalls and beach dunes), obstacles (such as buildings), and land coverage (for example a dense forest will impede tsunami movement more than pastoral land). For small amplitude tsunamis, the stage of tide may be a critical factor.

As well as inundating low lying coastal regions, tsunamis will also propagate up rivers and waterways much faster than they inundate some coastal zones.

## A.5 Tsunami hazard and Community Vulnerability

The preceding sections describe the processes that can influence the tsunami hazard at a specific geographic location. Once the hazard is quantified, vulnerability and risk assessments can be undertaken. Charvet et al. (2017) define tsunami risk as:

$$\text{Tsunami Risk} = \text{Tsunami Hazard} \times \text{Vulnerability} \times \text{Exposure}$$

Where exposure is the number of people, buildings and infrastructure at risk; and vulnerability is the likelihood of losses, defined as:

$$\text{Vulnerability} = \text{Fragility} \times \text{Loss Model}$$

Where fragility is the probability of damage given a particular tsunami intensity; and the loss model defines the probable losses (financial and casualty) for a given level of damage. The above definition being consistent with the risk assessment process defined in QFES (2018).

The vulnerability of a community to tsunami hazard can be categorized as physical (human casualties and structural damage), social, economic, and environmental (UNESCO, 2015 and UNISDR, 2017). The following relates to the physical aspects.

The science behind vulnerability and risk assessments is well developed for other coastal hazards that occur more frequently. There is extensive literature and guidelines regarding vulnerability metrics for riverine flood events, based on field and laboratory investigations. The Flood Hazard Guideline published by the Australian Institute for Disaster Resilience (AIDR, 2017) quantifies flood hazard as the product of flood depth and velocity. Figure A. 17 illustrates the combined general flood hazard vulnerability curves provided in the guideline, which set hazard thresholds that relate to the vulnerability of the community when interacting with floodwaters.

Further guidance in regards to human stability in riverine flood events can be found in Engineers Australia (2010), which is based on a review of previous laboratory experiments. The results are summarised in Table A. 1 as a function of the product of individual height and mass (H.M) and the product of depth and velocity (D.V).

However, there are fundamental differences in the physics of these two hazards. Riverine flooding of floodplains is generally characterised by the gradual and steady rise in water level over an extended period, with currents being typically low within the floodplain: the main cause of damage being from water damage. Their occurrence is much more frequent, and as such there has been significant field assessments and physical modelling investigations to develop vulnerability relationships.

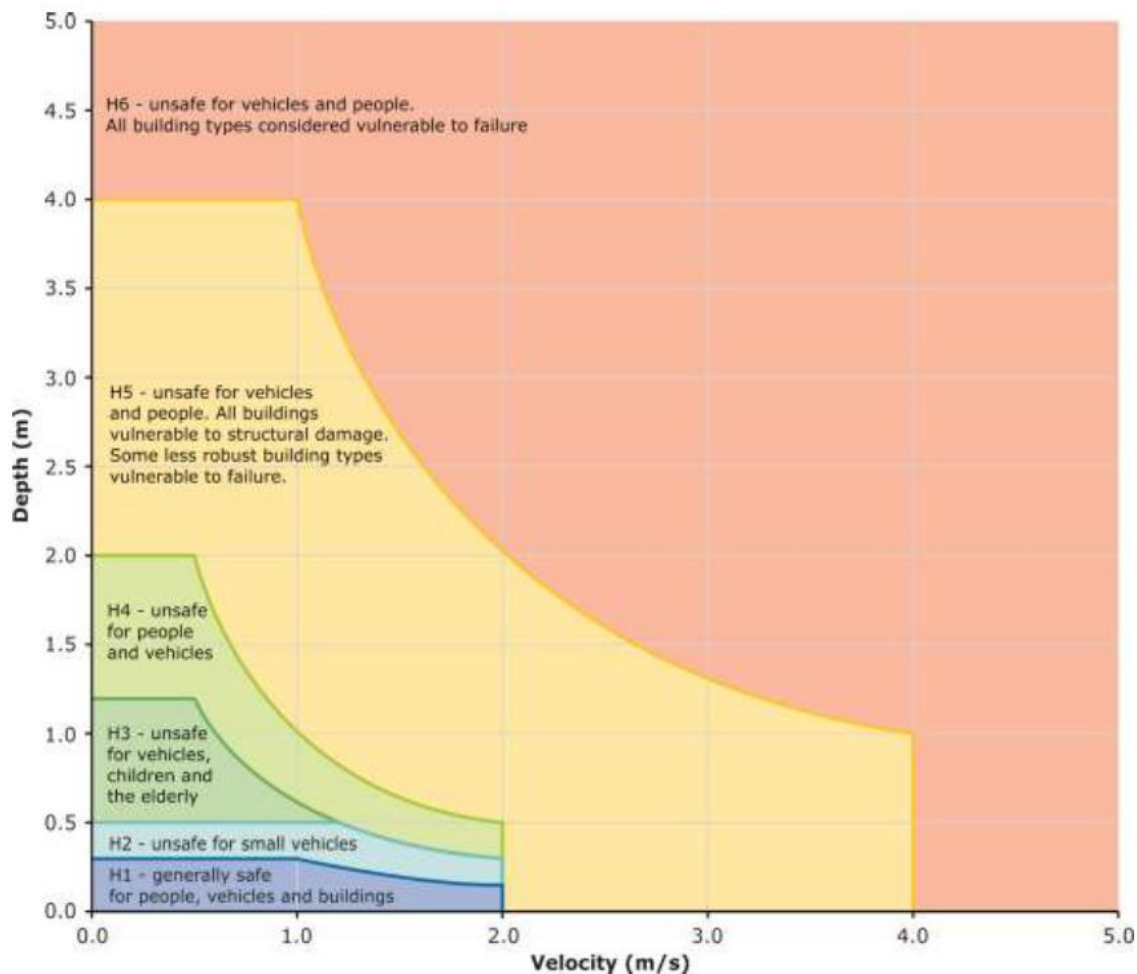


Figure A. 17 - General flood hazard vulnerability curves (AIDR, 2017).

Table A. 1 - Human Stability during flood event (reproduced from Engineers Australia, 2010).

D.V (m/s)	Infants, small children (H.M ≤ 25) and frail/older persons	Children (H.M = 25 to 50)	Adults (H.M > 50)
0	Safe	Safe	Safe
0–0.4	Extreme Hazard; Dangerous to all	Low Hazard	Low Hazard
0.4–0.6		Significant Hazard; Dangerous to most	
0.6–0.8		Extreme Hazard; Dangerous to all	Moderate Hazard; Dangerous to some
0.8–1.2			Significant Hazard; Dangerous to most
>1.2			Extreme Hazard; Dangerous to all

Although the overland flow associated with tsunami is predominantly horizontal (Bryant, 2014), the inundation is more rapid with stronger currents and turbulence. The sequence of a number of waves will see reversing currents. The formation of undular bores (refer Section A.4) can introduce additional forces on structures. Scour can be significant, compromising foundation stability. In addition, the occurrence of tsunami events with recorded damage assessments are much scarcer, relying on documented events post 2004.

The Joint Australian Tsunami Warning Centre (JATWC) provides warnings within Australia based on a no threat, marine warning or land warning. The following sections consider hazard and vulnerability metrics based on the latter two threats.

### **A.5.1 Marine Hazard**

Although tsunami inundation is perhaps the most considerable and obvious risk to the public, there can still be significant damage to maritime facilities from events that do not pose an inundation threat. Within ports and marinas, maritime assets are vulnerable to significant damage from strong currents and associated drag forces (Lynett et al., 2014). The following provides some guidance in relation to vessels and maritime structures.

#### **A.5.1.1 Maritime Users**

Hazards to maritime users from tsunami are most acute in nearshore areas as the tsunami wave enters shallower waters close to the shore.

Tsunamis can pose a significant risk to vessels of all sizes in nearshore areas and ports, due to wave steepness, high current velocities and debris. Tsunami forces on vessels at anchor are likely to impose significant loads on moorings. Due to the impact of tsunamis on the maritime industry from the 2004 and 2011 events, a considerable research effort has seen a variety of guides being produced for the marine industry on tsunami, including estimates of impact based on tsunami amplitude and current velocity (Muhari et al. 2015).

Lynett et al. (2014) undertook a review of recorded damage against measured and modelled tsunami current speeds within ports and harbours predominantly in California following the 2010 Chile and 2011 Great East Japan tsunamis. The results demonstrated distinct thresholds for different levels of damage (defined in Table A. 2) as shown in Figure A. 18, with initiation of damage occurring for speeds above 1.5 m/s. Muhari et al. (2015) developed loss functions for marine vessels based on a multivariate analysis of data collected from the 2011 Great East Japan tsunami together with numerical hydrodynamic modelling of flow velocities. Loss estimation surfaces were developed based on tsunami height, velocity, impact (from floating or static obstructions), and boat material. They found that their results were consistent with that of Lynett et al. (2014), with the model being more sensitive to velocity. They also concluded that collision is a major factor in the determination of vessel loss, significantly reducing the velocity and depth thresholds.

For recreational maritime users, Queensland Government guidance is to where possible moor your vessel and move to high ground. Otherwise, if at sea move offshore into deep water and stay there until further advised (Queensland Government, 2018). Lynett (2014) undertook hydrodynamic modelling for the Californian coast to examine a “safe” depth for evacuation of vessels should there be sufficient lead time prior to tsunami arrival. The modelling showed that navigable currents was the controlling factor, requiring depths greater than 50 m to reduce currents below 1 m/s, and depths greater than 180 m for currents below 0.5 m/s.

**Table A. 2 – Marine facility damage classification from Lynett et al. (2014).**

Damage Index	Damage Type
0	no damage/impacts
1	small buoys moved
2	1–2 docks/small boats damaged and/or large buoys moved
3	Moderate dock/boat damage (<25% of docks/vessels damaged) and/or midsized vessels off moorings
4	Major dock/boat damage (<50% of docks/vessels damaged) and/or large vessels off moorings
5	Extreme/complete damage (>50% of docks/vessels damaged)

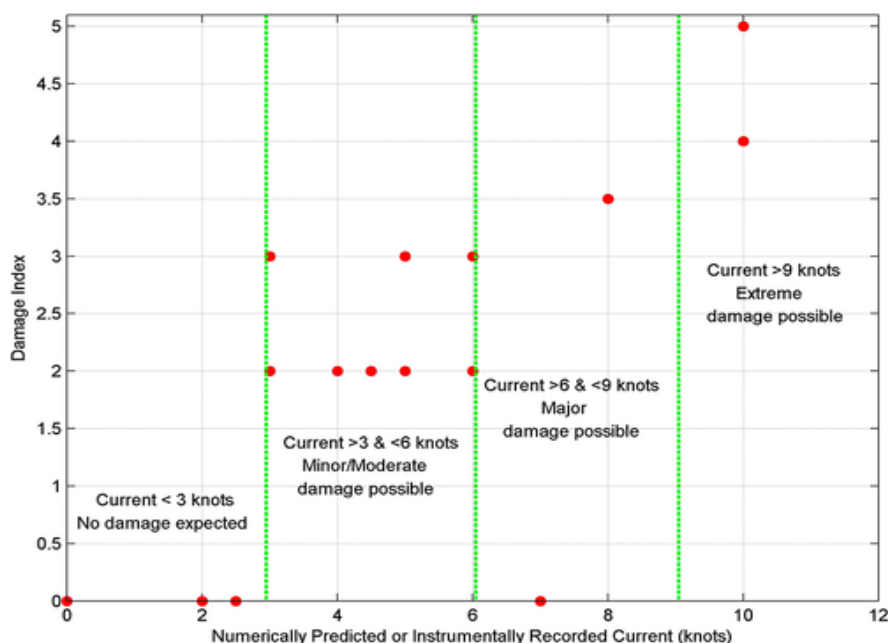


**Figure A. 18 - Damage against tsunami current speed from Lynett et al. (2014).**

**A.5.1.2 Maritime Structures**

Tsunamis have the potential to cause significant damage to coastal and estuarine structures due to the significant forces that can be applied to structures as they may be subject to hydraulic forces beyond tolerable design levels.

Tsunami waves apply exceptional hydraulic forces as they propagate over and around structures, dissimilar to surges and wind derived waves, potentially resulting in significant additional loading on a structure from wave impact forces and debris. Structures can also be impacted by scour due to increased current velocities and water depths. Although these forces are relatively well understood in terms of structure design, they are not well understood in the context of tsunami and are the subject of research.

Although the Australian design standards for maritime structures (Council of Standard Australia, 2002 and 2005) are rigorous in their requirements to assess the resilience of structures from a



variety of hydraulic impacts, the risk from tsunami is neither specifically identified nor particularly well understood.

For port facilities, some guidance is provided in Lynett et al. (2014) as described in the preceding section.

### A.5.2 Land Hazard

The obvious hazards associated with overland progression of tsunamis are inundation or flow depth and extent, high velocities, and debris. A number of factors influence building damage including hydrostatic forces, buoyant forces, hydrodynamic forces, surge forces, impact of floating objects, breaking wave forces, inundation duration and footing scour (Tinti, 2011).

Research into vulnerability measures has mostly developed post 2004, but particularly following the 2011 Great East Japan tsunami. As such, the tsunami community is still in the early stages of understanding how to quantify the physical and social vulnerability. Nevertheless, there is literature available that provides rough guidance. Wijetunge (2009) provides human stability criteria based on the experimental results of Takahashi (2005) as reproduced in Table A. 3.

**Table A. 3 - Human stability in tsunami based on laboratory experiments (Wijetunge, 2009).**

Depth, D (m)	Stability
D < 0.5	Stable, if V < 1.5 m/s
0.5 < D < 1.3	Unstable if V > -1.84D + 2.4
D > 1.3	Unstable for all V

This criteria is similar to classification H3 from the general flood hazard vulnerability curves (Figure A. 17). The above being based on the stability of people caught in currents and so should be considered only as a first approximation. Other factors will influence human stability such as floating debris.

Building vulnerability research has focused on developing empirical damage or fragility functions (probability of exceeding a given damage state based on a measure of tsunami intensity) for a range of structure types and predefined damage states based on post event assessments and laboratory experiments. Most of the recent work in this field has come from the 2011 Great East Japan tsunami. Figure A. 19 provides an example of the typical 2-D fragility functions as developed by Charvet et al. (2015) based on flow depth, where the damage state (DS) relates to the criteria defined by the Japanese Ministry of Land Infrastructure Tourism and Transport as summarized in Table A. 4, noting that they combined DS5 and DS6 as these damage states were seen to not be mutually exclusive.

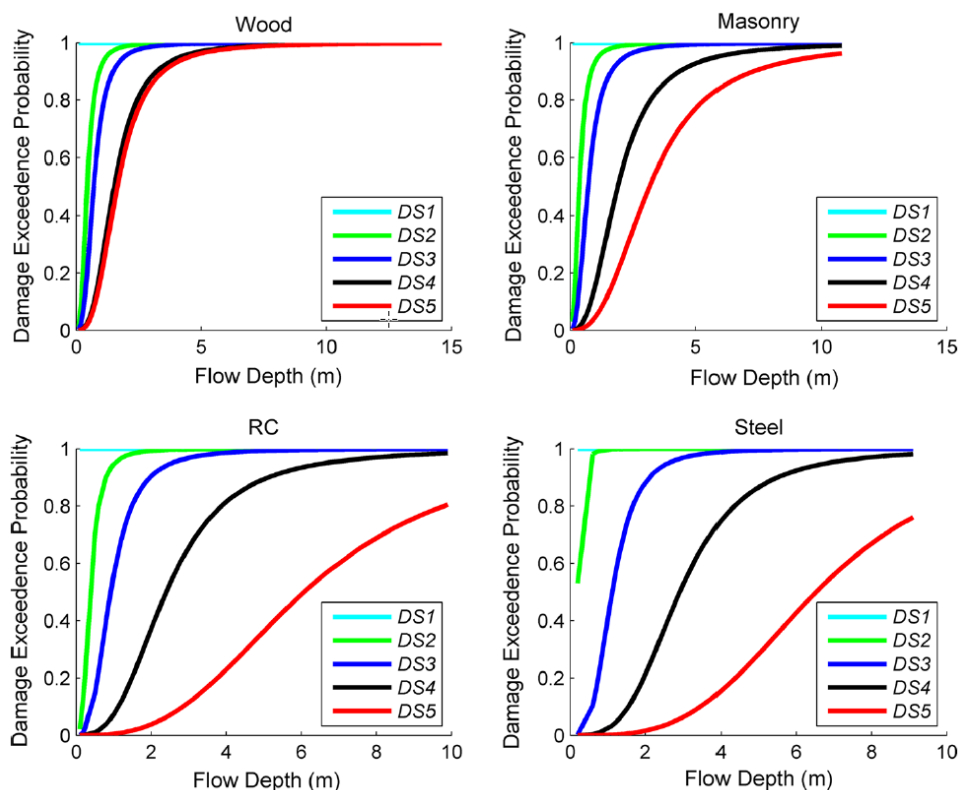


**Figure A. 19 - Two-dimensional fragility functions for Kesennuma City following the 2011 Great East Japan tsunami (Charvet et al., 2015).**

Charvet et al. (2015) also undertook a multivariate analysis using improved statistical methods to develop 3-D fragility surfaces based on flow depth, velocity, structure material, damage state, and debris impact; an example of which is provided in Figure A. 20. They found that flow depth alone is a poor predictor of damage for the stronger construction types (such as reinforced concrete (RC) and steel) at higher damage states, and suggested that both flow velocity and debris impact were important parameters (refer Figure A. 21). The work concluded that the approach provided better fits to the available damage data, but still showed a high level of uncertainty such that further research is required particularly into debris impact, numerical modelling methods for estimating velocities, scour effects, and the influence of additional parameters such as combined depth and velocity.

Charvet et al. (2017) undertook a review of the current state of knowledge in relation to estimating tsunami-induced building damage through fragility functions. The review found that flow depth is the main measure (referred to as Tsunami Intensity Measure or TIM in the paper) adopted in literature, as it can be readily determined from field assessments. Other information such as velocity is important at higher damage states, but difficult to measure in the field without pre-deployed instrumentation. Therefore, estimates of velocities rely on hydrodynamic models that are typically only validated for inundation depth or run-up extent. Park et al. (2013 and 2014) examined the sensitivity of modelled tsunami inundation water level, velocity and momentum flux to overland friction to show that although a tenfold reduction in friction had minor impacts on surface elevation (15% increase), velocity and momentum flux were more sensitive with increases of 95% and 208% respectively. When considering hydrodynamic forces (which are typically proportional to the velocity squared) then the sensitivity can become substantial.

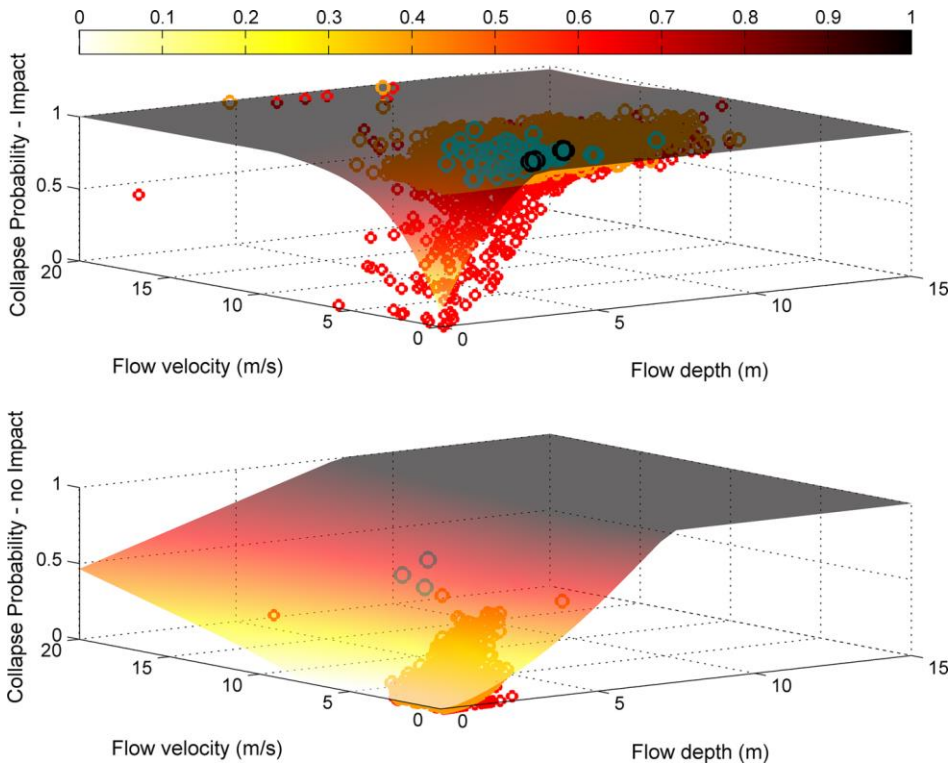








**Figure A. 20 - Example fragility surfaces showing the probability of collapse (DS5) for wood buildings, with and without debris impact (radius: 130 m) based on field survey data following the 2011 Great East Japan tsunami (Charvet et al., 2015).**



**Figure A. 21 - Schematic representation of the contributions of different tsunami intensity measures to the severity of observed damage (Charvet et al., 2015).**

**Table A. 4 - Damage state definitions used by the Japanese Ministry of Land Infrastructure Tourism and Transport following the 2011 Great East Japan Earthquake (source: Charvet et al., 2017).**

Damage	State	Description	Use	Image
DS1	Minor damage	Inundation below ground floor. The building can be reused by removing mud below the floor boards.	Possible to use immediately after minor floor and wall cleanup.	
DS2	Moderate damage	The building is inundated less than 1 m above the floor.	Possible to use after moderate repairs.	
DS3	Major damage	The building is inundated more than 1 m above the floor (below the ceiling)	Possible to use after major repairs	
DS4	Complete damage	The building is inundated above the ground floor level	Major work is required for re-use of the building	
DS5	Collapsed	The key structure is damaged, and difficult to repair to be used as it was before	Not repairable	
DS6	Washed away	The building is completely washed away except for the foundation	Not repairable	

Charvet et al. (2017) also concluded that fragility relationships that have been developed are not necessarily comparable or translatable to other locations due to a number of factors including choice of tsunami intensity measures, building codes (for example engineered structures in Japan versus non-engineered structures in Indonesia), differences in damage state criteria and mutual exclusiveness of each defined damage state, building classifications, field assessment approach (field survey by qualified personnel or remote sensing), completeness of database records, and variations in statistical approaches. Research into fragility functions following the 2011 Great East Japan tsunami also showed they can be location specific, sensitive to local bathymetry, topographic features, building distribution, and the presence of coastal defences. For locations that were also subject to the earthquake, it is difficult to separate earthquake related damage or contributions such as liquefaction. It was therefore concluded by Charvet et al. (2017) that for the

development of fragility functions for locations where damage data is not available, analytical methods for fragility function derivation based on structural analysis are required, incorporating multiple TIMs.

The above discussion outlines the complexity and issues of developing generic vulnerability curves for Tsunami. UNESCO (2015) provides some generic median damage states from Nanayakkara and Dias (2013) for single-storey buildings constructed from commonly used materials based on inundation depth (Table A. 5). The table is based on the median of data from Sri Lanka and Thailand during the 2004 Indian Ocean tsunami, as well as Samoa during the 2009 South Pacific tsunami. Data from the 2011 Great East Japan tsunami were intentionally omitted as these structures performed better given they were newly constructed with proper quality controls. It is likely that Australian building codes would also have higher quality controls.

**Table A. 5 - Median inundation depth ranges by construction and damage state (UNESCO, 2015).**

Damage State	Timber (T)	Masonry (M)	Reinforced Concrete (RC)
Complete (H6)	~1.6 m	2.3–2.5 m	5.4–7.3 m
Major structural (H5)	~1.3 m	~1.9 m	~3.5 m
Minor structural (H4)	~1.2 m	1.3 m	1.4–1.9 m
Non-structural (H3)	0.3–0.5 m	0.3–0.5 m	0.3–0.5 m

Figure A. 22 summarises Table A. 1 and Table A. 5 based on the lower limits for timber structures. Complete damage for masonry and reinforced concrete are also shown as lines. In Figure A. 22, H1 relates to “generally safe for people and buildings” adopted from the general riverine flood vulnerability curves (Figure A. 17), and H2 represents no structural damage. The figure only provides a general indication of potential vulnerability, and should only be used with due consideration of the limitations mentioned above.

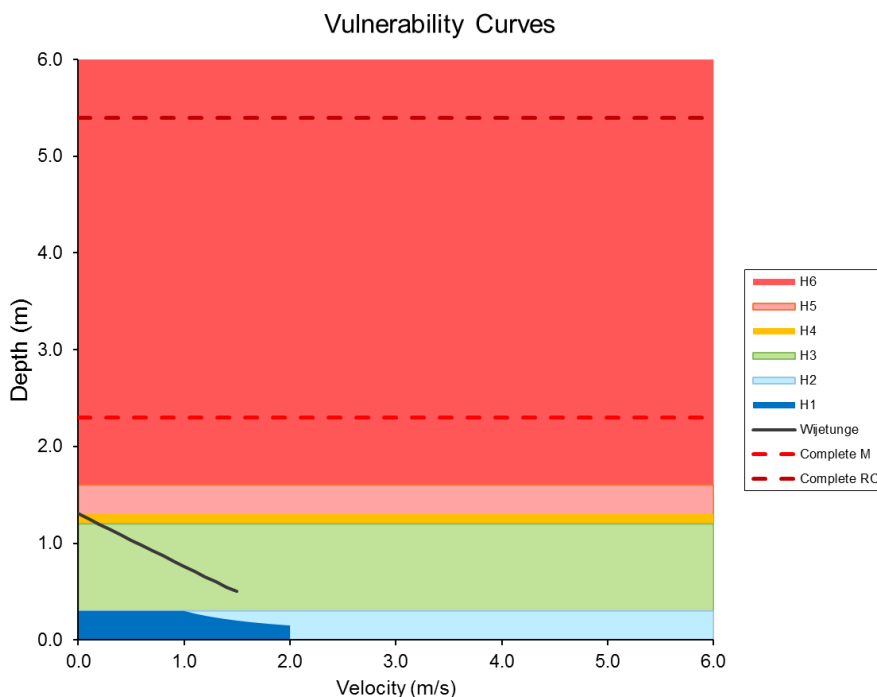


**Figure A. 22 - Combination of general vulnerability curves for tsunami inundation.**



## A.6 Further Information

As discussed above, tsunami generation, propagation and inundation can be complex. Further information can be found in UNESCO/IOC (2010), IOC (2012), IOC (2016), Murata et al. (2010), Bryant (2014), Mofjeld et al. (2004), Geist (1998 and 2009), Synolakis and Bernard (2006), and Borrero et al. (2015). Useful websites include those of National Oceanic and Atmospheric Administration (NOAA, 2018a), the International Tsunami Information Center (ITIC, 2018), and a website produced by the COMET program (UCAR, 2010).

## A.7 References

Australian Institute for Disaster Resilience (AIDR), 2017. Flood Hazard, Australian Disaster Resilience Guideline 7-3, 2<sup>nd</sup> Edition, prepared for the Australian Government Attorney-General's Department, p 30.

Abraimi, R., 2014. Modelling the 2010 Chilean Tsunami using the H<sub>2</sub>Ocean unstructured mesh model, MSc thesis, Civil Engineering and Geosciences, TUDelft, p 64, <https://doi.org/10.1186/s40562-017-0100-9>.

Adriano, B., Fujii, Y., and Koshimura, S., 2018. Tsunami source and inundation features around Sendai Coast, Japan, due to the November 22, 2016 M<sub>w</sub> 6.9 Fukushima earthquake, *Geoscience Letters* 5:2, p 12, <https://doi.org/10.1186/s40562-017-0100-9>.

Bernard, E.N., Mofjeld, H.O., Titov, V., Synolakis, C.E., and González, F.I., 2006. Tsunami: scientific frontiers, mitigation, forecasting and policy implications, *Phil. Trans. R. Soc. A* 364, pp 1989–2007, doi:10.1098/rsta.2006.1809.

Borrero, J.C., Lynett, P.J., and Kalligeris, N., 2015. Tsunami currents in ports, *Phil. Trans. R. Soc. A* 373: 20140372, p 19, <http://dx.doi.org/10.1098/rsta.2014.0372>.

Bryant, E., 2014. *Tsunami: The Underrated Hazard*, Third Edition, Springer, p 222.

Charvet, I., Macabuag, J., and Rossetto, T., 2017. Estimating Tsunami-Induced Building Damage through Fragility Functions: Critical Review and Research Needs, *Front. Built Environ.*, Vol 3(36), p 22, doi: 10.3389/fbuil.2017.00036.

Charvet, I., Suppasri, A., Kimura, H., Sugawara, D., and Imamura, F., 2015. Fragility estimations for Kesennuma City following the 2011 Great East Japan Tsunami based on maximum flow depths, velocities and debris impact, with evaluation of the ordinal model's predictive accuracy, *Nat.Hazards* 79, pp 2073–2099, doi:10.1007/s11069-015-1947-8.

Council of Standard Australia, 2002. *Structural Design Actions – General Principles*. (AS /NZS 1170-2002). SAI Global Pty Ltd.

Council of Standard Australia, 2005. *Guidelines for the design of maritime structures*. (AS /NZS 4997-2005). SAI Global Pty Ltd.

Engineers Australia, 2010. *Appropriate Safety Criteria for People, Stage 1 Report*, Australian Rainfall & Runoff Revision Project 10, P10/S1/006, April, p 21.

Fuller, J.D. and Mysak, L.A., 1977. Edge waves in the presence of an irregular coastline, *J. Phys. Oceanogr.*, Vol 7(6), pp 846–855.

- Geist, E.L., 1998. Local Tsunamis and Earthquake Source Parameters, *Advances in Geophysics*, Vol 39, pp 117–209, [https://doi.org/10.1016/S0065-2687\(08\)60276-9](https://doi.org/10.1016/S0065-2687(08)60276-9).
- Geist, E.L., 2009, Chapter 3 - Phenomenology of Tsunamis: Statistical Properties from Generation to Runup, *Advances in Geophysics*, Vol 51, pp 107–169, [https://doi.org/10.1016/S0065-2687\(09\)05108-5](https://doi.org/10.1016/S0065-2687(09)05108-5).
- Geist, E.L., Lynett, P.J., and Chaytor, J.D., 2009. Hydrodynamic modelling of tsunami from the Currituck landslide, *Marine Geology*, 264, pp 41–52.
- González, F.I., 1999. Tsunami!, *Scientific American*, May, pp 56–65.
- González, F.I., Satake, K., Boss, E.F., and Mofjeld, H.O., 1995. Edge Waves and Non-trapped Modes of the 25 April 1992 Cape Mendocino Tsunami, *Pure & Applied Geophysics*, Vol 144(3), September, pp 409–426, DOI: 10.1007/BF00874375.
- Horrillo, J., Knight, W., and Kowalik, Z., 2008. Kuril Islands tsunami of November 2006: 2. Impact at Crescent City by local enhancement, *J. Geophys. Res.*, Vol 113, C01021, p 12, doi: 10.1029/2007JC004404.
- Intergovernmental Oceanographic Commission (IOC), 2012. *Tsunami: The Great Waves*, Second Revised Edition, Paris, UNESCO, illus. IOC Brochure 2012-4. (English), p 16.
- Intergovernmental Oceanographic Commission (IOC), 2016. *Tsunami Glossary*, Third Edition, Paris, UNESCO, IOC Technical Series 85. (English, French, Spanish, Arabic, Chinese) (IOC/2008/TS/85 rev.2).
- International Tsunami Information Center (ITIC), 2018. Web page accessed in 2018, URL: <http://itic.ioc-unesco.org/index.php>.
- Kayal, J.R., 2016. *Seismic Waves and Earthquake Location*, Geological Survey of India, Lecture notes for a training course: Preparing for the Next Tsunami: Training in Seismology and Tsunami Warnings in the Indian Ocean Region, offered by Mooney, W.D., USGS, URL: <https://escweb.wr.usgs.gov/share/mooney/training%20courses.html>
- Lynett, P. J., Borrero, J., Son, S., Wilson, R., and Miller, K., 2014. Assessment of the tsunami-induced current hazard, *Geophys. Res. Lett.*, 41, pp 2048–2055, doi:10.1002/2013GL058680.
- Madsen, P.A., Fuhrman, D.R., and Schäffer, H.A., 2008. On the solitary wave paradigm for tsunamis. *J. Geophys. Res.*, Vol 113, C12012, p 22, doi:10.1029/2008JC004932.
- Madsen, P.A., Fuhrman, D.R., and Wang, B., 2006. A Boussinesq-type method for fully nonlinear waves interacting with a rapidly varying bathymetry, *Coast. Eng.*, 53, pp 487–504.
- Maritime Safety Queensland (MSQ), 2017. *Queensland Tide Tables: Standard Port Tide Times 2018*, Dept of Transport and Main Roads, Queensland Government, p 128.
- Mei, C.C., Stiassnie, M., and Yue, D. K.-P., 2005. *Theory and Applications of Ocean Surface Waves, Part 1: Linear Aspects*, Advanced Series on Ocean Engineering, Vol 23, World Scientific, pp 172–173.
- Mofjeld, H.O., González, F.I., Titov, V.V., Venturato, A.J., and Newman, J.C., 2007. Effects of Tides on Maximum Tsunami Wave Heights: Probability Distributions, *J. Atmos. Oceanic Technol.*, 24, 117–123, <https://doi.org/10.1175/JTECH1955.1>

- Mofjeld, H.O., Symons, C.M., Lonsdale, P., González, F.I., and Titov, V.V., 2004. Tsunami Scattering and Earthquake Faults in the Deep Pacific Ocean, *Oceanography*, Vol 17(1), pp 38–46.
- Mofjeld, H.O., Titov, V.V., González, F.I., and Newman, J.C., 2000. Analytic Theory of Tsunami Wave Scattering in the Open Ocean with Application to the North Pacific, NOAA Tech Memo OAR PMEL-116, , Jan, p 37.
- Mofjeld, H.O., Titov, V.V., González, F.I., and Newman, J.C., 2001. Tsunami scattering provinces in the Pacific Ocean, *Geophysical Res Letters*, Vol 28(2), Jan 15, pp 335–338.
- Muhari, A., Charvet, I., Tsuyoshi, F., Suppasri, A., Imamura, F., 2015 Assessment of tsunami hazards in ports and their impact on marine vessels derived from tsunami models and the observed damage data, *Natural Hazards*, 78 (2), pp. 1309–1328.
- Munger, S., and Cheung, K.F., 2008. Resonance in Hawaii waters from the 2006 Kuril Islands Tsunami, *Geophys. Res. Lett.*, Vol 35, L07605, p 7, doi: 10.1029/2007GL032843.
- Murata, S., Imamura, F., Katoh, K., Kawata, Y., Takahashi, S., Takayama, T. (eds), 2010. Tsunami: To Survive from Tsunami, *Advanced Series on Ocean Engineering*, Volume 32, World Scientific, p 302.
- Nanayakkara, K.I.U. and Dias, W.P.S., 2013. Fragility curves for tsunami loading, *International Conference on Structural Engineering & Construction Management*, Kandy.
- Neetu, S., Suresh, I., Shankar, R., Nagarajan, B., Sharma, R., Shenoi, S.S.C., Unnikrishnan, A.S., and Sundar, D., 2011. Trapped waves of the 27 November 1945 Makran tsunami: observations and numerical modeling, *Nat. Hazards*, Vol 59, pp 1609-1618, DOI: 10.1007/s11069-011-9854-0.
- Nielsen, P., 2012. Coastal and Estuarine Processes, *Advanced Series on Ocean Engineering*, Vol 29, World Scientific, p 343.
- NOAA, 2018a. Tsunami: The Tsunami Story (web page accessed 2018), URL: [https://www.tsunami.noaa.gov/tsunami\\_story.html](https://www.tsunami.noaa.gov/tsunami_story.html).
- Okada, Y., 1985. Surface Deformation due to Shear and Tensile Faults in a Half-Space, *Bulletin of the Seismological Society of America*, Vol 75(4), August, pp 1135–1154.
- Okada, Y., 1992. Internal Deformation due to Shear and Tensile Faults in a Half-Space, *Bulletin of the Seismological Society of America*, Vol 82(2), April, pp 1018–1040.
- Park, H., Cox, D.T., Lynett, P.J., Wiebe, D.M., & Shin, S., 2013. Tsunami inundation modeling in constructed environments: A physical and numerical comparison of free-surface elevation, velocity, and momentum flux, *Coastal Engineering*, Vol 79, pp 9-21, doi: <https://doi.org/10.9753/icce.v34.currents.1>
- Park, H., Wiebe, D., and Cox, D.T., 2014. Tsunami inundation modeling: sensitivity of velocity and momentum flux to bottom friction with application to building damage at Seaside, Oregon, *Coast. Eng. Proc.*, No 34, Korea, p 12. URL: [https://icce-ojs-tamu.tdl.org/icce/index.php/icce/article/view/7557/pdf\\_985](https://icce-ojs-tamu.tdl.org/icce/index.php/icce/article/view/7557/pdf_985)
- Queensland Government, 2018. Tsunami, URL: <https://www.qld.gov.au/emergency/dealing-disasters/disaster-types/tsunami>.

- Queensland Fire and Emergency Services (QFES), 2018. Queensland Emergency Risk Management Framework (QERMF) Risk Assessment Process Handbook, Queensland Government, p 53.
- Rabinovich, A.B., Stephenson, F.E., and Thomson, R.E., 2006. The California tsunami of 15 June 2005 along the coast of North America, *Atmosphere-Ocean*, Vol 44(4), pp 415-427, DOI: 10.3137/ao.440406.
- Rasyif, T.M, Kato, S., Syamsidik, Okabe, T., 2016. Influence of Small Islands against Tsunami Wave: Impact along Sumatra Island, *Journal of Japan Society of Civil Engineers*, Vol 72(2), pp I\_331-I\_336.
- Roeber, V., Yamazaki, Y., and Cheung, K. F., 2010. Resonance and impact of the 2009 Samoa tsunami around Tutuila, American Samoa, *Geophys. Res. Lett.*, Vol 37(21), L21604, p 8, doi: 10.1029/2010GL044419.
- Satake, K., 1987. Inversion of Tsunami Waveforms for the Estimation of a Fault Heterogeneity: Method and Numerical Experiments, *J. Phys. Earth*, Vol 35, pp 241–254.
- Stefanakis, T.S., Contal, E., Vayatis, N., Dias, F., Synolakis, C.E., 2014. Can small islands protect nearby coasts from tsunamis? An active experimental design approach, *Proceedings of the Royal Society A*, 470:20140575, p 20.
- Synolakis, C.E., Bardet, J.P., Borrero, J.C, Davies, H.L., Okal, E.A., Silver, E.A., Sweet, S., and Tappin, D.R., 2002. The slump origin of the 1998 Papua New Guinea Tsunami, *Proc. R. Soc. A*, Vol. 458, pp 763–789; DOI: 10.1098/rspa.2001.0915.
- Synolakis, S.E., and Bernard, E.N., 2006. Tsunami science before and beyond Boxing Day 2004, *Phil. Trans. R. Soc. A*, Vol 364, Issue 1847, pp 2231–2265, doi:10.1098/rsta.2006.1824.
- Synolakis C.E., and Skjelbreia J.E., 1993. Evolution of Maximum Amplitude of Solitary Waves on Plane Beaches, *J. Waterway, Port, Coastal, and Ocean Engineering*, Vol 119(3), ASCE, May, pp 323–342, doi: 10.1061/(ASCE)0733-950X(1993)119:3(323)
- Tadepalli, S., and Synolakis, C.E., 1994. The run-up of N-waves on sloping beaches. *Proc. R. Soc. Lond. A*, 445, pp 99–112, DOI: 10.1098/rspa.1994.0050.
- Tappin, D.R., Watts, P., and Grilli, S.T., 2008. The Papua New Guinea tsunami of 17 July 1998: anatomy of a catastrophic event, *Natural Hazards and Earth System Sciences*, 8, pp 243-266, <https://doi.org/10.5194/nhess-8-243-2008>.
- Tinti, S., Tonini, R., Bressan, L., Armigliato, A., Gardi, A., Guillande, R., Valencia, N., and Scheer, S., 2011. Handbook on tsunami hazards and damage scenarios: SCHEMA, Project No. 030963, JRC Scientific and Technical Reports, EUR 24691 EN, European Union, p 40.
- Truong, H.V.P, 2012. Wave-Propagation Velocity, Tsunami Speed, Amplitudes, Dynamic Water-Attenuation Factors, *Proc. 15<sup>th</sup> World Conf. on Earthquake Engineering*, Lisbon, p 10.
- United Nations Office for Disaster Risk Reduction (UNISDR), 2017. Words into Action Guidelines: National Disaster Risk Assessment, 2. Tsunami Hazard and Risk Assessment, p 9.
- University Corporation for Atmospheric Research (UCAR), 2010. Tsunami: Produced by the COMET Program (web site accessed 2018), URL: <http://www.torbenespersen.dk/Publish/tsunami/index.htm>

UNESCO, 2015. Tsunami risk assessment and mitigation for the Indian Ocean; knowing your tsunami risk – and what to do about it, IOC Manual and Guides No 52, Second Edition, p 160.

UNESCO/IOC, 2010. Where the First Wave Arrives in Minutes: Indonesian Lessons on Surviving Tsunamis Near Their Sources, IOC Brochure 2010-4, pp 36.

USGS, 2018a. The Science of Earthquakes (web page accessed in 2018), Earthquake Hazards Program, URL: <https://earthquake.usgs.gov/learn/kids/eqscience.php>

Wijetunge, J.J., 2009. Demarcation of High Hazard Areas Based on Human Stability Considerations in Tsunami Overland Flow, Engineer, Vol XXXXII (01), Institute of Engineers, Sri Lanka, pp 45-52.

Wong, R.H.C., Lin, H.Y., Chau, K.T., and Wai, O.W.H., 2008. Experimental study on edge wave effect inducing by tsunami at Phi-Phi Island (Thailand), 14<sup>th</sup> World Conference on Earthquake Engineering, Oct 12-17, Beijing, China, pp 9.

Yamazaki, Y., 2010. Depth-Integrated, Non-hydrostatic Model with Grid Nesting for Tsunami Generation, Propagation, and Run-up, PhD Thesis, University of Hawai'i, Manoa, pp 107.

Yamazaki, Y., and Cheung, K.F., 2011. Shelf resonance and impact of near-field tsunami generated by the 2010 Chile earthquake, Geophys. Res. Lett., Vol 38, L12605, p 8, doi: 10.1029/2011GL047508.



## Appendix B – Model Calibration

### B.1 Introduction

The standard approach to calibrating 2D hydrodynamic models involves adjusting model parameters such as bed roughness, horizontal eddy viscosity, and bathymetry to match measured water level and/or velocity data collected within the study area. This may involve a range of conditions that are expected to influence the local hydrodynamics. Once calibrated, the model is then validated against measured events.

As explained in Boswood (2013), the availability of measured tsunami events along the Queensland coast is scarce, and inundation mapping from historic events is non-existent. As tidal water level data are more readily available, the 2013 study (Stage 1) calibrated the regional models against tide water level predictions for 83 sites over a spring tide period in January to February 2011.

For consistency, the current study undertook to calibrate against predicted tides for the same period considered in the Stage 1 study (Boswood, 2013). However, due to the computation time required to model tides over the 39-day period for the fine resolution Stage 3 mesh, a subset of two weeks from 15–28 January 2011 was considered. This represented a spring to neap cycle.

### B.2 Tide Data and Boundary Conditions

Calibration is based on astronomical tides only (no meteorological component). Model results are compared against predicted tides for sites where tidal constituents are available. This provides a good measure of model skill with minimal complication from uncertainty in model boundary condition data that can occur by introducing meteorological components from forecast or hindcast models.

Boundary conditions were provided by a larger scale tide model of the Coral Sea, originally developed in 2006 (Callaghan et al., 2007), and later refined for Stage 1 (Boswood, 2013) (refer Figure B. 1). The open boundaries of the regional tide model are forced by water levels defined by eight harmonic constituents previously provided by the National Tidal Centre. Inland areas were omitted from the modelling to reduce computation times.

For this study, six prediction sites from the previous study were located within the study area (Caloundra Head, Tangalooma Point, Bongaree, Brisbane Bar, Brisbane Port Office, and Gold Coast Seaway). The sites at Noosa and Point Danger are outside the fine mesh region and were not included, together with the Nerang Site as it is not resolved within the current model. As these sites are outside the area of interest, their omission will not influence model skill.

### B.3 Assessment Approach

The calibration undertaken in Stage 1 involved assessing the skill of the model. The assessment was based on the Index of Agreement (IofA) (Wilmott, 1981), the Coefficient of Determination ( $R^2$ ) (Kreyszig, 1999), along with the Root Mean Square Error (RMSE) normalised to the amplitude of the Highest Astronomical Tide (HAT) (that is, the height of HAT above Mean Sea Level (MSL)). The criteria adopted are detailed in Table B. 1. The skill scores provide a statistical measure of agreement between the observed (predicted tides) and modelled data.

**Table B. 1 - Skill score classification (Boswood, 2013).**

Criteria	lofA	R <sup>2</sup>	RMSE (percentage)
excellent	>0.95	>0.925	<10
satisfactory	0.85–0.95	0.85–0.925	10–20
poor	0.5–0.85	0.5–0.85	20–30
reject	<0.5	<0.5	>30

The resulting calibration for Stage 1 indicated that over 90 per cent of the 83 sites to be of excellent agreement and 99 per cent to be above satisfactory based on this criteria. Only one site was deemed to be poor, but the tide site is located within Runaway Bay on the Gold Coast which is not adequately resolved within the Stage 1 mesh (Boswood, 2013).

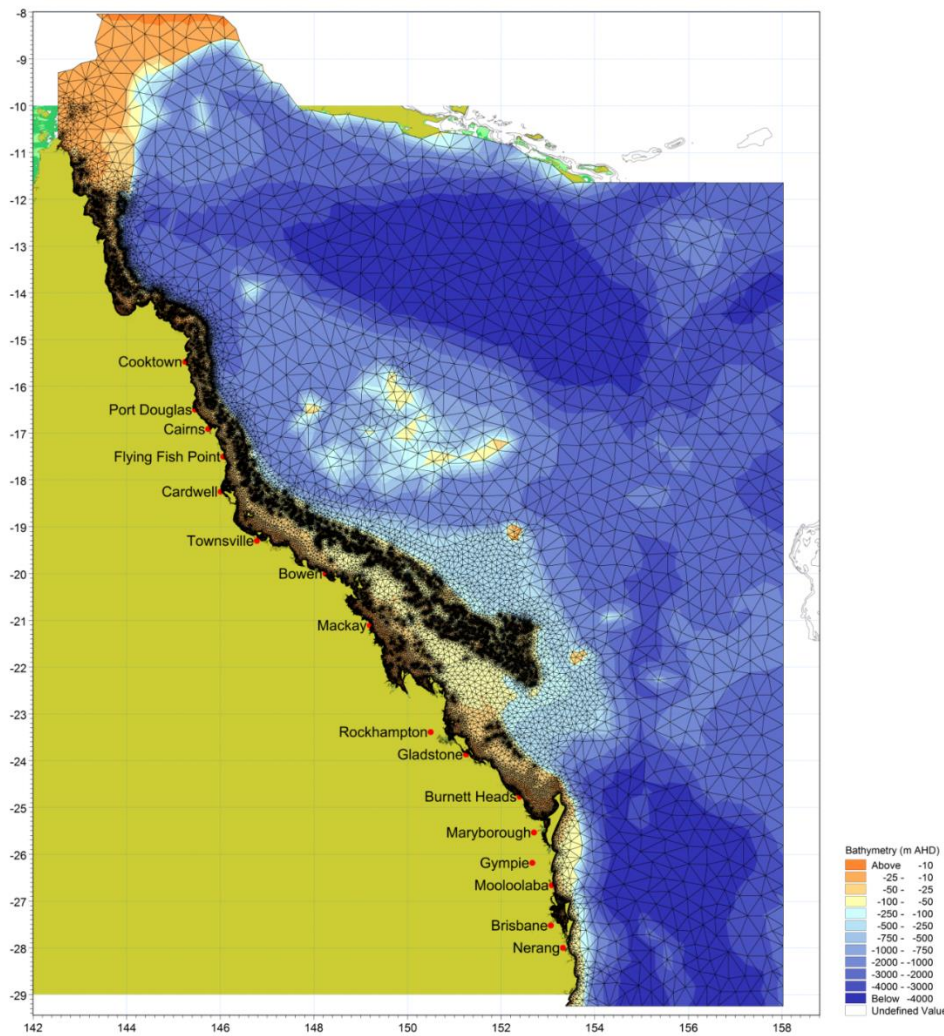


**Figure B. 1 - Regional tide model domain (Boswood, 2013).**

### B.4 Calibration Results

A range of uniform Manning’s roughness values between  $n=0.02$  to  $0.03$  (Manning’s  $M = 50$  to  $33.3$ ) were tested, as well as increased roughness in the rivers. The horizontal eddy viscosity was also tested based on depth dependent values, and a constant value using the Smagorinsky

formulation (Smagorinsky, 1963). Each scenario was scored in a similar way to the Stage 1 assessment and the best performing scenario overall was chosen for final modelling.

Increases in roughness had little influence on the open coast sites due to the narrow continental shelf, as noted in Stage 1. The influence was more notable within Moreton Bay and the Brisbane River, with some reduction in ranges and increased lag in tidal phase. Changes in eddy viscosity had little impact on the tides.

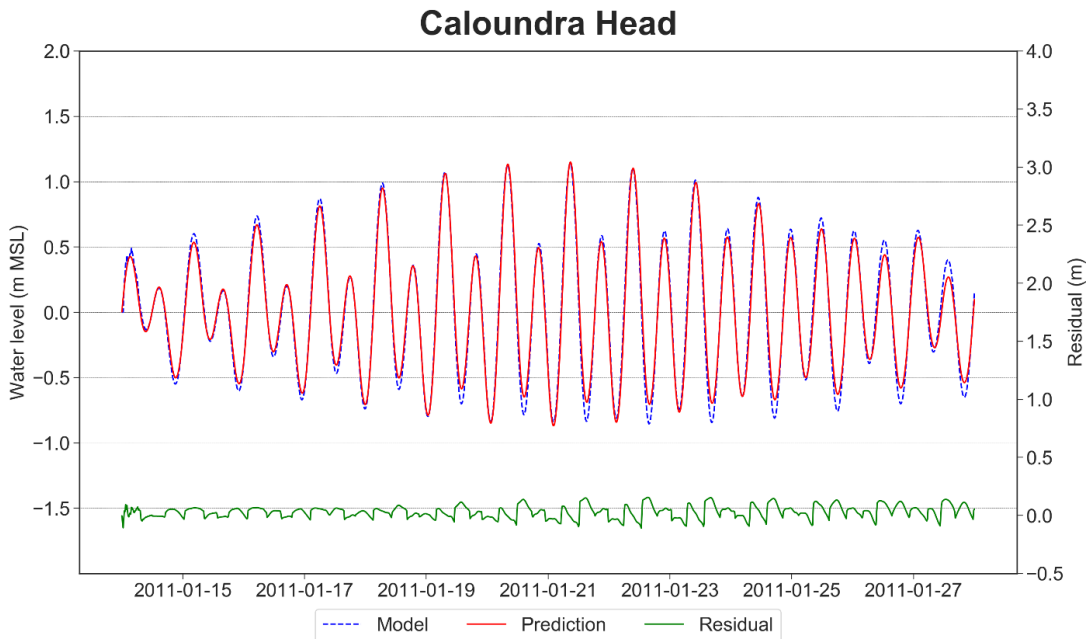


**Figure B. 2 - A comparison of the modelled results for the final calibration scenario at Caloundra Head.**

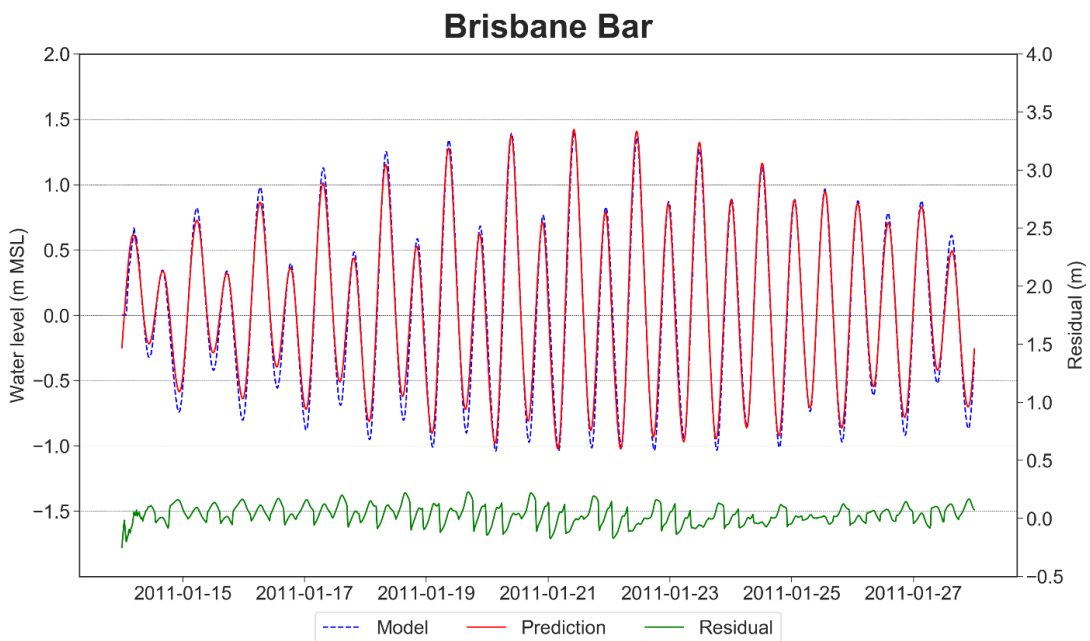


**Figure B. 3 - A comparison of the modelled results for the final calibration scenario at Brisbane Bar.**

Figure B. 2 and Figure B. 3 demonstrate the performance of the model for the final calibration parameters (constant Manning's M of 40 and constant Smagorinsky value of 0.28) at Caloundra Head (ocean side site), and Brisbane Bar (within Moreton Bay) respectively. The skill for all of the chosen six tide sites within the study area scored excellent for the lofA,  $R^2$  and RMSE. This is an improvement to the previous calibration during Stage 1, an expected outcome given the finer resolution and improved bathymetry data sets applied to Stage 3. The results indicate that the model captures the hydrodynamics associated with long period tides.

## **B.5 References**

Boswood, P.K. 2013. Tsunami Modelling along the East Queensland Coast, Report 1: Regional Modelling. Brisbane: Department of Science, Information Technology, Innovation and the Arts, Queensland Government, p 111.

Callaghan, D.P., Boswood, P.K., and Voisey, C., 2007. Modelling Queensland Tides from the Gold Coast to Cooktown, Coasts and Ports 2007, Engineers Australia, 18-20 July, Melbourne.

Kreyszig, E., 1999. Advanced engineering mathematics, Vol. New York: John Wiley, p 1156.

Smagorinsky, J., 1963. General Circulation Experiment with the Primitive Equations, Monthly Weather Review, 91(3), pp 99-164.

Wilmott, C.J., 1981. On the validation of models. Physical Geography, Vol. 2(2). Pp 184-194.

## Appendix C – Validation and Sensitivity Testing

### C.1 Introduction

The original Stage 1 model (Boswood, 2013) was validated against the 2007 Solomon Islands tsunami event that was captured by the then Queensland Environmental Protection Agency's (EPA) storm tide monitoring network. Given the purpose of Stage 1 was to assess nearshore amplification up to the 10 m depth contour, this model was coarser than the current mesh and did not include overland flooding (i.e. a fixed land boundary at RL -0.5 m AHD). The previous validation was therefore revisited for the current mesh.

### C.2 2007 Solomon Islands Tsunami Event

On 01 April 2007, at about 20:39:58 UTC, an 8.1 magnitude earthquake occurred at latitude 8.481° south and longitude 156.978° east as a result of shallow thrust faulting along the boundary of the Pacific plate with the Australia, Woodlark, and Solomon Sea microplates (Hayes et al., 2017). The epicentre of the quake was about 43 km south southeast of Gizo in the Solomon Islands, and approximately 540 km west northwest of the capital Honiara (EPA, 2007). The earthquake (which lasted for more than one minute) generated a tsunami that devastated the local islands with run-up heights up to 12.1 m, resulting in 52 deaths and destroying 2,500 buildings (McAdoo et al., 2008 and NOAA, 2018b). Over three hours later, the tsunami started to reach the Queensland coastline. The waves that were measured by a number of Queensland tide gauges were of much smaller magnitude. Amplitudes along the east coast of Queensland were typically less than 0.1 m with the exception of Clump Point and Rosslyn Bay, which recorded in the order of 0.25 metres (EPA, 2007).

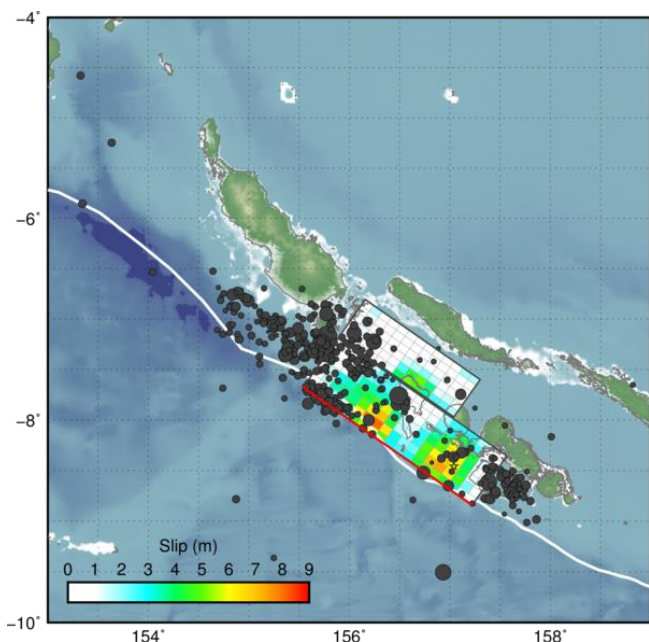


**Figure C. 1 - Surface projection of the slip distribution for the 2007 Solomon Island earthquake superimposed on GEBCO bathymetry (USGS: <https://earthquake.usgs.gov/earthquakes/eventpage/usp000f83m#finite-fault>).**

A number of sources describe the sea bed deformations with some variations. NOAA (2018b) refers to an uplift of up to 3.6 m and subsidence down to 1.5 m, resulting in reports of tsunami



waves between 2 to 10 m. USGS (2018b) have the origin at latitude 8.466° south and longitude 157.043° east with a depth of 24 km (last updated 7 February 2017). Their preliminary finite faults analysis is shown in Figure C. 1 based on two segments with a strike of 305 degrees and dip of 14 and 30 degrees respectively. Their modelling of the earthquakes implies a fault area of 200 x 80 kilometres.

Based on a fault area of 180 x 60 km, a 300 degree strike and 14 degree slip, Koshimura (2018) developed the deformation map shown in Figure C. 2. Further information about the earthquake can be found in Fisher et al. (2007) and Chen et al. (2009).

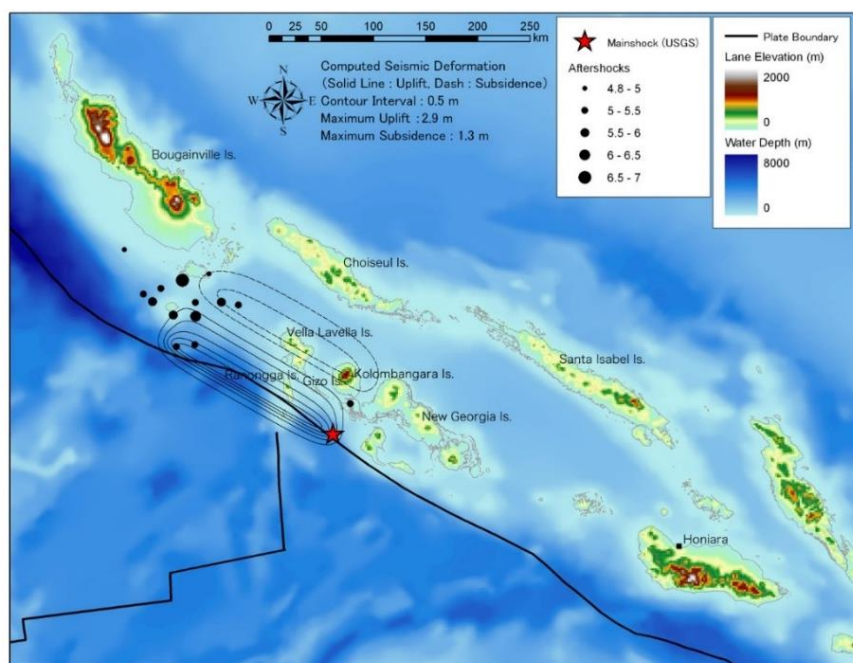


**Figure C. 2 - Seabed deformation during 2007 Solomon Island earthquake (Dr S Koshimura: [http://www.tsunami.civil.tohoku.ac.jp/hokusai2/disaster/07\\_Solomon/event.html](http://www.tsunami.civil.tohoku.ac.jp/hokusai2/disaster/07_Solomon/event.html))**

### C.3 Tsunami Event Data and Boundary Conditions

The 2007 Solomon Island tsunami event was captured by the then Queensland Environmental Protection Agency's (EPA) storm tide monitoring network at a 1 min sampling rate. Unfortunately, there are no measurements available within Moreton Bay for this event. Only two sites were available within the model domain: Gold Coast Seaway and Mooloolaba.

Boundary conditions for the Stage 3 model, in the form of water level and depth averaged velocity time series, were obtained from the Stage 1 validation model (as shown in Figure C. 3).

The offshore boundary is located at 158° longitude. The north-east corner has been clipped to be more parallel with the wave crest, connecting to the south-east extent of Papua New Guinea (refer Figure C. 3). As the tsunami was generated from an earthquake some 500 km north of the north-east corner of the mesh, boundary conditions in the form of a varying water level time series along the open offshore boundaries were provided courtesy of Geoscience Australia (GA) and consists of a maximum leading wave ranging between 0.7 m in the north and 0.05 m in the south. Although the land boundary was based on a GIS shapefile polyline representing 0 m AHD, the depths along the boundary interpreted from the gbr100 DEM varied between -1.5 m and -15 m AHD. The mesh consists of 1,179,240 triangular elements with areas generally ranging from 17 km<sup>2</sup> offshore to 31,000 m<sup>2</sup> near the coast. This equates approximately to an equivalent spatial resolution of 6 km

offshore to 250 m along the coast. Finer meshes with equivalent spatial resolutions down to 50 m were incorporated in the vicinity of storm tide gauge locations. Tides were excluded, with the tsunami time series applied to a constant water level set to Mean Sea Level (MSL). The mesh extent and modelled maximum water levels are shown in Figure C. 3.

The Stage 1 model was re-run to provide time series output of water level and depth averaged velocities at the 1,000 m depth contour. This was then used as boundary conditions for the Stage 3 model.

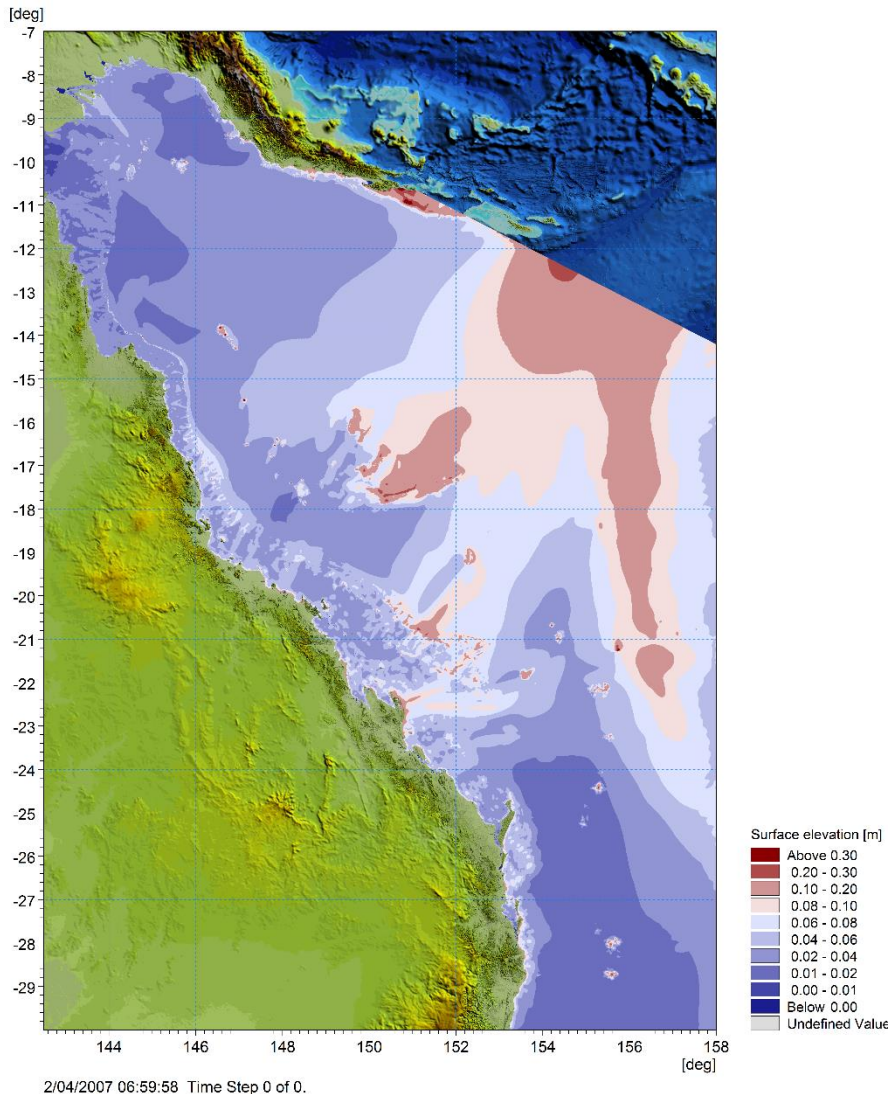


**Figure C. 3 - Stage 1 mesh domain and maximum water level for 2007 Solomon Islands tsunami model validation.**

## C.4 Validation Results

The results of the validation for the Stage 3 mesh are provided in Figure C. 4 and Figure C. 5 for Gold Coast Seaway and Mooloolaba respectively, and are summarised in Table C. 1 in terms of the maximum amplitude and Table C. 2 for arrival times. The two locations are within the model domain but outside of the finer mesh within the study region. The Mooloolaba monitoring site was located at the pilot jetty in the Mooloolah River. The river is not resolved within the Stage 3 mesh as it is outside the study region. A location just offshore was used for this comparison. The Gold Coast Seaway monitoring site was located at the southern end of the Broadwater. The resolution in

this area is better represented than the original model, but is still relatively coarse. It therefore may not pick up the complex interactions with bathymetry, bank protection works and shoreline/bank configuration. Being in river entrances, the two locations will be influenced by tidal currents, particularly the Gold Coast Seaway. These currents are not represented in the model.

There is also some uncertainty associated with the boundary water level time series as there were no offshore measurement sites in the Coral Sea to validate the Stage 1 model against, and as described in Pedersen et al. (2005) and Luger and Harris (2010), it is possible that there may be some numerical dispersion with a 6 km offshore mesh resolution. Sensitivity testing demonstrated that the model became too dispersive when the offshore mesh resolution was increased. The boundary conditions for the Stage 1 model are also the result of a model run from Geoscience Australia.

Despite these limitations, the modelled results perform well against the measured data in terms of arrival times and the amplitude of the leading wave. Table C. 2 provides the measured and modelled arrival times relative to the time of the earthquake. The arrival time is defined as the time when the leading edge of the tsunami deviates by more than 1 cm from mean sea level. Determination of the recorded arrival times for the monitoring sites can be complicated by the tsunami amplitude being comparable in magnitude to the background meteorological fluctuations preceding the event. There is only a one minute difference for Mooloolaba. There is an eight minute difference for the Gold Coast. However, this may be due to differences in locations as the model does not define the Nerang River. Both model sites perform well on the leading wave amplitude, but underestimate the higher subsequent wave. They also do not capture the higher frequency oscillations observed in the measured data. This is most likely due to local scale interactions such as reflections that are not captured with the coarser mesh in these areas. This is a plausible conclusion when we look at the results of the Stage 1 model for Mooloolaba (Figure C. 5). The Stage 1 model includes the Mooloolah River and we can see it captures the height of the largest wave. Both model results compare well for the first three waves.

**Table C. 1 - Measured and modelled maximum tsunami amplitude for the 2007 Solomon Islands tsunami.**

Site	Location	Measured Maximum Amplitude (m)	Stage 1 Max Amplitude (m)	Stage 3 Max Amplitude (m)
Mooloolaba	Pilot jetty within Mooloolah River	0.12	0.10	0.07
Gold Coast Seaway	Within the Broadwater	0.10	0.04	0.05
Gold Coast Seaway Entrance	Model point on the open coast near Seaway entrance	-	0.12	0.12

**Table C. 2 - Tsunami arrival times following the 2007 Solomon Islands earthquake for select tide sites.**

Site	Measured Arrival Time (h:min)	Stage 1 Model (MSL) Arrival Time (h:min)	Stage 3 Model (MSL) Arrival Time (h:min)
Mooloolaba	4:11	4:09	4.11
Gold Coast Seaway	4:28	4:20	4.20

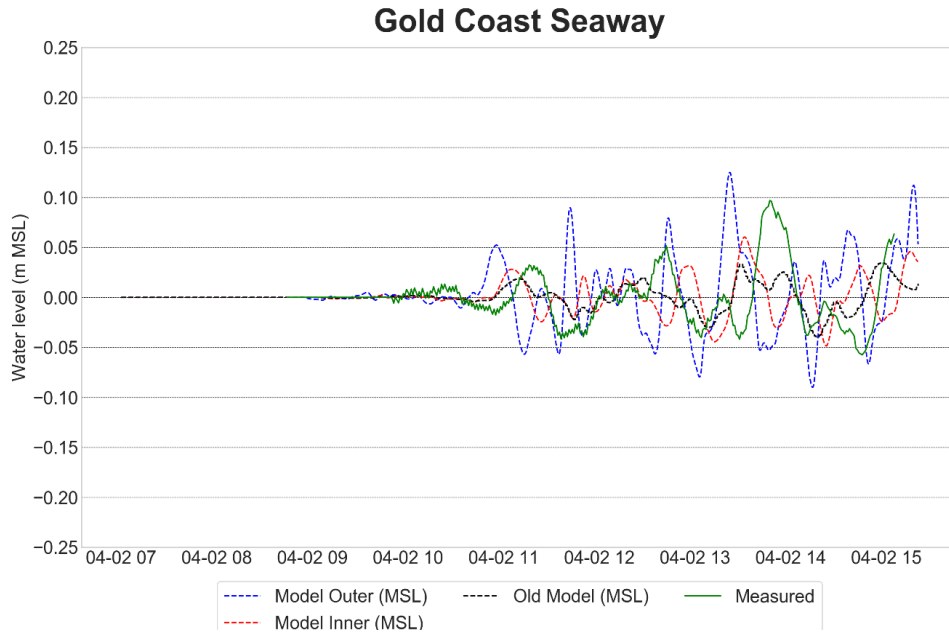


**Figure C. 4 - Solomon 2007 tsunami model results near Gold Coast Seaway.**

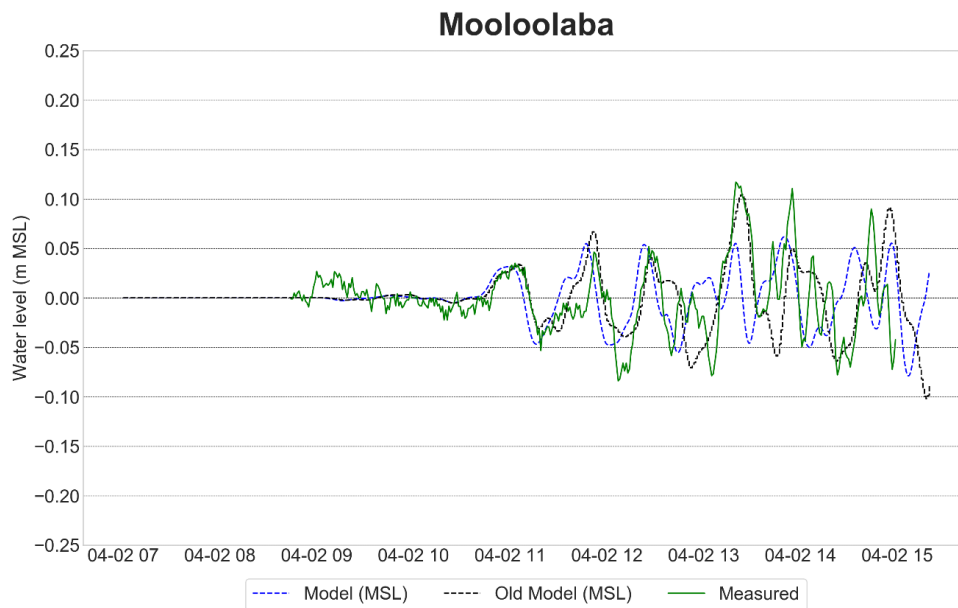


**Figure C. 5 - Solomon 2007 tsunami model results near Mooloolaba.**

Some sensitivity testing was undertaken by varying the roughness and horizontal eddy viscosity parameters as described in the tide calibration. However, there were only marginal changes to the modelled water levels, most likely contributable to the very small amplitudes being modelled.

In general, the validation exercise for the 2007 Solomon Island tsunami event supports the use of MIKE21FM and the developed mesh for tsunami propagation studies. It is noted though that this validation has relied solely on one event.

## C.5 Sensitivity Testing

The calibration phase demonstrated that for tides, the model behaviour in terms of amplitude and phase were slightly sensitive to roughness, and to a lesser degree, horizontal eddy viscosity. This was more noticeable within the shallow bay. Similar checks for the validation phase show lesser sensitivity. Cardno (2013) undertook an assessment of tsunami inundation risk for the New South Wales government. Sensitivity testing undertaken in that study indicated that for seabed roughness, the model was not particularly sensitive, and a Manning's roughness ( $n$ ), of 0.02 was adopted. The report also discussed sensitivity to tides, structures, and overland roughness. It did not discuss viscosity as a sensitivity parameter.

To further test model sensitivity, a number of runs were undertaken for the 10,000 year ARI at HAT. As with tides, Manning roughness values in the range 0.02 to 0.03 were tested, as well as a constant eddy viscosity, and viscosity defined by the Smagorinsky formulation (Smagorinsky, 1963). The results are demonstrated for select locations in Table C. 3 and Table C. 4, with Figure C. 6 and Figure C. 7 showing the water level time series for varying roughness and viscosity respectively for a location near the Brisbane Bar.

Although not shown here, the results for the open ocean showed similar results to Cardno (2013). That is, the tsunami is not particularly sensitive to open ocean seabed roughness and eddy viscosity. However, within the bay, the model is sensitive to both parameters.

As there were no monitoring sites within the bay for the validation, a constant seabed roughness of 0.02 and a constant Smagorinsky coefficient of 0.28 (default value) were adopted. Overland roughness was defined by interpolation of the roughness mapping described in Appendix D.

**Table C. 3 - Percentage change in maximum water level relative to the Smagorinsky eddy viscosity option for select sites.**

Site	Max WL (Smagorinsky)	% Change (Viscosity = 5)	% Change (Viscosity = 10)	% Change (Viscosity = 20)
Bongaree	0.573	-1	-1	-3
Brisbane Bar	0.633	-2	-2	-4
Brisbane Port Office	0.608	-7	-9	-13
Caloundra Head	2.946	0	0	0
Gold Coast Seaway	4.578	0	0	0
Mooloolaba	3.737	0	0	0
Nerang River	5.435	0	0	0
Noosa Head	3.613	0	0	0
Tangalooma Point	0.573	-1	-2	-4



**Table C. 4 - Percentage change in maximum water level relative to a Mannings number, n = 0.025 for select sites.**

	Mannings 0.025	Mannings 0.02	Mannings 0.03
Bongaree	0.573	19%	-26%
Brisbane Bar	0.633	18%	-27%
Brisbane Port Office	0.607	21%	-32%
Caloundra Head	2.945	1%	-3%
Gold Coast Seaway	4.577	3%	-6%
Mooloolaba	3.736	5%	-10%
Nerang River	5.435	4%	-4%
Noosa Head	3.613	4%	-9%
Runaway Bay	1.306	13%	-22%
Tangalooma Point	2.436	19%	-32%

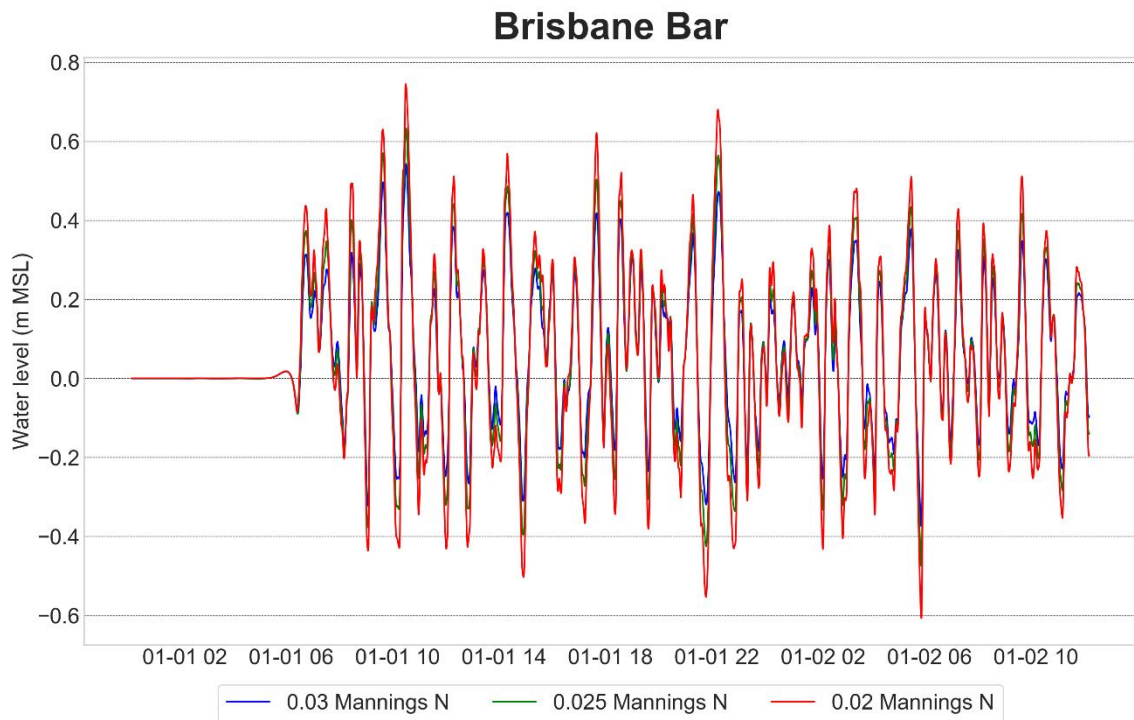


**Figure C. 6 - Sensitivity testing of roughness for 10,000 year ARI event.**

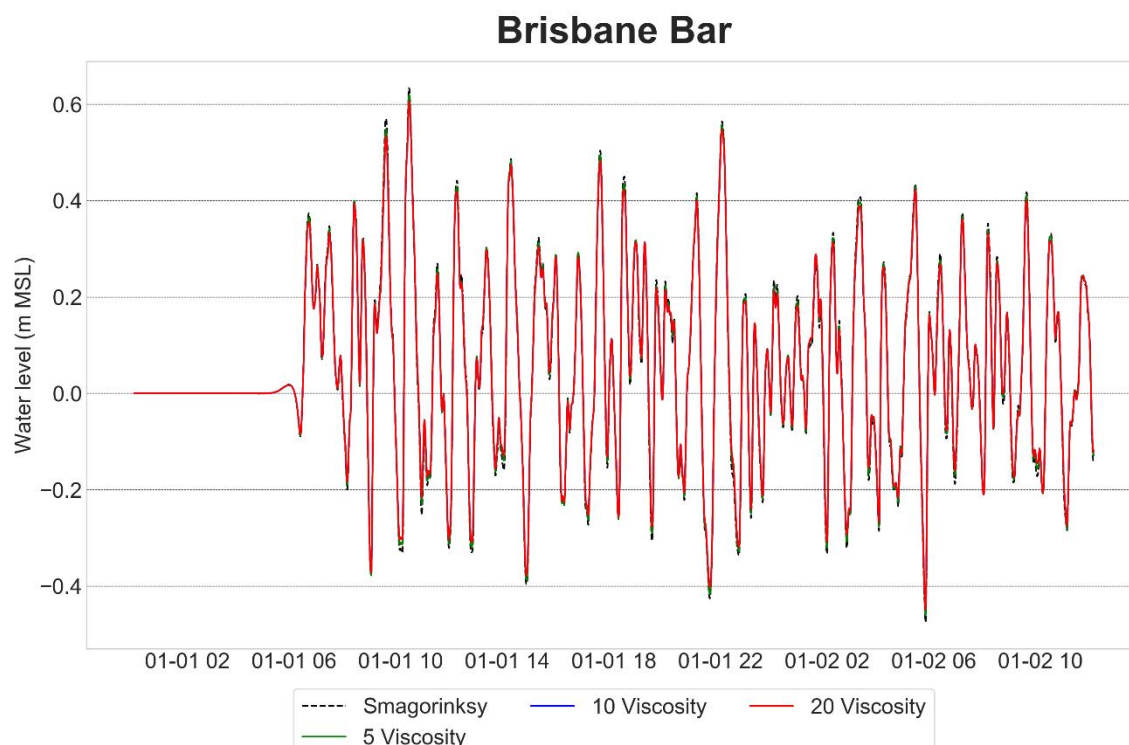


**Figure C. 7 - Sensitivity testing of horizontal eddy viscosity term for 10,000 year ARI event.**

## C.6 References

Boswood, P.K. 2013. Tsunami Modelling along the East Queensland Coast, Report 1: Regional Modelling. Brisbane: Department of Science, Information Technology, Innovation and the Arts, Queensland Government, p 111.

Cardno,.2013. NSW Tsunami Inundation Modelling and Risk Assessment, Report prepared for the NSW State Emergency Service and the Office of Environment and Heritage, p 64.

Chen, T., Newman, A.V., Feng, L., and Fritz, H.M., 2009. Slip distribution from the 1 April 2007 Solomon Islands earthquake: A unique image of near-trench rupture, *Geophysical Research Letters*, Vol 36, L16307, p 6, URL: <https://doi.org/10.1029/2009GL039496>.

Hayes, G.P., Myers, E.K., Dewey, J.W., Briggs, R.W., Earle, P.S., Benz, H.M., Smoczyk, G.M., Flamme, H.E., Barnhart, W.D., Gold, R.D., and Furlong, K.P., 2017. Tectonic summaries of magnitude 7 and greater earthquakes from 2000 to 2015: U.S. Geological Survey Open-File Report 2016–1192, p 148, <https://doi.org/10.3133/ofr20161192>.

Environmental Protection Agency (EPA), 2007. Solomon Islands tsunami, Fact Sheet, FS 2007-2, May, p 3.

Fisher, M.A., Geist, E.L., Sliter, R., Wong, F.L., Reiss, C., and Mann, D.M., 2007. Preliminary Analysis of the Earthquake ( $M_w$  8.1) and Tsunami of April 1, 2007, in the Solomon Islands, Southwestern Pacific Ocean, *Science of Tsunami Hazards*, Vol. 26(1), p 19.

Koshimura, S., 2018. The Tsunami Disaster of 01 April 2007 in the Vicinity of Solomon Sea (web page accessed in 2018), Disaster Control Research Center, Tohoku University, Japan, URL: [http://www.tsunami.civil.tohoku.ac.jp/hokusai2/disaster/07\\_Solomon/event.html](http://www.tsunami.civil.tohoku.ac.jp/hokusai2/disaster/07_Solomon/event.html).

Luger, S.A., and Harris, R.L., 2010. Modelling Tsunamis Generated by Earthquakes and Submarine Slumps Using MIKE 21, International MIKE by DHI Conference, Copenhagen, 6 - 8 September 2010, p 13.

McAdoo, B.G, Fritz, H.M., Jackson, K.L., Kalligeris, N., Kruger, J., Bonte-Graptin, M., Moore, A.L., Rafiau, W.B., Billy, D., and Tiano, B., 2008. Solomon Islands Tsunami, One Year Later, EOS, Transactions, American Geophysical Union, Vol 89(18), 29 April, pp 169–176.

NOAA, 2018b. 2007 Solomon Island Tsunami Event (web page accessed in 2018), National Centers for Environmental Information, URL: [https://www.ngdc.noaa.gov/nndc/struts/results?EQ\\_0=3037&t=101650&s=9&d=100,91,95,93&nd=display](https://www.ngdc.noaa.gov/nndc/struts/results?EQ_0=3037&t=101650&s=9&d=100,91,95,93&nd=display)

Pedersen, N.H., Rasch, P.S., and Sato, T., 2005. Modelling of the Asian Tsunami off the Coast of Northern Sumatra. 3<sup>rd</sup> Asia-Pacific DHI Software Conference, Kuala Lumpur, Malaysia, 21–22 February.

Smagorinsky, J., 1963. General Circulation Experiment with the Primitive Equations, Monthly Weather Review, 91(3), pp 99–164.

USGS, 2018b. M 8.1 – Solomon Islands (web page accessed in 2018), Earthquake Hazards Program, URL: <https://earthquake.usgs.gov/earthquakes/eventpage/usp000f83m#executive>.

## Appendix D – Overland Roughness Mapping

### D.1 Background

The Mike21 software seeks to balance the external forces acting on a mesh cell with the local resistant forces. As a tsunami travels overland, it will experience obstacles and land cover that will obstruct or impede its motion. Including such structures within the model requires very fine mesh of 1 to 2 metres. Even smaller scale is required to capture features such as trees. However, the computation time of such a fine resolution over large extents becomes prohibitive, being considerably slower than prototype time and requiring large storage capacity for result files. At very fine resolution, the flow interaction with buildings can further complicate the problem. For problems focused on inundation extent and depths, a simplified approach has been broadly and successfully applied (for example Gayer et al., 2010). The approach replaces the obstacles with a representative roughness that replicates the behaviour of the obstacle in resisting the inland flow.

Typically, overland grid sizes are limited by computation (and storage) requirements. For inundation extent, grid sizes in the order of 5 to 50 m are typical for built-up areas, with larger sizes in areas of mostly uniform vegetation. These models are based on a “bare earth” DEM, that is the structures have been removed leaving only the ground surface. To facilitate the effect of obstacles, an apparent roughness is adopted, the value of which depends on the type and coverage of the obstacle relative to the area of consideration. Syme (2008) considered the apparent roughness to be a valid option for freshwater flood modelling, as this tries to replicate the effect of water being restricted as it flows through the building, whilst preserving the full storage covered by the building.

Roughness coefficients are typically adjusted to match measured inundation levels. However, such data for a tsunami event is lacking for the study region. Other approaches include determining roughness coefficients from physical models (for example Aida (1977), or Kotani et al. (1998)), or by adjusting numerical model inundation extents to match smaller scale numerical models that include buildings as solid structures (for example Gayer et al. (2010) or Cardno (2013)). MLITT (2012) provides guidance for tsunami inundation modelling and gives the roughness coefficients from Kotani et al. (1998) as an example. Stage 2 (Boswood, 2013b) adopted three values representing: ocean and waterways; beach and dune system; and built-up areas based on a range of values from Aida (1977), Kotani et al. (1998), Cardno (2013), and Garber et al. (2011).

Bricker et al. (2015) undertook a review of roughness values used in tsunami modelling. The paper concluded that the values provided by Kotani et al. (1998) were smaller than those based on field measurements and large-scale experiments for open channel flow (for example Chow (1959), Arcement and Schneider (1984), and Gibson (2005)). They attributed this to the physical model scales not being large enough to avoid the effects of surface tension and viscosity. Housing-density-dependent and flow-depth dependent urban Manning’s  $n$  relations (Koshimura et al., 2009) produce values similar to those found in open channel flow literature. Bricker et al. (2015) conclude that tsunami models would benefit from leveraging roughness values from open channel flow literature, and cites the work of Bunya et al. (2010), which provides an extensive list of Manning’s values based on land use mapping for a storm surge modelling study.

The approach applied to this study was the development of a detailed roughness map based on land use. Further detail is provided in the subsequent section.

## D.2 Roughness Map Generation

Manning's values for onshore areas were chosen following a literature review of values as discussed above. The final list of values is provided in Table D. 1, based on the work of Bricker et al. (2015), Bunya et al. (2010), and Cardno (2013). This list has been purposely kept to a minimum, to reduce complicated areas that are at present, impossible to verify given the lack of tsunami inundation levels for actual events. It is expected that this will produce a more conservative result.

A number of different datasets were used to generate a land use map, listed below (refer to Table D. 1 for details), for which roughness values were then applied:

- Queensland Land Use Mapping – QLUMP;
- Queensland Digital Cadastral Database – QDCDB;
- Queensland Wetland Habitat Mapping.

The Queensland Land Use Mapping Program (QLUMP) was the principle dataset used. This is an aggregated product derived from a number of sources, including remote sensing and field survey developed and maintained by DES in collaboration with other government departments and councils. The dataset provides a series of land use categories and types which are sorted by a code. These were then mapped against the land use types identified in the literature review (refer Table D. 1). This provided the base layer for roughness mapping as it has no gaps. However for the purposes of detailed roughness mapping it missed a number of key elements including roads and detail in urban and coastal areas.

**Table D. 1 - Table of Manning's values used with the model domain.**

Land Use Category	Manning's n	Manning's M
Coastal Waters	0.025	40
Roads	0.02	50
Wetland Barren	0.030	33.33
Wetland Shrub	0.045	22.22
Grassland	0.030	33.33
Farmland	0.040	25
Coastal Woody Wetland	0.070	14.28
Forest	0.070	14.28
Low Density Urban	0.050	20
Medium Density Urban	0.100	10

To improve the QLUMP base dataset a number of subsequent layers were used, the QDCDB provided detailed cadastral information for roads and urban areas. Manning's numbers were assigned based on attribute information which contained details on land use. The Wetland Habitat Mapping layer was also used to better define vegetation areas in the coastal floodplains; this allowed better inclusion of Mangroves and Wetlands which have different roughness characteristic but were not separated within the QLUMP data. These supplementary layers were then stamped into the QLUMP data to produce a complete roughness map. Results were then reviewed against aerial mapping to produce the final roughness map. Figure D. 1 shows the roughness map for Bribie Island.



The final land use map has the associated Manning’s n and Manning’s M (adopted by the MIKE21 software and is the reciprocal of Manning’s n) within the attribute table, to convert the product into a roughness map. These are then tied to the model domain mesh node points using a spatial join and those values are ingested into MIKE21.

It is important to note that the final roughness values applied within the model are interpolations at the mesh nodes and therefore the resolution of the roughness map used within the model domain was dependant on the resolution on the model mesh. Figure D. 1 shows good agreement with the original roughness map.

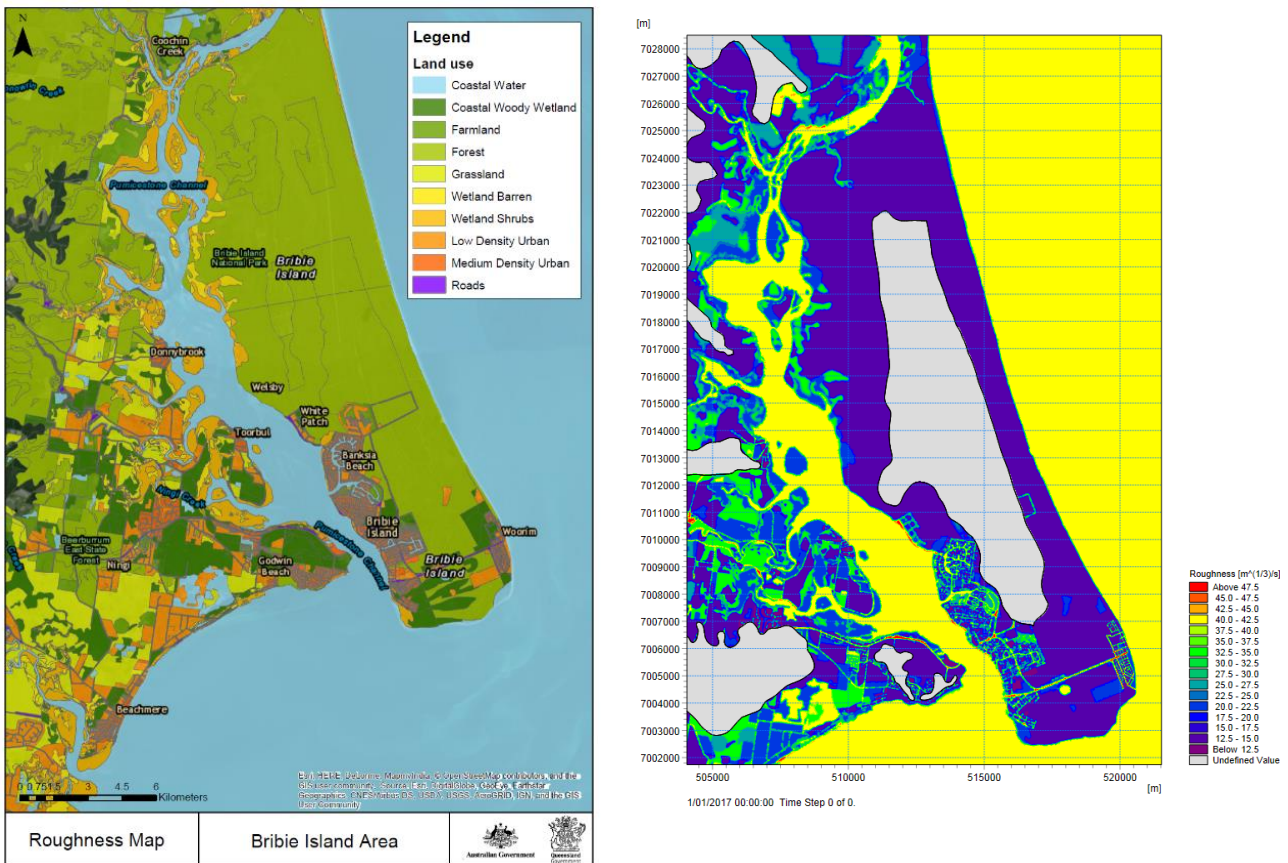


**Figure D. 1 - Land use map example for Bribie Island, compared with the roughness map interpolated for the MIKE21 model.**

### D.3 References

Arcement, G.J. Jr. and Schneider, V.R., 1984. Guide for Selecting Manning's Roughness Coefficients for Natural Channels and Flood Plains, Report No. FHWA-TS-84-204, Federal Highway Administration, Also published as US Geological Survey Water Supply Paper 2339 [1989].

Aida, I., 1977. Numerical experiment for inundation of tsunamis. Susaki and Usa, in the Kochi Prefecture. Bulletin of Earthquake Research Institute, University of Tokyo, 52: pp 441–460. (In Japanese).

Boswood, P.K., 2013b. Tsunami Modelling along the East Queensland Coast, Report 2: Sunshine Coast. Brisbane: Department of Science, Information Technology, Innovation and the Arts, Queensland Government, p 96.

- Bricker, J.D., Gibson, S., Takagi, H., and Imamura, F., 2015. On the Need for Larger Manning's Roughness Coefficients in Depth-Integrated Tsunami Inundation Models. *Coastal Engineering Journal*, volume 57(2), June, p 13, <https://doi.org/10.1142/S0578563415500059>
- Bunya, S., Deitrich, J.C., Westerink, J.J., Ebersole, B.A., Smith, J.M., Atkinson, J.H., Jensen, R., REsio, D.T., Luettich, R.A., Dawson, C., Cardone, V.J., Cox, A.T., Powell, M.D., Westerink, H.J., and Roberts, H.J., 2010. A High-Resolution Coupled Riverine Flow, Tide, Wind, Wind Wave, and Storm Surge Model for Southern Louisiana and Mississippi. Part I: Model Development and Validation, *Monthly Weather Review*, Vol. 18, pp 345–377.
- Cardno, 2013. NSW Tsunami Inundation Modelling and Risk Assessment, Report prepared for the NSW State Emergency Service and the Office of Environment and Heritage, p 64.
- Chow, V. T., 1959. *Open-Channel Hydraulics*, McGraw-Hill Book Company, New York, p 113.
- Garber, S., Treloar, D., Beadle, C., Hanslow, D., and Opper, S., 2011. Validation of Tsunami Modelling along the NSW Coast, 20<sup>th</sup> NSW Coastal Conference, Tweed Heads, 8-11 November, 18pp.
- Gayer, G., Leschka, S., Nöhren, I., Larsen, O., Günther, H., 2010. Tsunami inundation modelling based on detailed roughness maps of densely populated areas, *Natural Hazards and Earth System Sciences*, pp 1679-1687.
- Gibson, S., 2005. Unsteady HEC-RAS Model of the downtown reach of the Truckee River, HEC, PR-58, p 39.
- Koshimura, S., Oie, T., Yanagisawa, H., and Imamura, F., 2009. Developing fragility functions for tsunami damage estimation using numerical model and post-tsunami data from Banda Aceh, Indonesia," *Coastal Eng. J.* 51(3), pp 243–273.
- Kotani, M., Imamura F. & N. Shuto., N., 1998. Tsunami run-up simulation and damage estimation by using GIS. In: *Proc. of Coastal Eng., JSCE*, vol. 45 (1), pp 356–360. (In Japanese)
- MLITT., 2012. Guide to determining the potential tsunami inundation, Seacoast Office, Water and Disaster Management Bureau, Ministry of Land, Infrastructure, Transport and Tourism, Version 2.0 (temporary translation), p 82.
- Syme, W.J., 2008. Flooding in Urban Areas – 2D Modelling Approaches for Buildings and Fences, 9<sup>th</sup> National Conference on Hydraulics in Water Engineering, Engineers Australia, Darwin, 23–26 September, p 8.

## Appendix E – Tsunami Arrival Times

The following tables provide the arrival times for various Average Recurrence Intervals (ARIs) and subduction zones. The locations are shown in the following figures.

The boundary conditions showed two characteristics of the leading wave. The leading wave generated from the Kermadec-Tonga (KT) subduction zone exhibited a drawdown prior to the leading wave, symptomatic of a leading depression N-wave (LDN). Whilst the South America (SA) and New Hebrides (NH) wave forms were similar to a leading elevation N-wave (LEN) in form. Due to the differing leading wave forms, different criteria were developed for calculating arrival times for each subduction zone scenario as outlined below:

- Kermadec-Tonga – defined as a deviation of 1 cm away from the still water level.
- New Hebrides – defined as an up-crossing deviation of 0.75 cm or down-crossing of 1 cm from the still water level.
- South America – defined as an up-crossing or down-crossing of 1 cm from the still water level.

**Table E. 1 - Arrival time statistics (hours: minutes after earthquake) for locations within Moreton Bay by ARI and subduction zones of Kermadec-Tonga (KT), New Hebrides (NH), and South America (SA).**

Arrival Time (hours: minutes after earthquake) In Morton Bay									
ARI (year)	750			3,000 (MSL)	3,000			10,000	
Source	KT	NH	SA	KT	KT	NH	SA	NH	KT
1. Beachmere	5:52	4:31	19:01	5:55	5:49	4:33	19:20	4:34	5:46
2. Bongaree	5:34	4:16	18:46	5:35	5:31	4:16	19:04	4:16	5:28
3. Brighton–Sandgate	6:00	4:36	19:10	6:07	5:57	4:43	19:29	4:44	5:56
4. Brisbane Airport	5:57	4:33	19:06	6:04	5:54	4:40	19:24	4:41	5:53
5. Bulwer	5:00	3:42	18:10	4:57	4:56	3:42	18:28	3:42	4:54
6. Cleveland	5:37	4:27	18:47	5:46	5:34	4:24	19:07	4:23	5:31
7. Clontarf	5:58	4:34	19:06	6:05	5:55	4:39	19:24	4:40	5:52
8. Deception Bay	6:02	4:34	19:11	6:14	5:59	4:43	19:30	4:45	5:58
9. Dunwich	5:19	4:16	18:30	5:27	5:15	4:06	18:50	4:05	5:13
10. Goodwin Beach	5:42	4:22	18:51	5:46	5:38	4:24	19:10	4:24	5:36
11. Manly	5:50	4:29	18:58	6:08	5:48	4:35	19:16	4:33	5:45
12. Pine River	6:12	4:48	19:21	6:20	6:10	4:54	19:39	4:55	6:08
13. Redcliffe	5:43	4:23	18:53	5:45	5:40	4:26	19:12	4:26	5:38
14. Redland Bay Victoria Point	5:50	4:40	19:00	6:03	5:47	4:40	19:19	4:28	5:44
15. Scarborough	5:46	4:24	18:55	5:49	5:43	4:27	19:13	4:39	5:40
16. South Bay Islands	5:49	4:41	18:59	6:02	5:46	4:34	19:17	4:33	5:43
17. South Morton Island Inside	4:53	3:23	18:04	4:57	4:50	3:39	18:23	3:40	4:48
18. Wellington Point	5:49	4:31	18:57	6:10	5:46	4:34	19:15	4:33	5:43

**Table E. 2 - Arrival time statistics (hours: minutes after earthquake) for locations within the Brisbane River by ARI and subduction zones of Kermadec-Tonga (KT), New Hebrides (NH), and South America (SA).**

Arrival Time (hours: minutes after earthquake) in Brisbane River									
ARI (year)	750			3,000 (MSL)	3,000			10,000	
Source	KT	NH	SA	KT	KT	NH	SA	NH	KT
19.Port of Brisbane	5:50	4:29	19:00	5:57	5:47	4:32	19:19	4:30	5:45
20.Newstead Park	6:23	5:00	19:33	6:31	6:21	5:08	19:50	5:06	6:20
21.Kangaroo Point	6:34	5:10	19:41	6:42	6:31	5:18	19:59	5:16	6:30
22.St Lucia	6:54	5:31	20:02	7:04	6:52	5:38	20:20	5:35	6:50
23.Indooroopilly	7:11	5:49	20:19	7:22	7:09	5:54	20:36	5:51	7:08

**Table E. 3 - Arrival time statistics (hours: minutes after earthquake) for locations outside Moreton Bay by ARI and subduction zones of Kermadec-Tonga (KT), New Hebrides (NH), and South America (SA).**

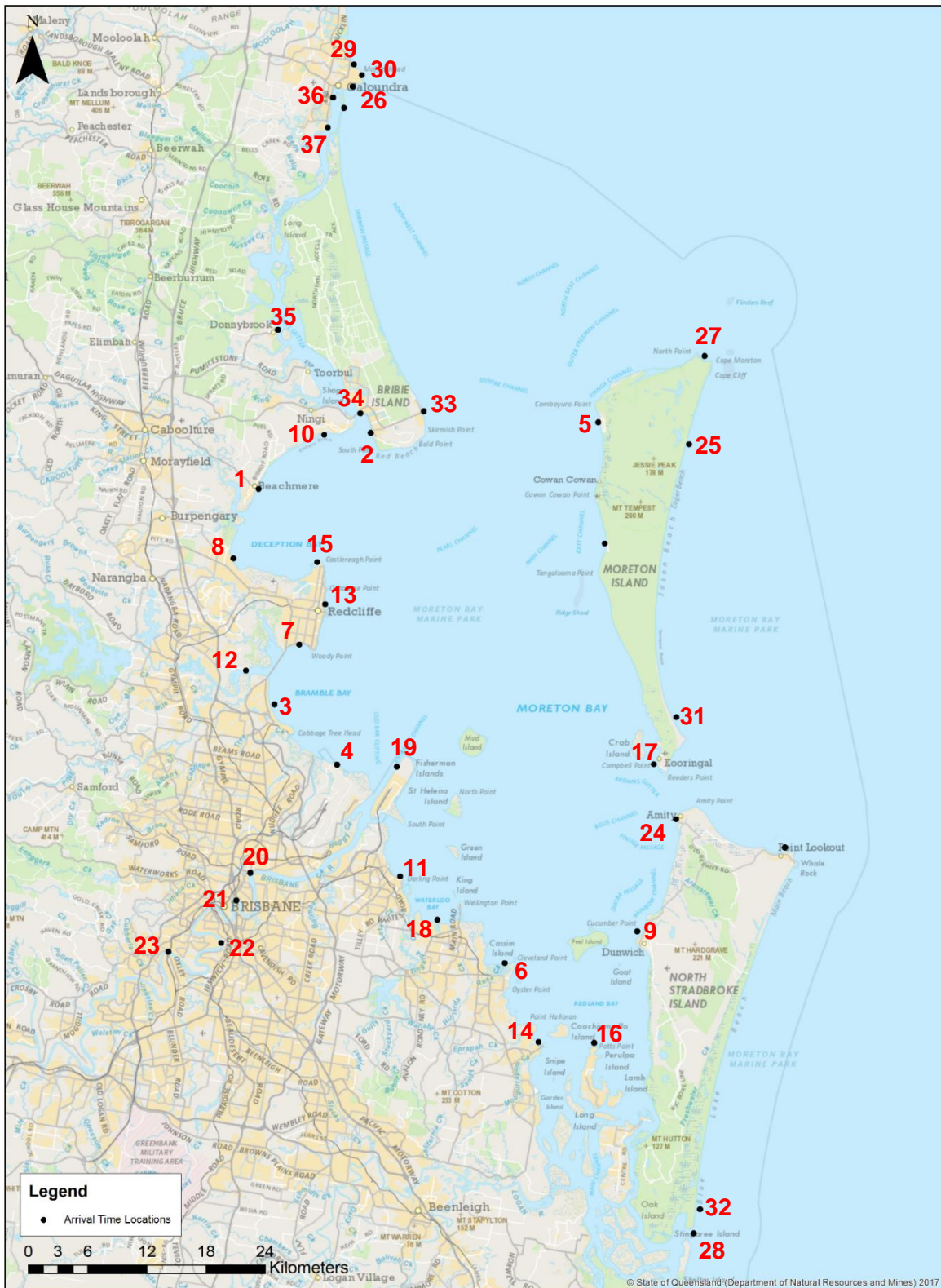
Arrival Time (hours: minutes after earthquake) outside Morton Bay									
ARI (year)	750			3,000 (MSL)	3,000			10,000	
Source	KT	NH	SA	KT	KT	NH	SA	NH	KT
24.Amity	4:47	3:13	17:57	4:46	4:44	3:31	18:17	3:33	4:43
25.Blue Lagoon Campsite	4:33	3:05	17:43	4:30	4:30	3:15	18:03	3:17	4:29
26.Caloundra	4:57	3:28	18:09	4:55	4:55	3:39	18:28	3:41	4:53
27.Cape Moreton	4:33	3:08	17:44	4:30	4:30	3:15	18:03	3:17	4:28
28.Jumpinpin	4:44	3:14	17:47	4:42	4:41	3:28	18:07	3:30	4:40
29.Moffat Beach	4:56	3:28	18:07	4:54	4:53	3:38	18:27	3:39	4:52
30.Shelly Beach	4:56	3:28	18:07	4:54	4:53	3:37	18:26	3:39	4:52
31.South Morton Island Outside	4:37	3:01	17:47	4:35	4:34	3:21	18:07	3:23	4:33
32.South Stradbroke Island	4:41	3:11	17:45	4:39	4:39	3:26	18:05	3:28	4:38
33.Woorim	5:10	3:43	18:21	5:10	5:07	3:52	18:41	3:54	5:06

**Table E. 4 - Arrival time statistics (hours: minutes after earthquake) for locations within Pumicestone Passage by ARI and subduction zones of Kermadec-Tonga (KT), New Hebrides (NH), and South America (SA).**

Arrival Time (hours: minutes after earthquake) Pumicestone Passage									
ARI (year)	750			3,000 (MSL)	3,000			10,000	
Source	KT	NH	SA	KT	KT	NH	SA	NH	KT
34.Pumicestone Passage	5:38	4:20	18:49	5:39	5:35	4:20	19:07	4:20	5:32
35.Donnybrook	6:19	5:05	19:38	6:52	6:16	4:59	19:52	4:57	6:12
36.Golden Beach	5:06	3:42	18:17	5:06	5:02	3:48	18:36	3:49	5:01
37.Pelican Waters	5:18	3:57	18:29	5:24	5:14	3:59	18:47	3:58	5:12



Based on the above criteria, events from the New Hebrides have the shortest arrival time of just over four hours after the earthquake, with events from South America arriving much later at over 18 hours.



Tsunami Modelling  
Morton Bay

Locations where arrival time  
was calculated from model domain

